Strain Concentrations in Polyethylene Geomembranes Adjacent to Seams and Scratches

by

Jake Andresen

A Thesis Presented in Partial Fulfillment
of the Requirements for the Degree
Master of Science

Approved April 2017 by the
Graduate Supervisory Committee:

Edward Kavazanjian Jr., Chair
Sandra Houston,
Claudia Zapata

ARIZONA STATE UNIVERSITY

May 2017

ABSTRACT

Laboratory testing was conducted to quantify strain concentrations adjacent to seams and scratches in high density polyethylene (HDPE) geomembranes. The tensile strain profile of remnants meeting the ASTM criteria for wide-width tensile testing from samples of field seams recovered for construction quality assurance testing was evaluated using digital image correlation (DIC). Strains adjacent to scratches on laboratory prepared samples loaded in tension were also measured using DIC. The tensile strain in the zone adjacent to a seam and the tensile strain adjacent to a scratch were compared to the tensile strains calculated using theoretical strain concentration factors. The relationship between the maximum tensile strain adjacent to a seam and the global nominal strain in the sample was quantified for textured and smooth geomembranes of common thicknesses. Using statistical analysis of the data, bounds were developed for the allowable nominal tensile strain expected to induce maximum tensile strains adjacent to the seam less than or equal to the typical yield strain of HDPE geomembranes, at several confidence levels. Where nominal strain is the global or average strain applied to the sample and maximum strain is the largest tensile strain induced in the sample.

The reduction in the nominal yield strain due to a scratch in a HDPE geomembrane was also quantified. The yield strain was approximately the same as predicted using theoretical strain concentration factors. The difference in the average measured maximum strains adjacent to the seams of textured and smooth HDPE geomembranes was found to be statistically insignificant. However, maximum strains adjacent to extrusion welded seams were somewhat greater than adjacent to fusion welded seams for nominal strains on the order of 3% to 4%. The results of the testing program suggest that the nominal tensile

strain should be limited to 4% around dual hot wedge seams and 3% around extrusion fillet seams to avoid maximum strains equal to 11%, a typical yield strain for HDPE geomembranes.

ACKNOWLEDGMENTS

The research project described herein was made possible due to the contributions of several individuals and organizations which deserve mention. Firstly, the guidance and experience of my advisor, Dr. Edward Kavazanjian, Jr, was invaluable, without which the project would never have moved forward. My thanks to the members of my thesis committee, Dr. Sandra Houston and Dr. Claudia Zapata for their advice and time spent aiding me in my graduate studies. I would like to thank Mr. Sam Allen of TRI Environmental, Dr. Allen Marr of Geotesting Express, and Mr. Carl Apicella of AEG, A Tetra Tech Company for providing the field samples of geomembrane seams used in this study. The work detailed in Chapter 4 was funded in part by the National Science Foundation (NSF) Geomechanics and Geotechnical Hazards program of the Civil, Mechanical, and Manufacturing Innovation Division (CCMI) under the Network for Earthquake Engineering Simulation Research program under Grant # CMMI 1208026, "NEESR: Performance-based Seismic Design of Geomembrane Liner Systems for Waste Containment. The authors are grateful for this support. However, any opinions or positions expressed in this paper are the opinions and positions of the authors only, and do not reflect any opinions or positions of the NSF.

Finally, I would like to thank Dr. Angel Gutierrez for his aid in the laboratory testing setup and research assistant Sarah Montgomery for her help in performing the laboratory testing for this project.

TABLE OF CONTENTS

Page

CHAPTER Page

CHAPTER Page

CHAPTER Page

LIST OF TABLES

LIST OF FIGURES

Figure Page

Figure Page

Figure Page

Figure Page

PREFACE: PREVIOUS WORK

Chapter 4 of this work includes the journal paper entitled "Experimental Evaluation of HDPE Geomembrane Seam Strain Concentrations", which was accepted for publication in Geosynthetics International on 23 January 2017. I am the second author of the work. The first and third authors are Dr. Edward Kavazanjian and Dr. Angel Gutierrez respectively.

The journal paper is based upon tensile testing performed upon seamed HDPE geomembrane samples. Digital image correlation (DIC) was used to capture the tensile strain perpendicular to the seams across the surface of the sample. I was responsible for the testing and data collection, as well as the post processing and data analysis for the project.

To facilitate data collection, I learned to successfully operate the available DIC equipment to capture the images needed to calculate the deformation and related strain fields across the sample surfaces. The apparatus setup includes proper camera positioning, lighting, exposure adjustment, focus, and calibration of the spatial relationship between the image capture cameras and test sample. I worked with Dr. Angel Gutierrez to run the tensile tests and image capture process simultaneously.

During the journal review process, I performed several tests, with aid from undergraduate research assistant Sarah Montgomery, to generate the mean and standard deviation values needed for the validation of accuracy and precision of the DIC measurements.

Following data collection, I compiled the graphical representations of the strain fields by performing the post processing required in the DIC software, VIC3D. Further, I created the comparison charts and table which constitute the primary result of the study. The charts include a comparison of the average and maximum tensile strains to the average

strain adjacent to the seam across the sample and the bending strain prediction generated using the Giroud (1995) equations for strain concentrations in geomembranes adjacent to seams. A summary of the results must include the following two key points. Firstly, the tensile strain measured adjacent to the seam across the width of the sample was found to be relatively close to that predicted using the Giroud (1995) equations for bending strain in geomembranes adjacent to seams. The discrepancy can be explained by inconsistencies in the geomembrane created during the welding of the bars used to secure the samples during welding, and possibly edge effects. Secondly, the localized maximum tensile strain measured in the sample was found to be on the order of 3 to 4 times the nominal tensile strain. These findings prompted further study into field geomembrane seam samples as opposed to the laboratory prepared samples used in this project.

Dr. Edward Kavazanjian and Dr. Angel Gutierrez were the primary writers for the paper, incorporating images generated by myself as well as supplementing these with further images. Dr. Kavazanjian served as the primary advisor regarding the direction of the testing, appropriate assumptions, and necessary data collection. Dr. Gutierrez served as the project lead, and aided in the laboratory testing for the project.

CHAPTER 1. INTRODUCTION

1.1 Objective and Scope

This dissertation was prepared in partial fulfillment of the requirements for graduation with a Master of Science in Geotechnical Engineering from the School of Sustainable Engineering and the Built Environment at Arizona State University. The methodology and results contained herein are the product of testing performed at Arizona State with the help of Angel Gutierrez, PhD, under the advisement of Dr. Edward Kavazanjian.

Two distinct studies are included herein with the following objectives. 1) characterization of the nominal tensile strain in high density polyethylene (HDPE) geomembranes loaded in tension across fields seams which is likely to induce a maximum strain exceeding the yield strain, and 2) evaluation of the reduction in nominal yield strain due to a scratch in a geomembrane loaded in tension. Giroud et al. (1994) and Giroud (1993) present the theoretical equations for strain concentrations in geomembranes adjacent to seams subjected to tensile loads and for reductions in yield strains due to scratches in geomembranes, respectively. In this work, the Giroud et al. (1994) strain concentration factors are compared to experimentally measured strains on field seamed HDPE geomembrane samples with two thicknesses, 1 mm (40 mil) and 1.5 m (60 mil), from three sources (TRI Environmental, Geotesting Express, and AEG), and with two textures (smooth and rough). 1 mil designates 1 milli-inch, 0.001 inches. The reduction in yield strain due to scratches of varied depths was also evaluated experimentally and compared to the theoretical values from Giroud (1993).

1.2 Motivations

In the process of developing a method for evaluating the integrity of geosynthetic elements of waste containment systems, Kavazanjian et al. (2013) performed numerical analyses on two lined landfills subject to strong ground motions in the 1994 Northridge earthquake. Earthquake induced cracking and associated tears in the liner at the Chiquita Canyon Landfill in response to the Northridge event, shown in Figure 1-1, provided a unique opportunity for an in-depth study with regard to geomembrane liner system failure modes in response to strong shaking and large strain behavior. A forensic study following the damage by EMCON Associates (1994) presents a great deal of information on the strength properties of the liner system interface and insight into the failure mechanism.

Arab (2011) developed a finite difference model to back analyze the seismic response of the Chiquita Canyon landfill liner system in the Northridge event. The state-of-the art finite difference model was used to predict tensile strains in the vicinity of the observed tears in the side slope liner (Kavazanjian et al., 2013). The locations of tensile strains induced in the geomembrane by waste placement and the earthquake were accurately predicted in the geomembrane, but the magnitude of the tensile strains adjacent to the tears was well below yield. To explain why the geomembrane tore at these locations, strain concentrations adjacent to seams loaded in tension and the reduction in yield stress due to scratches in the geomembrane had to be considered to reduce the factor of safety for yield of the geomembrane to below 1.0 (Kavazanjian et, al., 2013). The theoretical seam strain concentration factors developed by Giroud et al. (1995) and the theoretical reduction in tensile yield strain due to a scratch developed by Giroud (1994) were employed in this

analysis. While these factors have a sound theoretical basis, they have never been experimentally verified.

Figure 1-1: Geomembrane tear at Cell C, Chiquita Canyon Landfill following the 1994 Northridge earthquake

The work presented herein experimentally evaluates strain concentrations in geomembranes adjacent to seams loaded in tension and the reduction in yield strain due to a scratch loaded in tension and to compare these values to the theoretical values predicted

by Giroud (1994) and Giroud et al. (1995). The testing program considered the effect of seam type, geomembrane surface texture, and geomembrane thickness on the maximum tensile strain adjacent to the seam. Statistical analysis of the data is used to establish confidence levels for the maximum nominal strain such that the maximum tensile strain adjacent to a seam is below yield. The effect of a scratch in a geomembrane loaded in tension was also evaluated experimentally.

1.3 Organization of this Dissertation

This work presented herein adheres to the following organizational structure. Chapter 2 includes background information on HDPE geomembranes as it applies to this work, including information on geomembrane seams and the geomembrane stress-strain relationship. Background information pertaining to strain concentrations, greater detail into the events motivating this work, and information on the liner failure at the Chiquita Canyon landfill are also included in Chapter 2. Chapter 3 introduces Digital Image Correlation, the technique used to measure the tensile strains in the geomembrane, and the associated techniques and computer programs used in the analysis presented herein. Furthermore, the best practices for sample preparation for DIC of a geomembrane in tension are discussed in Chapter 3 based upon the literature and personal experiences during this study. Chapter 4 details previous work on experimental evaluation of geomembrane seam strain concentrations in factory made seams. Chapter 5 details the experimental evaluation of geomembrane seam strain concentrations in field seams. This section includes statistical analyses to establish confidence bounds on the extent of the maximum strain. Chapter 6 details the experimental evaluation of the reduction in yield strain in geomembranes due to scratches. Chapter 7 includes a summary of the project work and a discussion of sources

of error, assumptions, and experimental and data processing challenges which may be encountered when attempting to replicate the experiments described herein, as well as thoughts regarding relevant research which may strengthen the confidence in the results of this project.

CHAPTER 2. BACKGROUND

2.1 Geomembranes

Geomembranes are low permeability materials used in solid waste, liquid and gas containment. Geomembranes can be used as landfill liners, vapor/gas barriers, and in the construction of lakes and ponds. Geomembranes may be constructed from a variety of polymers, including high density polyethylene (HDPE), low density polyethylene (LDPE), polyvinyl chloride (PVC), and chlorosulfonated polyethylene (CSPE). Geomembranes are typically supplied in rolls or as prefabricated panels and subsequently seamed in the field.

HDPE is a commonly used polymer for waste containment due to high chemical resistance. LDPE is often used for other containment applications requiring a higher ductility. Other polymers such as PVC are also occasionally used in containment systems. HDPE liners incorporated into a waste containment system are typically manufactured in 100 feet rolls with a width of 22.5 feet. The rolls are laid out at the site and seamed in the field via welding processes.

HDPE geomembranes are chemically stable and therefore tend to be difficult to glue, but do melt at temperatures above 140°C (Muller, 2007) making thermal welding the preferred method for joining HDPE geomembranes. Thermal welding heats the HDPE polymer above its melting point and induces a rheological process where the melted materials flow and subsequently mix to form a connection upon cooling.

2.2 Seams in Geomembranes

The two welding processes typically employed to create a seam joining two geomembrane rolls in the field are fusion welding and extrusion welding. Fusion welds connect the two geomembrane panels directly using heat and pressure while extrusion

welds use an intermediate material, typically also HDPE, to join the two panels together. (Figure 2-1). Fusion welds include hot wedge seams and dual hot wedge seams, while extrusion welds include extrusion fillets and extrusion lap seams. In the case of landfill liners where large areas of HDPE are to be joined, the two most common weld types are extrusion fillet welds and dual hot wedge welds. Figure 2-1 from Giroud (2005) shows the fusion, extrusion lap, and extrusion fillet seam types.

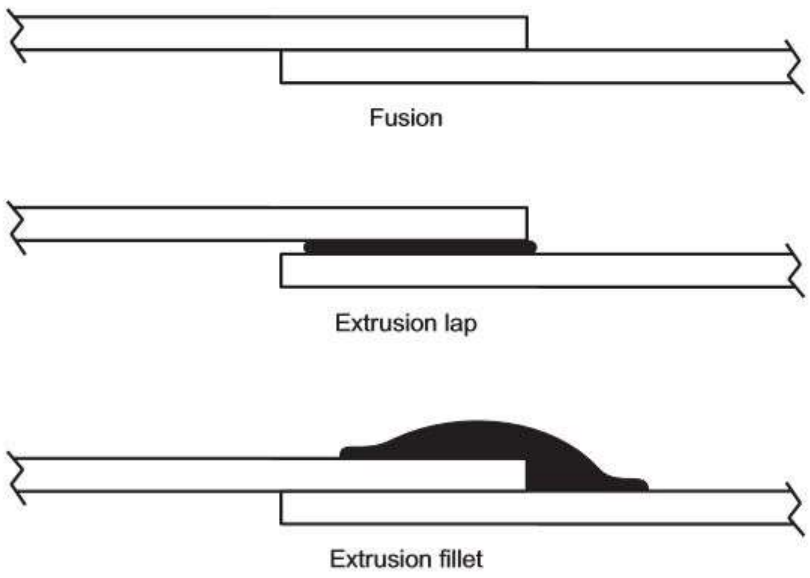

Figure 2-1: Typical seams used to join geomembranes

The dual hot wedge seam is comprised of two fusion weld separated by a channel. A picture of a dual hot wedge seam is shown in Figure 2-2. The channel allows for nondestructive seam integrity testing and the dual seams provide an additional factor of safety. Dual hot wedge welds are formed using a heated wedge that moves between the overlapping geomembrane panels. Guide rollers ensure contact between the wedge and the geomembranes while squeeze rollers press the melted geomembrane layers together. Figure 2-3 shows a diagram of the heated wedge with the two tracks used to form the two

seams separated by a channel. Figure 2-4 presents a cross section illustration of the welding apparatus.

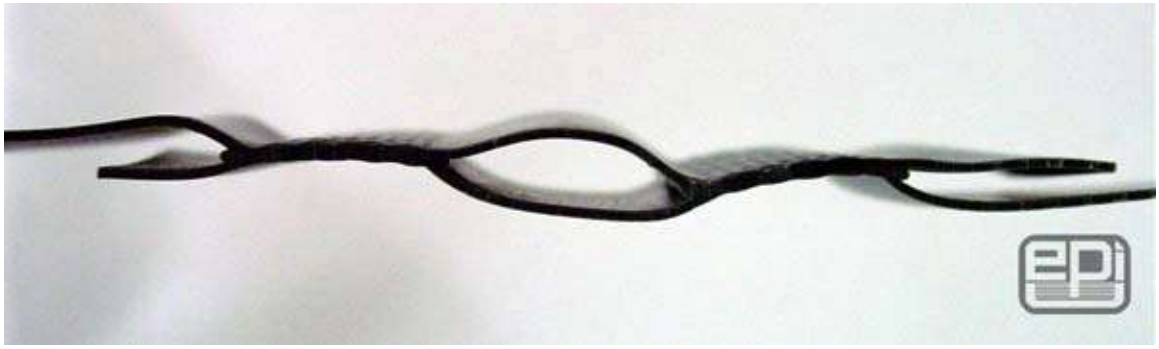

Figure 2-2: Dual hot wedge seam cross section

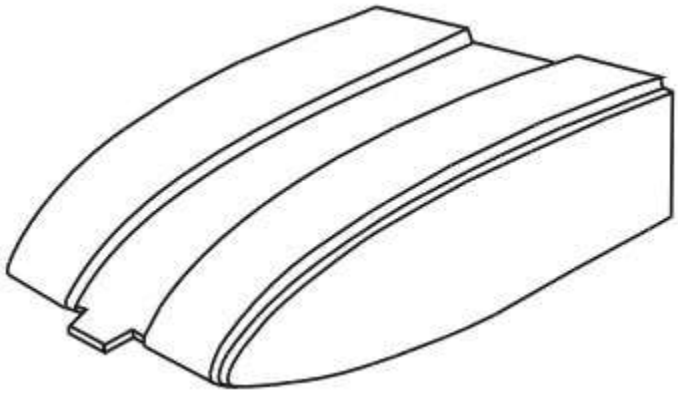

Figure 2-3: Diagram of dual wedge track with test channel (Muller, 2007)

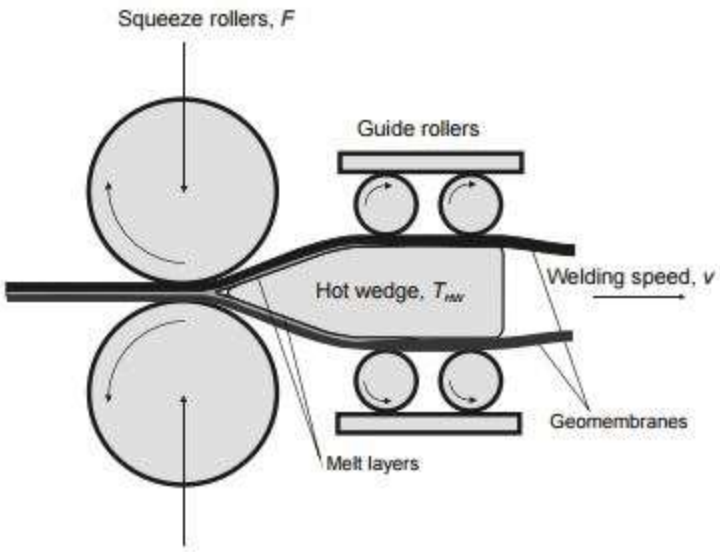

Figure 2-4: Sketch of the heated dual wedge weld apparatus (Muller, 2007)

Extrusion fillet welding consists of merging a strand of extrudate material along with the overlapping geomembrane sections (Figure 2-1). The extrudate is usually composed of the same or similar material as that of the geomembrane as the flow properties must be similar to make an effective weld. The area over which the weld will sit must be prepared by grinding of the surface layer and preheating the surface to counteract the poor heat transfer between the extrudate strand and the geomembrane. The seaming process is more labor intensive than the hot wedge method and is difficult to nondestructively test for integrity in an effective manner. Therefore, extrusion welding is typically only used in areas of the liner where the geometry does not allow the use of the wedge apparatus.

The integrity of landfill liners depends upon the tensile strength and leak tightness of the seams. Liners are tested for seam strength in the laboratory and for tightness in the field. Laboratory tests to test seam strength are performed on field samples cut from the geomembrane. The resulting section of the seam from which the sample has been cut is patched and the patch is welded with an extrusion fillet. Some seam strength testing is

typically conducted in the field. However, most seam strength testing is conducted on the geomembrane sample in a certified testing laboratory according to ASTM D6392-12 or a similar standard.

Potential leaks in the geomembrane seams are detected in the field using a tightness test which varies according to the seam type. If there is a test channel, e.g., the channel in a dual track fusion weld, large lengths of the seam may be sealed off and pressurized. If the channel fails to hold the pressure within the guidelines of ASTM D5820-95, individual sections must be tested until the leak is found. The leak is then typically patched using an extrusion fillet weld to secure the patch. In the absence of a test channel, as is the case with extrusion fillet seams, a vacuum box is used to seal sections of the seam. The seam is covered in a soap film, a vacuum pressure is applied to the chamber, and the seam is monitored for soap bubbles. If bubbles are observed, a leak is present and the seam must be sealed using a patch secured by extrusion fillet welding.

2.3 Geomembrane Stress-Strain Behavior and Localized Strain

The stress-strain relationship for geomembranes is highly non-linear and varies according to material microstructure and type. For instance, the stress-strain relationship of HDPE is fundamentally different from that of a low density polyethylene (LDPE) (Giroud, 1984). Geomembranes may be described as exhibiting a yield peak, yield plateau, or neither. Figure 2-5 below presents the results of a simple mathematical model using an n-order parabola (Giroud, 1984) developed for geomembranes which exhibit yield peak behavior. Yield peak behavior is characterized by a drop in strength following exceedance of a certain strain (yield). The yield strain typically occurs at between 10 and 15 percent

(Giroud, 1984), with 11 percent being common for many commercially available geomembranes.

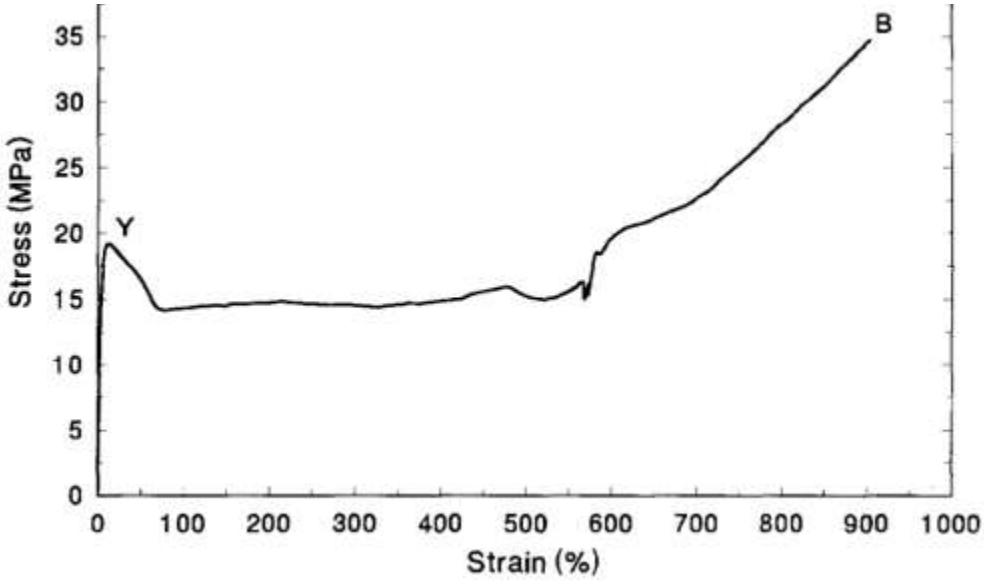

Figure 2-5: HDPE stress-strain behavior

Geomembranes with a stress strain curve exhibiting a yield peak (such as HDPE) are significantly influenced by scratches on the surface of the geomembrane. It has been shown by Giroud (1984) that geomembranes may break at an average (or nominal) tensile strain below yield, if they are scratched. The following rationale has been presented (Giroud, 1994) which explains seemingly premature tearing and breaking due to scratches in geomembranes.

Consider a geomembrane with peak yield behavior which is scratched and subjected to a tensile load. The reduction in thickness at the scratch results in an increased stress and associated strain at the location of the reduced thickness (Figure 2-6 from Giroud 1994). The unmarred area has a lower strain, represented by the nominal tensile strain across the geomembrane. Depending upon the scratch depth and original geomembrane

thickness, the yield strain may be exceeded at the scratch resulting in excessive deformation or tearing.

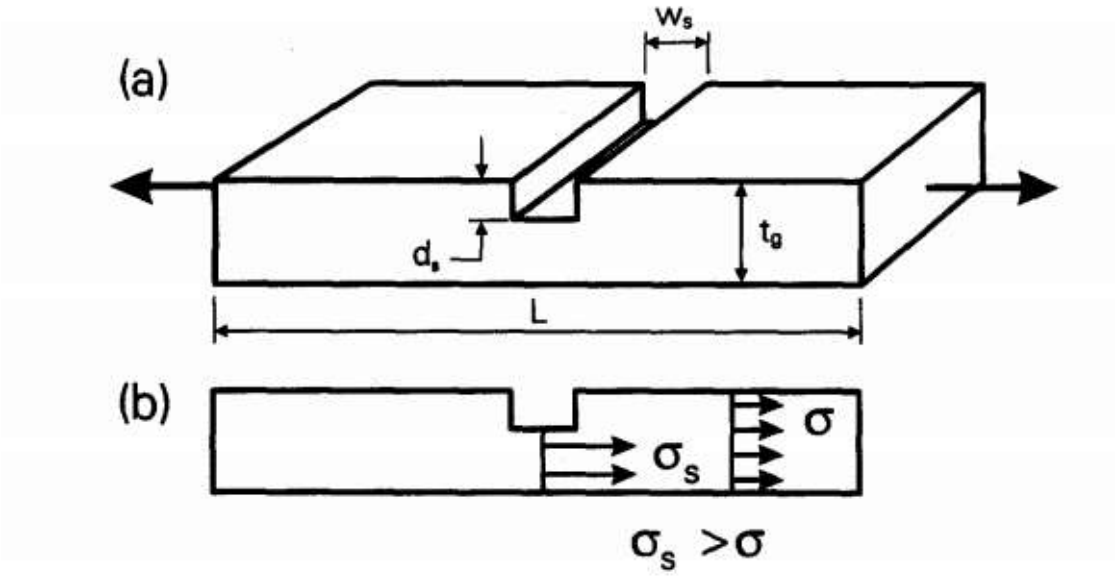

Figure 2-6: Reduction of geomembrane thickness and subsequent stress amplification

2.4 Giroud Strain Concentration Factors for Geomembranes Away from Seams

Field observations show that geomembranes fail at tensile strains well below the yield strain of the material. Giroud et al. (1995) attributes this to strain concentrations due to defects and imperfections (such as scratches), bending, and geometric changes near the seam. Giroud et al. (1995) identified bending at seams oriented parallel to the tensile load as a major source of strain concentrations. The seam must rotate when loaded in tension to allow the geomembrane on either side of the seam to be in the same plane. The maximum bending strain occurs immediately adjacent to the seam as shown in Figure 2-7 from Giroud (2005).

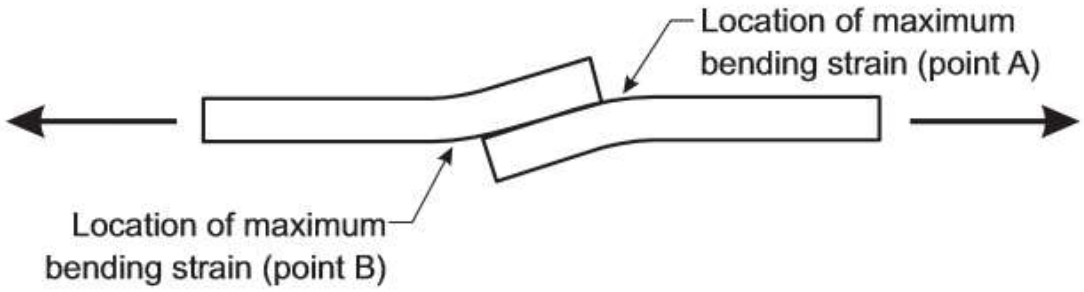

Figure 2-7: Bending strain at seams in geomembranes under tensile loads (Giroud, 2005)

Giroud et al. (1995) developed theoretical relationships for the incremental strain due to bending adjacent to a seam loaded in tension for extrusion and fusion welds. Figure 2-8 presents plots developed by Giroud for typical seam widths and geomembrane thicknesses. Strain increments for geomembranes with extrusion lap, extrusion fillet, and fusion welds are provided as a function of seam thickness. Equations are presented to allow calculation of strain increments for other lengths and thickness. As illustrated in Figure 2-8, the incremental strain due to bending in 1 mm (40 mil) geomembranes increases non-linearly at low normal tensile strains (under 0.3%) and progresses with a strongly linear relationship to increasing tensile strain from that point onward. The incremental bending strain in 2 mm (80 mil) thick geomembranes from fusion weld seams is non-linear at tensile strains up to 0.5% and then increases in a linear fashion with increasing tensile strain. The incremental bending strains associated with the extrusion lap and extrusion fillet seams increase at a similar rate after 0.5% tensile strain, but the linear relationship is not as strong.

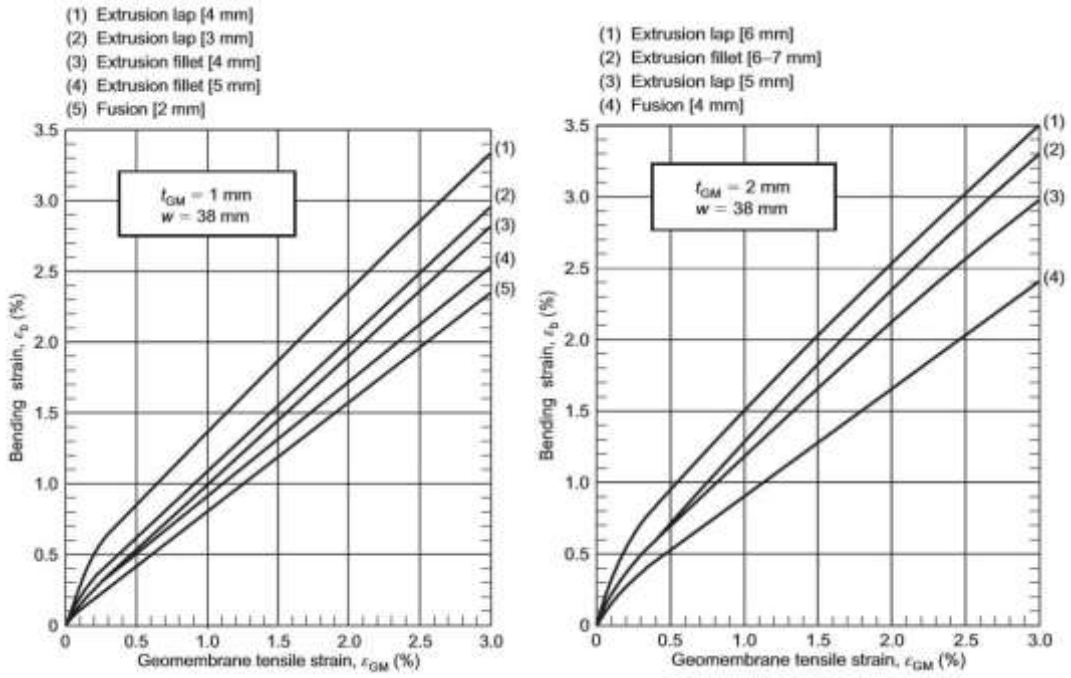

Figure 2-8: Incremental bending strains vs. normal geomembrane tensile strain for extrusion lap, extrusion fillet, and fusion welds for seams in 1 mm (40 mil) and 2 mm (80 mil) geomembranes (Giroud, 2005)

2.5 ASU Study -Numerical model utilizing Giroud Equations to Predict Geomembrane Failure

The Northridge earthquake occurred in January 1994 in the north-central San Fernando Valley of Los Angeles. The Chiquita Canyon landfill was one of the closest landfills to the epicenter of the earthquake and the only landfill to report damage to the geomembrane component of the lining system (Matasovic et al., 1995). There were five waste disposal areas comprising the Chiquita Canyon landfill and two of those areas were found to have tears in the geomembrane. (Matesovic et al., 1995). A damage assessment of the Chiquita Canyon landfill performed by EMCON Associates (1994) following the

Northridge earthquake provided a detailed description of the tears encountered in the geomembrane.

The tears in the side slope liners at the Chiquita Canyon landfill following the Northridge Earthquake were discovered in areas designated as Canyons C and D. Both areas were found to have tears towards the top of the slope. In Canyon C a tear, measuring 4 m long and 0.24 m wide was found close to the anchor trench near the top of the side slope (Augello et al, 1995). Three parallel tears measuring 27 m long and 0.3 m wide were discovered a month after the earthquake in Canyon D. The tears were near the anchor trench towards the top of the side slope (EMCON Associates, 1994). The tear in the geomembrane liner on the side slope of Canyon C was concluded to have started at the extrusion fillet weld used to weld a patch over a quality control cut-out during the liner construction (EMCON Associates, 1994). The crack then proceeded to propagate perpendicular to the direction of tensile loading (EMCON Associates, 1994) as shown in Figure 2-9. The geomembrane liner in Canyon D had three tears at the top of the side slope. The first tear began at the vertical seam and the grind lines (i.e., scratches) next to the seam. The second tear propagated from an area with an extrusion fillet seam over a flat extrusion seam, as sketched in Figure 2-10. The third tear propagated from the vertical seam and was caused by the stress concentrations associated with the grinding lines (EMCON Associates, 1994).

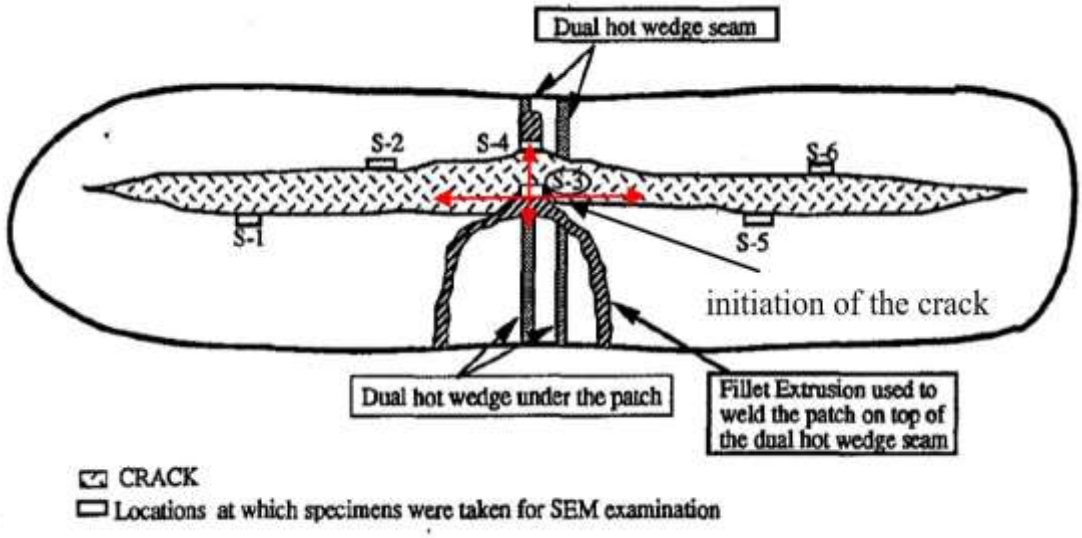

Figure 2-9: Canyon C geomembrane tear (EMCON Associates, 1994)

The tears in both Canyons C and D occurred at the top of the side slopes where the tensile stresses due to slipping of the waste against the geomembrane are greatest (Arab, 2011). The crack in the Canyon C landfill which began at a seam and propagated perpendicular to the tensile strain may have been subjected a bending strain concentration which contributed to the failure.

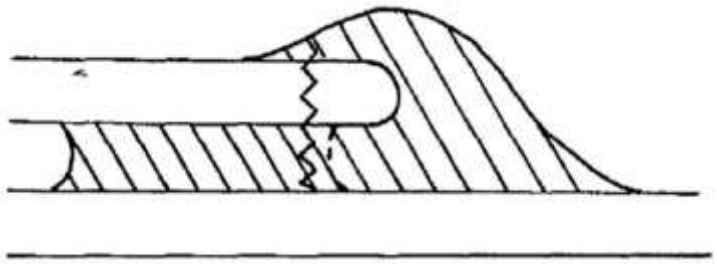

Figure 2-10: Crack in a doubly seamed liner area in Canyon C (EMCON Associates, 1994)

Numerical analysis conducted at Arizona State University of the liner system at the Chiquita Canyon landfill performance during the Northridge earthquake predicted tensile strains in the geomembrane at the crest of the side slopes (Kavazanjian et al., 2013). The study was conducted using a model that explicitly predicts geomembrane

strains. While the model predicted that the location of the tears in the geomembrane corresponded to the locations of maximum tensile strains in the geomembrane, the magnitude of the tensile strain was well below yield. However, once strain concentrations were considered the factor of safety for yield fell below 1.0 (Kavazanjian et, al., 2013).

CHAPTER 3. DIGITAL IMAGE CORRELATION

3.1 DIC Concept and Use for Materials Property Testing

Strain concentrations are highly localized and, in some cases, the maximum strain is transient throughout a tensile loading test. Traditional strain gauges do not provide sufficient resolution to monitor localized strain concentrations at geomembrane seams. However, Digital Image Correlation (DIC) provides a method with sufficient resolution for this purpose. Using DIC, a displacement field is generated over a sample. The displacement field is then differentiated numerically to capture the strain field including the localized strain concentrations. DIC is the collection of displacement data through the capture and subsequent comparison of high resolution photos as a sample deforms. The data is processed to establish the relative deformation between recognizable points on the sample. The strain field is then determined from this deformation field. To make DIC measurements, high resolution cameras are first setup in a manner which allows for proper focus and lighting. Following the acquisition of a reference image, subsequent photos are captured throughout the deformation of the sample. The photos are compared to the reference image and all subsequent images, providing a powerful tool for determining the deformation of the sample and the corresponding strain field. The sample must be prepared in such a way that the area of interest is covered in a relatively dense pattern of distinct speckles. These distinct speckles may be a natural pattern due to the texture of the sample or the product of sample preparation.

For the purposes of this study, the primary variable of interest is the strain perpendicular to seams and scratches. Conventional strain data collection involves the placement of strain gages on the sample at critical points. The resolution of strain gages is

not enough to capture the localized nature of the strain concentrations. The advantages of DIC will become clear in the following analysis. When attempting to find regions of localized strain within the sample it is necessary to obtain a density of data on the sample deformation which is not feasible with conventional strain gages.

3.2 DIC Deformation Algorithm Capture Theory

The image capture software used in the testing described herein was VIC Snap, a product from Correlated Solutions, Inc. (Correlated Solutions, 2016). This software allows for the direct input from two high resolution cameras (Figure 3-1). A single camera may be used for a two dimensional analysis, but the addition of the second camera allows the option to create a three dimensional model which shows the contours of the sample in three dimensions during deformation.

Figure 3-1: VIC Snap software interface using two cameras with overlapping fields of view

The processing and analysis of the images captured for this project was done in the partner program to VIC Snap, VIC 3D, also from Correlated Solutions, Inc. Analysis of

data with VIC3D is dependent on two sets of images: calibration images and test images. A series of calibration images must be taken which merge spatial relationships between the cameras and the sample. The test images document the deformation of the sample over the course of the test. VIC3D allows the extraction of a variety of parameters from the test images including the strain field. Several tools are available in VIC 3D to present and compare data.

DIC algorithms work by using pixel intensity values to calculate the deformation of between points. A subsequent best match is found by comparing the image similarity to the reference subset (Take, 2014). Sample preparation is a key component of accurate deformation measurements and three notable instances may occur where inaccuracy will occur. Figure 3-2 taken from Take, 2014 summarizes the algorithm reaction to a subset with no texture, subsets with an edge or line feature, and a subset with a repeating pattern. Essentially, these features on the sample surface result in an unsuccessful identification of the actual pattern deformation.

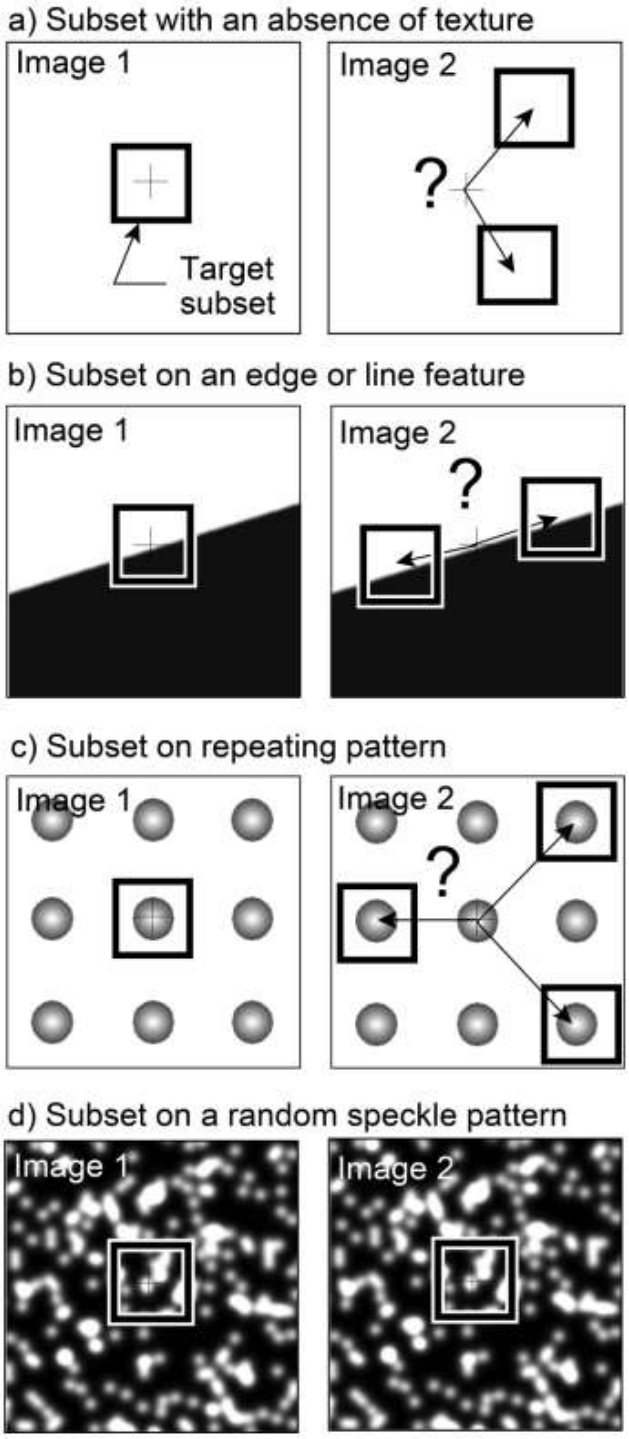

Figure 3-2: DIC algorithm reaction to surface features (Take, 2014)

3.3 Sample Preparation

"The single most important factor influencing the precision and accuracy of DIC is image texture" (Take, 2014 p 1202). Therefore, a variety of texturing schemes were attempted and tested upon remnants and unused geomembrane samples. The most common sample preparation method in materials-based testing is the application of a random speckling with paint (Take, 2014). The smooth HDPE samples were all black and of uniform texture. Figure 3-2 illustrates the inability of the DIC algorithm to obtain a match in this context. Similarly, the textured samples have a repeating pattern of textures as well as a constant color intensity, making the surface unsuitable for DIC.

The following paint color schemes were considered. A white speckling applied directly onto the black HDPE and a solid white coat overlain by a black random speckling. The first scheme was found to be less effective due to reflection of the lighting system off the relatively reflective HDPE material. The resulting deformation field was discontinuous and unacceptable for the purposes of this study. The application of a white base coat overlain by a black speckling worked well when prepared to the following specifications.

In a sample preparation employed herein, a flat paint (e.g., Rustoleum Flat Spray Paint) was used for both the base and speckling coat. Other forms of paint such as gloss and semi-gloss were found to have issues similar to those encountered with the surface of HDPE, e.g., reflection of light and the resulting discontinuous deformation profiles across the sample. The black speckling must be random (as opposed to a uniform grid) with speckles being relatively close in size. The target speckle was to be no larger than 1mm and the target density was 50 percent. The speckling was applied primarily through

manipulation of a spray paint can at an appropriate angle and application rate. Figure 3-3 shows a sample from which an appropriately continuous deformation profile, sufficient for the purposes of this study, was obtained.

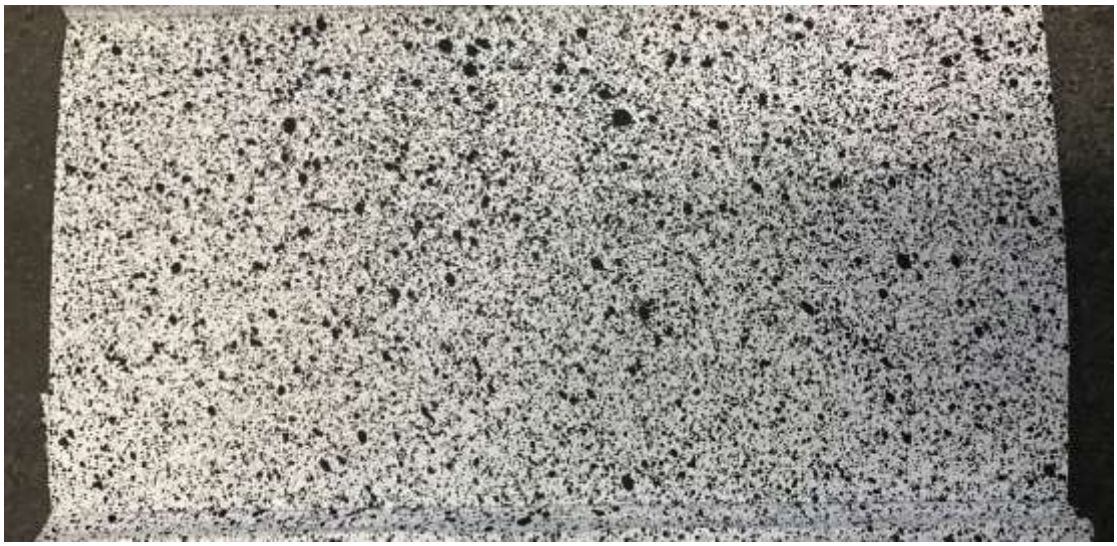

Figure 3-3: Appropriate speckle pattern applied to the surface of an HDPE geomembrane sample

Sufficient bond strength between HDPE and the applied paint, such that the strain of the sample itself was captured as opposed to the layers of paint upon the surface, was an initial concern. Studies on the effect of paint thickness by Perez et al. (2015) show that paint thicknesses over 30 μm result in an underestimation of the true strain using DIC. Coating thicknesses under this limit were found to have no strain underestimation. Perez et al. (2015) found that the application of a background paint layer and speckling layer do not exceed 20 μm. The value of 20 μm is based upon five trials conducted with five separate research groups who employ DIC for materials testing purposes. As such, strain underestimation due to the paint-HDPE interface is not considered a source of significant error in this study. Researchers wishing to recreate this experiment should note that when using commercially available spray paint, there is a window of time

following initial application of the white basecoat in which the tensile test must be performed. Over the course of testing, samples which were tested over one week from initial preparation were found to be at risk for cracking. The paint becomes too brittle to withstand large deformations (greater than 5 percent) which invalidates the test results. Cracking and crumbling of paint during testing was avoided by performing the testing within two to three days of initial spray paint application to the sample.

CHAPTER 4. EXPERIMENTAL EVALUATION OF GEOMEMBRANE SEAM STRAIN CONCENTRATIONS IN FACTORY-MADE SEAMS

ABSTRACT: Laboratory testing was conducted to evaluate strain concentrations adjacent to high density polyethylene (HDPE) geomembrane seams loaded in tension perpendicular to the seam. Strains concentrations were evaluated using digital image correlation (DIC) on samples meeting the ASTM criteria for wide-width tensile testing. The tensile strain in the zone of strain concentration adjacent to the seam from the DIC analysis was compared to the strain predicted using theoretical seam strain concentration factors. While the average strain in the zone of strain concentration was relatively close to the theoretical value, the maximum tensile strain in this zone was significantly greater than the value predicted using the theoretical strain concentration factors. For average (global) tensile strains on the order of 3%, maximum strains measured by DIC in the zone of strain concentration were on the order of 9% to 11%, compared to values on the order of 5% to 6% predicted using the theoretical strain concentration factors. These findings suggest that the allowable tensile strain for HDPE geomembranes that will be loaded in tension perpendicular to the seam should likely be less than 4% and that construction quality assurance (CQA) samples for destructive testing should not be recovered from areas where the geomembrane may be loaded in tension.

4.1. Introduction

Strain concentrations are recognized as an important issue in establishing the allowable tensile strains for geomembrane liners. Theoretical analysis by Giroud et al. (1995) established that loading in tension perpendicular to the seam was one source of strain concentrations in geomembrane liners. The yield strain of a typical high density

polyethylene (HDPE) geomembrane subject to uniaxial tension is on the order of 11% to 14%. However, the allowable tensile strain for HDPE geomembranes is typically on the order of 4% in practice in the United States while European practice calls for an allowable global tensile strain on the order of 3% (Peggs et al. 2005), at least in part due to strain concentrations.

Tears were observed in the Chiquita Canyon landfill HDPE geomembrane at two locations following the 1994 Northridge earthquake. Numerical analyses by Kavazanjian et al. (2013) yielded maximum tensile strains due to the earthquake loading of less than 3% at the locations of these tears. Kavazanjian et al. (2013) invoked seam strain concentration factors presented in Giroud et al. (1995) and Giroud (2005) to help explain why the geomembranes tore at these locations. Forensic analysis indicated that the tears emanated from seams for extrusion welded patches recovered for construction quality assurance (CQA) testing (EMCON 1994) that were loaded in tension perpendicular to the seam, supporting the Kavazanjian et al. (2013) interpretation.

Giroud et al. (1995) showed that the bending required for two geomembranes of constant thickness joined at a seam to remain co-planar away from the seam when loaded in tension induced additional (incremental) tensile strains adjacent to the seam. Figure 4-1 illustrates the Giroud et al. (1995) concept of seam strain concentrations due to bending, wherein the incremental tensile strains are induced at points A and B adjacent to and on the opposite edges of the seam.

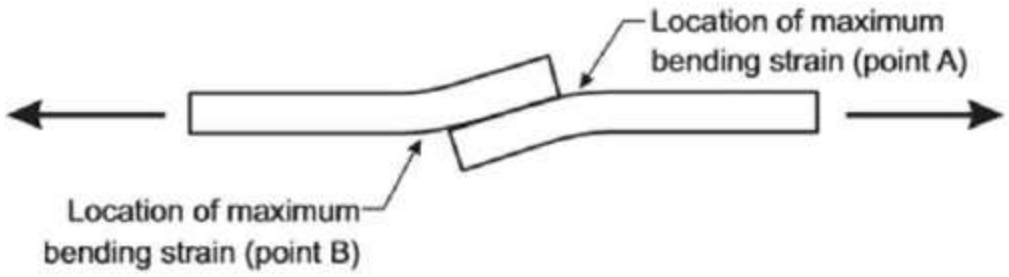

Figure 4-1: Location of incremental bending strains induced adjacent to a seam in a geomembrane loaded in tension (Giroud 2005).

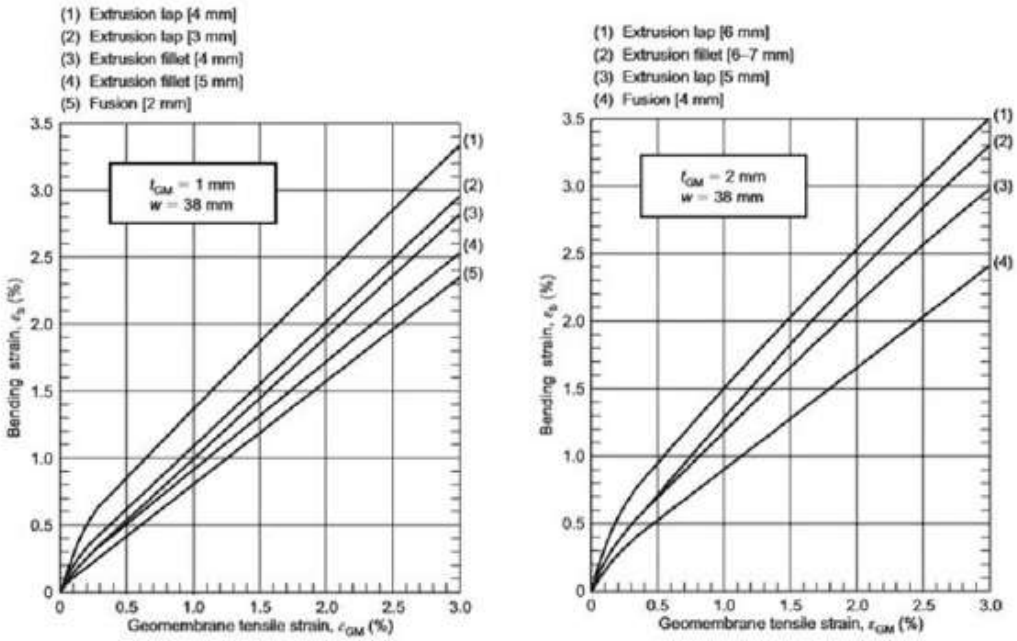

Figure 4-2: Incremental bending strains vs. normal geomembrane tensile strain for different seam types for 0.001m (40mil) and 0.002 m (80 mil) geomembranes (Giroud, 2005)

Figure 4-2 graphically illustrates the strain concentration factors developed analytically by Giroud et al. (1995) for two different HDPE geomembrane thicknesses for a seam width of 30 mm for both extrusion welded and fusion welded seams, the two types of welds evaluated experimentally in this paper. As illustrated in this figure, the

incremental strain adjacent to the seam depends not only upon the seam thickness and seam width, but also on the type of seam and the thickness of the seam itself. Figure 4-3 illustrates the types of seams typically employed in practice for polyethylene geomembranes considered by Giroud et al. (1995), including extrusion fillet weld seams, wherein a bead of resin is applied where the edge of one geomembrane panel overlaps another, and fusion weld seams, wherein two overlapping geomembrane panels are fused together under pressure and temperature. Included in Figure 4-3 is a double track fusion seam, the most common type of seam used to join HDPE geomembrane panels in landfill practice, wherein adjacent geomembrane panels are fused together along two separate tracks, leaving an open channel in between the tracks to facilitate non-destructive testing of seam integrity by air pressure testing.

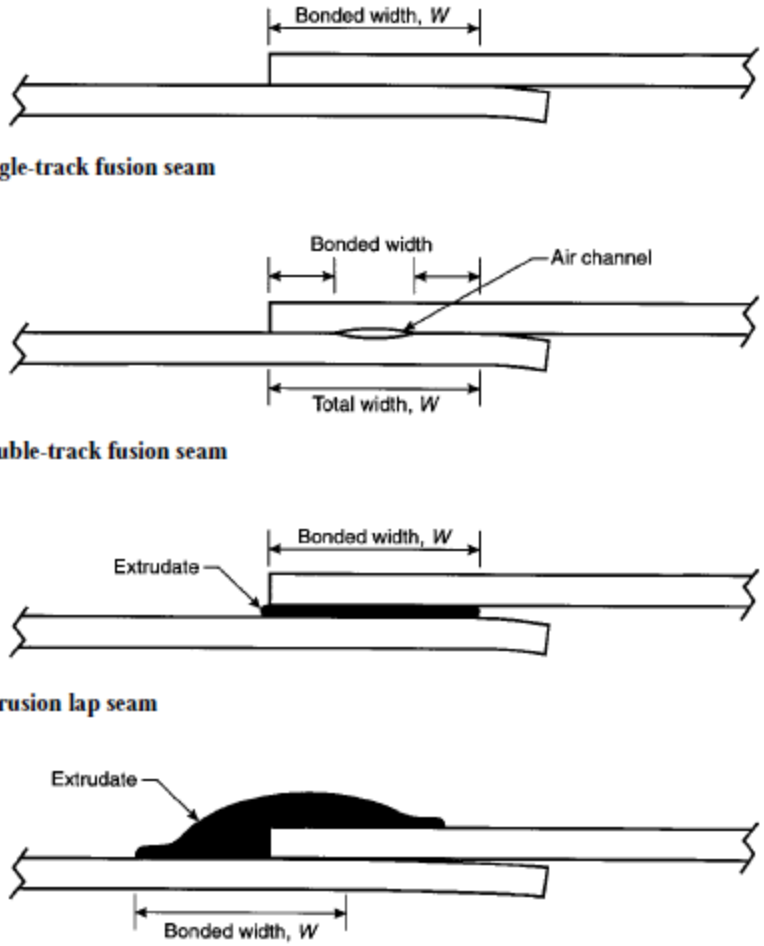

Figure 4-3: Typical seams used with polyethylene geomembranes (Giroud et al., 1995)

Figure 4-2 indicates that in HDPE geomembranes seam strain concentrations can double the average tensile strain near the seam for typical seams used in practice. Giroud et al. (1995) and Giroud (2005) presents equations that can be used to calculate the seam strain concentration factors for any set of values of geomembrane thickness, geomembrane modulus, seam width, and seam thickness. While these seam strain concentration factors are theoretically sound, no physical measurements have ever been obtained to evaluate their accuracy. Therefore, a testing program was developed to experimentally evaluate

strain concentrations at HDPE geomembrane seams loaded in tension perpendicular to the seam.

4.2. HDPE Geomembrane Samples

HDPE geomembrane samples 1 mm (40 mil) and 2 mm (80 mil) in thickness with extrusion and fusion seams were prepared by a leading United States geomembrane manufacturer for the seam strain concentration testing program. The samples were prepared using the commercially available HDPE geomembrane produced by the manufacturer. Each sample was 135 mm-long x 150 mm-wide. Two 135 mm-long x 40 mm-wide HDPE bars were welded on each end of the sample so the sample could be clamped between the jaws of a loading frame. The middle section of the sample (i.e., the section between the bars) was therefore 75 mm-tall by.150 mm-wide, satisfying ASTM D4885-01 requirements for wide-width tensile testing (ASTM 2011). Figure 4-4 illustrates the configuration of the samples with the bars in place.

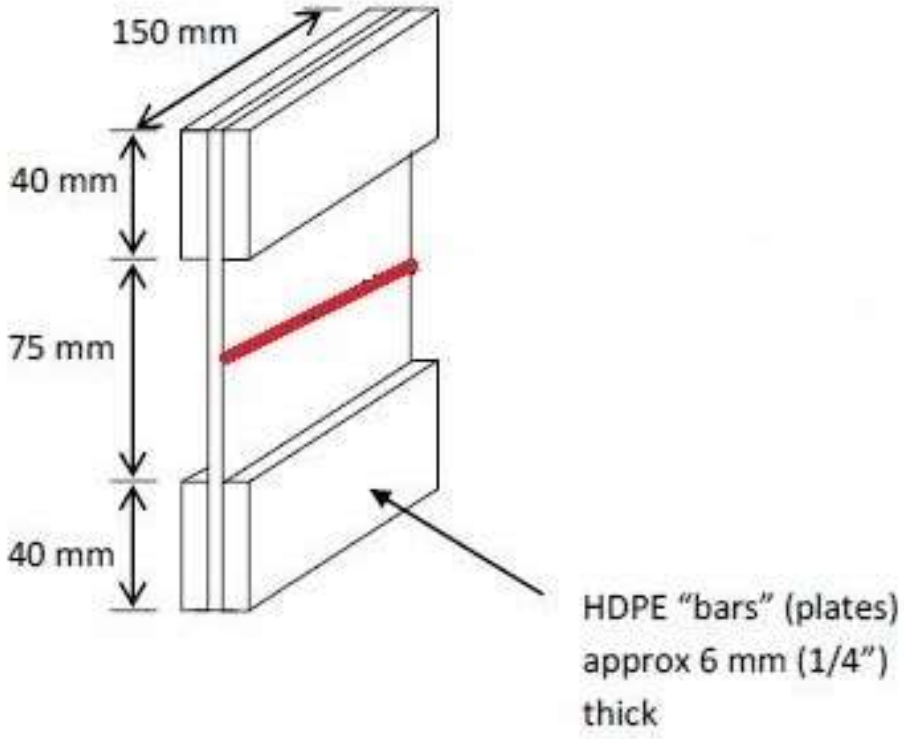

Figure 4-4: HDPE geomembrane sample prepared for tensile testing

Six (6) seamed HDPE geomembrane samples were tested in uniaxial tension to experimentally evaluate seam strain concentrations. The strain field in these samples, including strain concentrations adjacent to the seams, was measured using digital image correlation (DIC). Additional testing was conducted on unseamed samples to quantify the precision and accuracy of the measurements. Three (3) of the seamed geomembrane samples were 1 mm-thick while the other 3 samples were 2 mm-thick. Each 3-sample group consisted of one sample with a horizontal extrusion weld across the middle of the sample, and two samples with a double track fusion weld across the middle of the sample. The width and thickness of the seams on the 6 seamed samples, essential parameters in the Giroud et al. (1995) equations for geomembrane seam strain concentrations, are presented in Table 4-1 along with geomembrane thickness and sample designation.

Table 4-1: Summary of seamed geomembrane tensile test results

Sample	*seam type*	*W (m x 10^{-3})*	*t_{gm} (m x 10^{-3})*	*t_s (m x 10^{-3})*	*ε_{AVG} (%)*	*ε_{Giroud} (%)*	*ε_{DIC} (%)*	
							Max	*Average*
40S1C	extrusion fillet	40.72	1	4.24	0.10	0.21	0.53	0.03
					0.90	1.72	4.79	1.38
					2.78	5.44	9.50	7.44
40S2B	dual hot wedge (fusion)	48.92	1	2.15	0.49	0.86	1.30	0.39
					1.83	3.15	5.60	2.57
					3.50	6.03	11.40	5.48
40S2C	dual hot wedge (fusion)	48.86	1	2.14	0.38	0.67	2.76	1.75
					1.85	3.19	6.51	4.53
					3.61	6.23	10.87	8.88
80S1C	extrusion fillet	41.84	2	6.43	0.36	0.79	2.80	0.59
					1.45	2.91	5.00	1.10
					2.89	5.72	11.60	5.59
80S2A	dual hot wedge (fusion)	52.75	2	4.26	0.34	0.66	1.00	0.86
					1.36	2.40	3.70	2.80
					2.70	4.69	6.30	5.10
80S2B	dual hot wedge (fusion)	52.49	2	4.12	0.36	0.70	1.21	0.76
					1.30	2.33	3.69	3.06
					2.83	4.99	9.22	6.52

4.3 Testing Apparatus

A standard loading frame for triaxial testing of soil was modified to conduct wide-width geomembrane tensile tests in accordance with ASTM D4885 using the geomembrane samples with the bars attached. The bars on each end of the sample were slid into grips at each end of the loading frame and a tensile load was applied to the sample. The clamp system was designed to minimize the potential for strain concentrations along the grip points. Figure 4-5 shows the testing apparatus and clamping system used in the testing program.

Figure 4-5: Geomembrane clamping and loading system with sample inserted, ready to be tested

4.4. Test Program

4.4.1 DIC Image Correlation (DIC) Equipment Setup

The DIC equipment includes a tripod on which two LED lights are mounted, two high resolution cameras, and a computer that runs the software for image capture. The image capturing software used on this project was VIC Snap (Correlated Solutions, 2016). The equipment is setup so the cameras are imaging the sample from different angles but have the same size image and field of view in the viewfinder. The lights have to be adjusted to provide approximately the same amount of exposure for each camera. Furthermore, ideally, the lighting should be uniform across

the surface that is being analyzed. Differences in light coverage across the sample surface should be minimized and mirrored in the images captured by the two cameras. Any necessary exposure adjustments should be done by adjusting the lighting, with slight adjustments on the cameras themselves being the last resort. Once proper exposure is achieved, the camera focus is adjusted to obtain clear, crisp images from both cameras. Figure 4-6 shows the DIC equipment setup. After proper exposure and focus is obtained on both camera images, the DIC equipment must be calibrated.

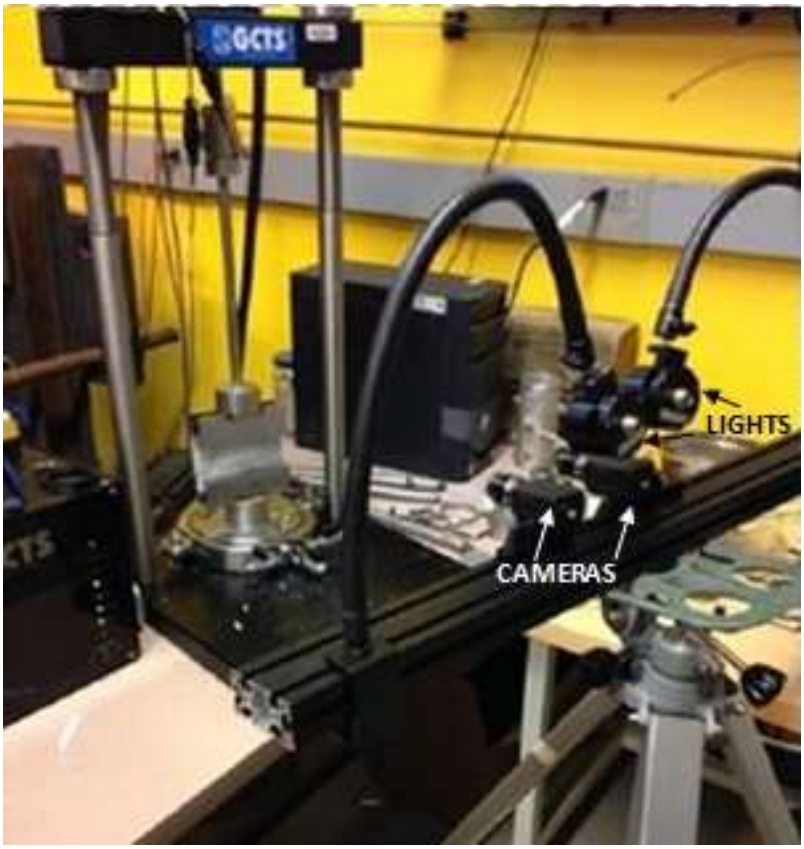

Figure 4-6: Test setup for DIC analysis of geomembrane samples loaded in tension

4.4.2 DIC Calibration

Calibration of the DIC setup consisted of removing the HDPE sample from the triaxial clamps and inserting a 105 mm-wide x 75 mm-high calibration plate with black dots 1.5 mm in diameter spaced 7.5 mm center to center in a square grid pattern. Figure 4-

7 presents an image of the calibration plate. The calibration plate is rotated along its three axes by hand. While the calibration plate is being rotated, a series of photos are taken with the cameras. These photos are then imported into the VIC3D and used to calibrate the test setup. The calibration process compares the differences between each image that is imported into VIC3D. A score that reflects the differences in the calculated calibration plate geometry for each image is given at the end of the calibration. This score indicates if the test setup is adequate. If the cumulative error is below 1%, the calibration is satisfactory and testing may be conducted. If not, calibration images are retaken and another calibration analysis is conducted as sometimes the calibration is not satisfactory due to human error. If the calibration still yields unsatisfactory results the equipment setup must be re-aligned.

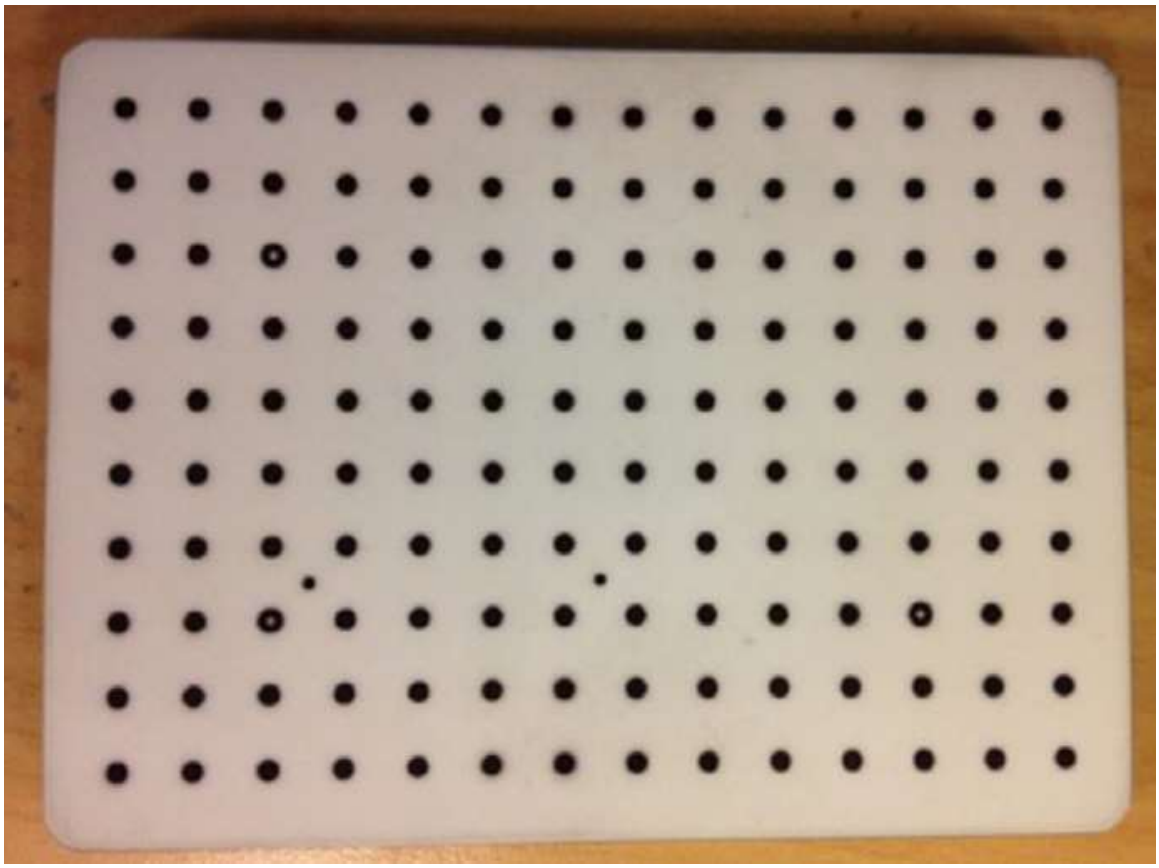

Figure 4-7: Calibration plate for DIC testing

4.4.3 **Tensile Test Apparatus Setup**

Once calibration of the DIC setup was complete, the geomembrane sample was slid into place between the jaws of the uniaxial tensile testing apparatus. Once the sample was in place, a small tensile load was applied to firmly seat the sample on the clamps. The seating load was the tensile load required to remove all slack from the sample, evaluated visually. Once the sample was seated, the sample was deformed in tension at a strain rate of 10% per minute in accordance with the ASTM 4885 standard for wide-width tensile testing of geomembranes.

4.4.4 **HDPE Geomembrane Sample Preparation**

Because the strain concentrations associated with a geomembrane seam are extremely localized, they cannot be measured using strain gages or other conventional strain measurement techniques. Therefore, DIC was employed to measure the strain field around the seam (and over the entire geomembrane sample). For a DIC test to be effective, the surface of the sample must be prepared in a manner such that distortions of the sample can be optically detected. A sample of uniform color or texture, e.g. an entirely black sample, would not be amenable to DIC measurements. High gloss surfaces can also make DIC measurement ineffective due to reflections from the high intensity lighting used to illuminate the sample. Therefore, preparation of the samples for DIC measurements consisted of first applying a uniform coat of white non-gloss paint on the surface of the sample. Once the white non-gloss paint was dry, a random pattern of black speckles was applied over the white background and allowed to dry.

The details of the speckle pattern are of great importance in acquiring proper results from the DIC measurements. If a speckle is too large, a data gap is created in the analysis.

However, if a speckle is too small the image analysis program may not recognize it. Changes in speckle density can also create gaps in the data. Figure 4-8 shows an un-seamed HDPE sample properly prepared for DIC strain field measurements.

Figure 4-8: HDPE sample prepared with speckle pattern for DIC analysis

4.5. Accuracy and Precision of DIC Measurements

Tests were conducted on unseamed samples to evaluate the accuracy and precision of the DIC measurements. Accuracy was evaluated by comparing the average global strain evaluated by the DIC measurements using VIC 3D to the nominal global strain evaluated based upon the length of the sample between the grips and measurements of the displacement of the grips securing the sample made using a linear varying displacement transducer (LVDT). Precision was evaluated by loading the sample to a strain below yield five times and comparing the DIC strain measurements from each trial at nominal strains

(strains based upon LVDT measurements) of 0.17, 0.35, 1, and 3 percent. The accuracy and precision measurements were made on 2 different samples.

VIC 3D calculates the strain field based upon differentiation of the displacement field of the sample determined by comparison of two images taken at different times. Therefore, a reference image for the unstrained state of the sample is required upon which the DIC analysis is based. In this testing program, the reference image was taken after the seating load was applied to the geomembrane samples. Using the reference image as the baseline, VIC 3D computes a deformation and strain field over the area of interest based upon the relative movement of the speckles.

Results of the accuracy and precision tests are presented in Table 4-2. The mean strain from 5 trials based upon the DIC measurements was typically within 10 percent of the strain based LVDT measurements. Except at the smaller nominal strains (0.17 and 0.35 %), the strain from the DIC measurements was greater than the nominal strain from the LVDT measurements. The standard deviation from 5 measurements on the same sample was increased as the strain increased, but the variance (the standard deviation divided by the mean) decreased as the strain increased. While the variance at the smaller nominal strains (0.17 and 0.35 %) for Sample 1 was relatively high (up to 45%), at the largest nominal strain (3 %) was only 6% for Sample 1 and 3% for Sample 2.

Table 4-2: Comparison of nominal percent strain based upon LVDT measurements to mean and standard deviation percent strain from DIC measurements on an unseamed sample loaded below yield five times

LVDT	Sample 1			Sample 2		
	Mean	Std. Dev.	Variance	Mean	Std. Dev.	Variance
0.17	0.153	0.067	44%	0.171	0.016	9%
0.33	0.326	0.101	31%	0.359	0.012	11%
1.00	1.073	0.129	12%	1.110	0.029	3%
3.00	3.330	0.200	6%	3.389	0.086	3%

4.6. Seamed Sample Testing

4.6.1 **Testing Program**

Each sample was assigned a unique identifier that consisted of three components: sample thickness, seam type, and a letter at the end to differentiate between samples of the same thickness (in mil) and seam type. Extrusion fillet seams were designated S1 while dual hot wedge (fusion) seams were designated S2. Therefore, for instance, 80S2B designated the 2 mm (80 mil) -thick dual hot wedge seam sample labeled B. Table 4-1 presents the sample designation (indicating the type of seam), seam width, seam thickness, and geomembrane thickness for each seamed sample.

The tensile tests on the seamed samples were typically conducted up to a maximum seam strain of about 14-16%, at which point it was assumed that the geomembrane had yielded locally. The strain field across each sample was computed using VIC3D. The average tensile strain over the entire sample between the grips and the maximum strain and the average strain near the seam were calculated at three times during each test. These strains were typically calculated once at an average strain less than 1%, once at an average

strain at around 1%, and once at an average strain between 2% and 4%. Table 4-1 presents the average and maximum strains adjacent to the seams along the line of seam strain concentration at these three times and the strain concentration values predicted using the Giroud et al. (1995) strain concentration factors.

4.6.2 **VIC 3D Analysis**

Figure 4-9 shows the results of the VIC 3D analysis for a non-seamed sample. While the average strain over the sample was approximately 6% in this image, the sample exhibits strains between 4% to 8%, with the largest strain at the center of the sample. This behavior was typical for non-seamed samples at average strains larger than 3% and is believed due to the boundary conditions associated with the tensile test, including the limited width of the samples and the way the grips held the samples at the bottom and top of each sample. At strains of less than 3%, the strain field was relatively uniform over the area between the grips of the testing apparatus, although some minor strain concentrations were often observed near the clamps, likely due to non-uniformity of the bars welded to the ends of the sample for gripping purposes. Based upon the non-uniformity in the sample strain at large strains observed in the non-seamed sample, seam strain concentrations were not evaluated at average sample strains much greater than 3%.

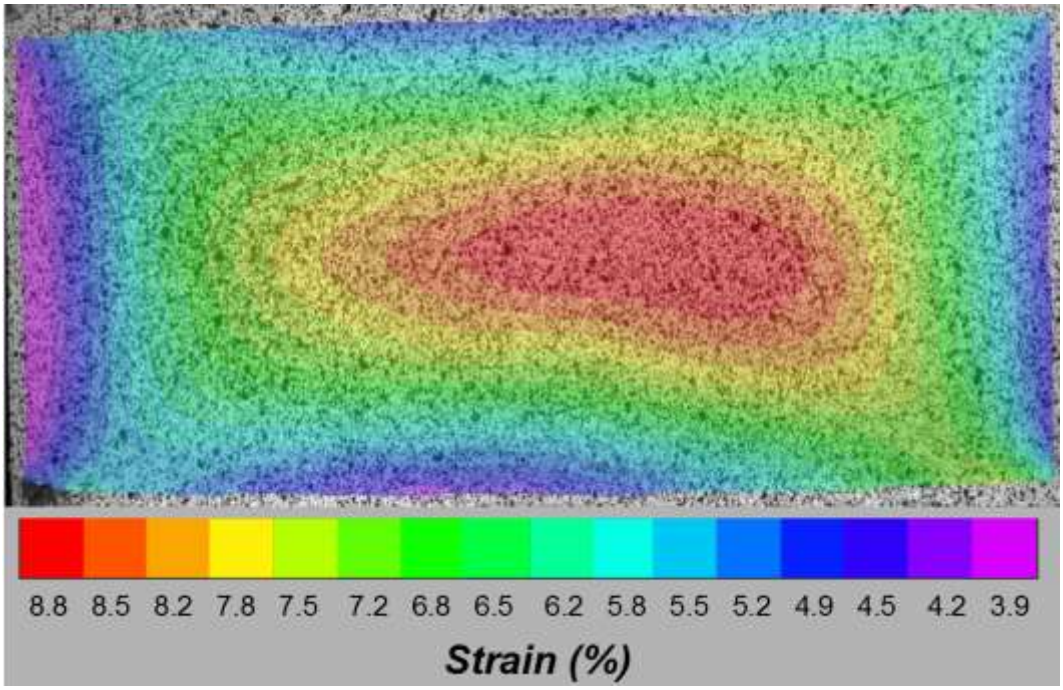

Figure 4-9: Strain field from DIC for 2 mm non-seamed sample at 6.1% average strain (sample dimensions 150 mm – wide by 75 mm tall)

Figure 4-10 shows the computed strain field for 2 mm (80-mil) extrusion fillet seam sample at an average strain over the mid-section of the sample of 0.36%. The strain concentration adjacent to the seam is clearly visible as the yellow and red band that spreads longitudinally across the sample, with an average strain of 0.59% and a maximum strain of 2.8% along this line. Application of the Giroud et al. (1995) strain concentration factors at this stage of the test resulted in a strain adjacent to the seam of 0.89%, relatively close to the average strain measured experimentally but significantly less than the maximum measured value.

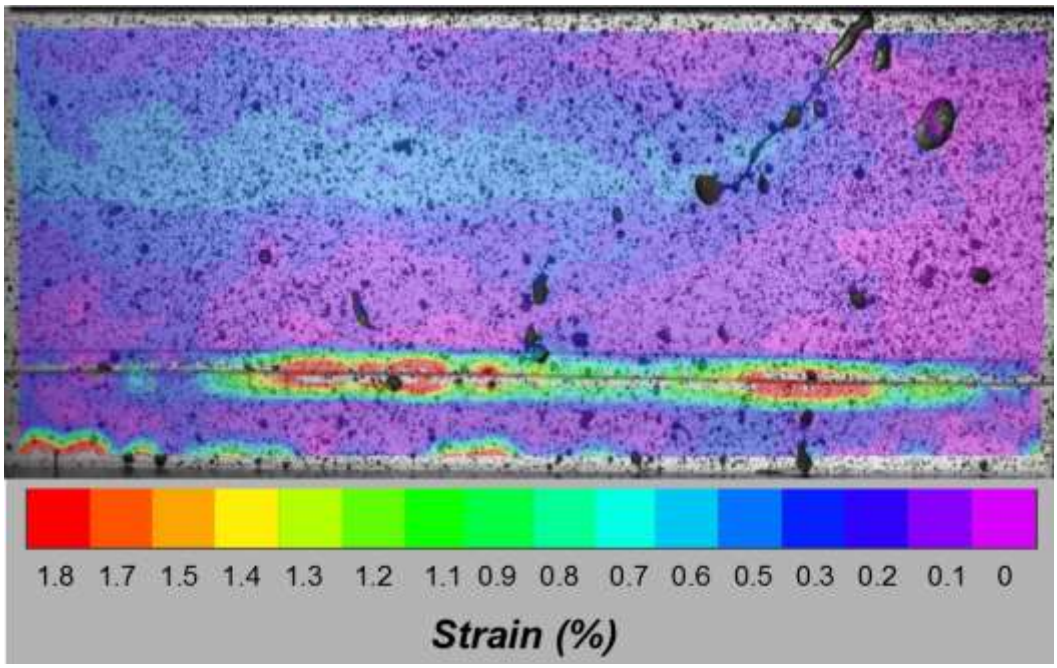

Figure 4-10: Strain field from DIC for 2-mm extrusion fillet sample at 0.36% average strain (Sample 80S1C dimensions: 150 mm wide by 75 mm tall with seam thickness of 6.4 mm)

Figure 4-11 shows an example strain field for a 2 mm (80-mil) dual hot wedge fusion seam sample with an average strain of 2.7%. Again, it can be seen that there is a clear strain concentration adjacent to the seam. In this case, the measured average strain adjacent to the seam was 5.1% and the maximum strain adjacent to the seam was 6.3%. Application of the Giroud et al. (1995) strain concentration factors at this stage of the test resulted in a strain adjacent to the seam of 4.91%, once again approximately equal to the average strain measured experimentally but less than the maximum measured value.

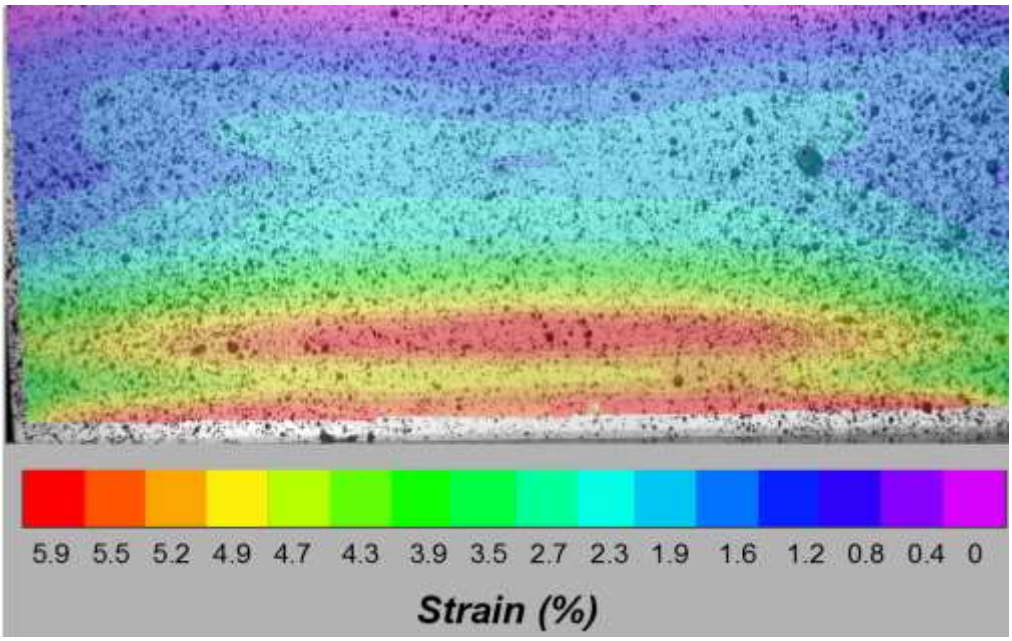

Figure 4-11: Strain field from DIC for 2-mm dual hot wedge seam sample at 2.7% average strain (Sample 80S2A dimensions 150 mm wide by 75 mm tall with seam thickness 4.26 mm)

4.7. Summary of Test Results

Table 4-1 summarizes the results of the tests conducted on seamed HDPE samples tested to evaluate strain concentrations. Table 4-1 includes the values for ε_{AVG}. the nominal average strain of the HDPE sample based upon DIC measurements, $(\varepsilon_{DIC})_{AVG}$, the average value of the strain in the geomembrane adjacent to the seam as measured by DIC, $(\varepsilon_{DIC})_{MAX}$, the maximum strain adjacent to the seam measured using DIC, and ε_{Giroud}, the theoretical maximum strain adjacent to the seam found using the equations from Giroud et al. (1995) for the three strain levels at which DIC analysis was conducted.

Figures 5-12 to 5-17 are graphical representations of the results in Table 1, comparing four strain values: the nominal (global) average sample strain (ε_{AVG}), the strain adjacent to the geomembrane seam based upon the Giroud et al. (1995) strain concentration factors (ε_{Giroud}), the average strain in the geomembrane adjacent to the seam from DIC ($(\varepsilon_{DIC})_{AVG}$), and the maximum strain in the geomembrane adjacent to the seam from DIC

($(\varepsilon_{DIC})_{MAX}$), for each set of seamed samples (1 mm and 2 mm geomembrane thicknesses, extrusion and fusion welds). These figures and the corresponding data in Table 1 show that the discrepancy between the strain predicted using the Giroud et al. (1995) strain concentration factors and the measured maximum values increases as the nominal (global) average strain increased, sometimes with the maximum strain reaching twice the value predicted by the Giroud et al. (1995) equations and up to four times the magnitude of the nominal average (global) strain over the entire sample at nominal average strains on the order of 3%.

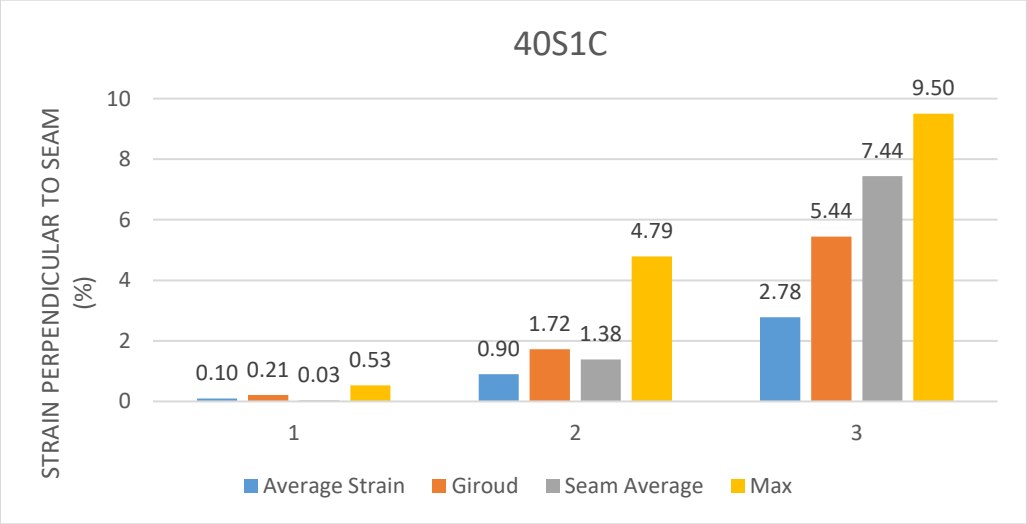

Figure 4-12: Histogram for 1-mm (40-mil) extrusion fillet seam strains (Sample 40S1C)

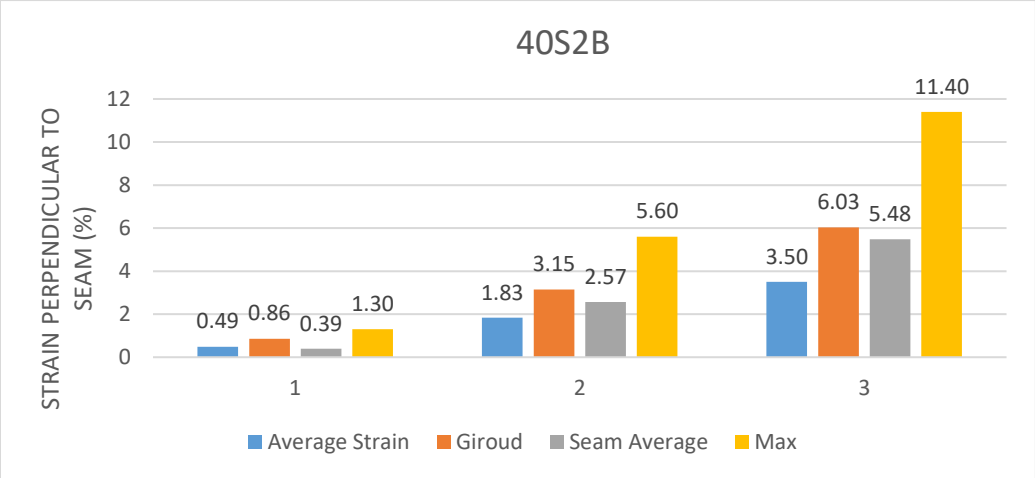

Figure 4-13: Histogram for 1-mm (40-mil) dual hot wedge seam strains (Sample 40S2B)

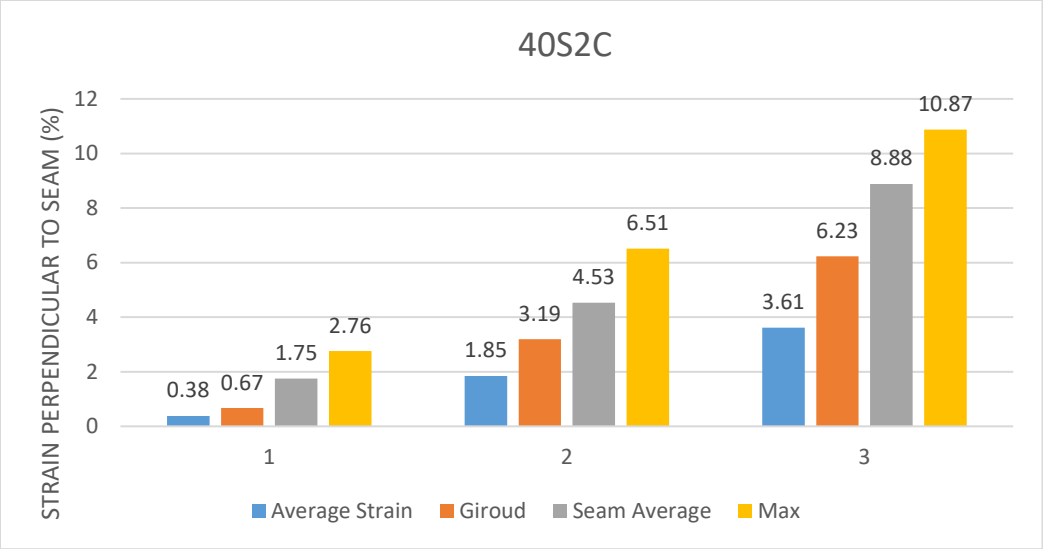

Figure 4-14: Histogram for 1 mm (40-mil) extrusion fillet seam strains (Sample 40S2C)

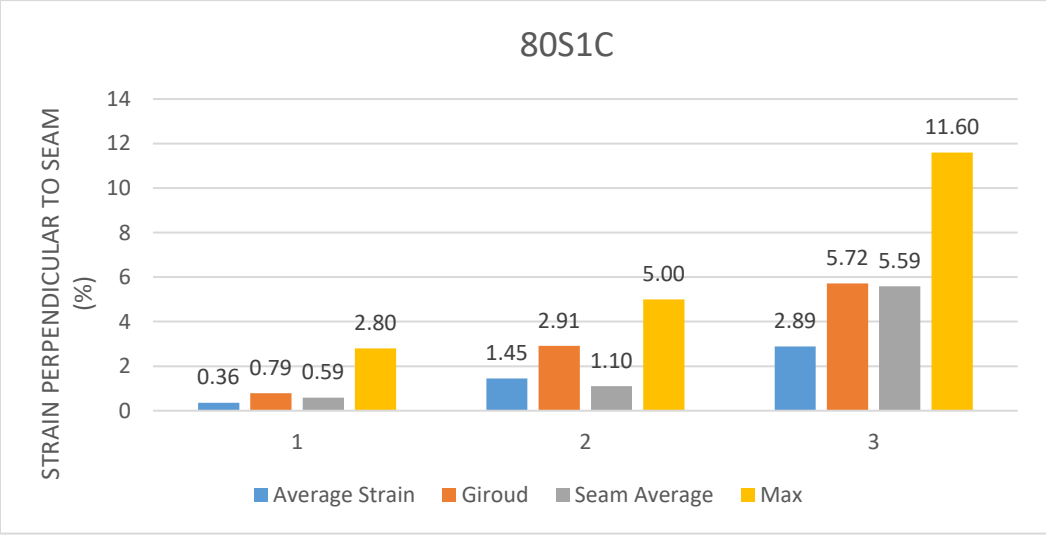

Figure 4-15: Histogram for 2 mm (80-mil) extrusion fillet seam strains (Sample 80S2A)

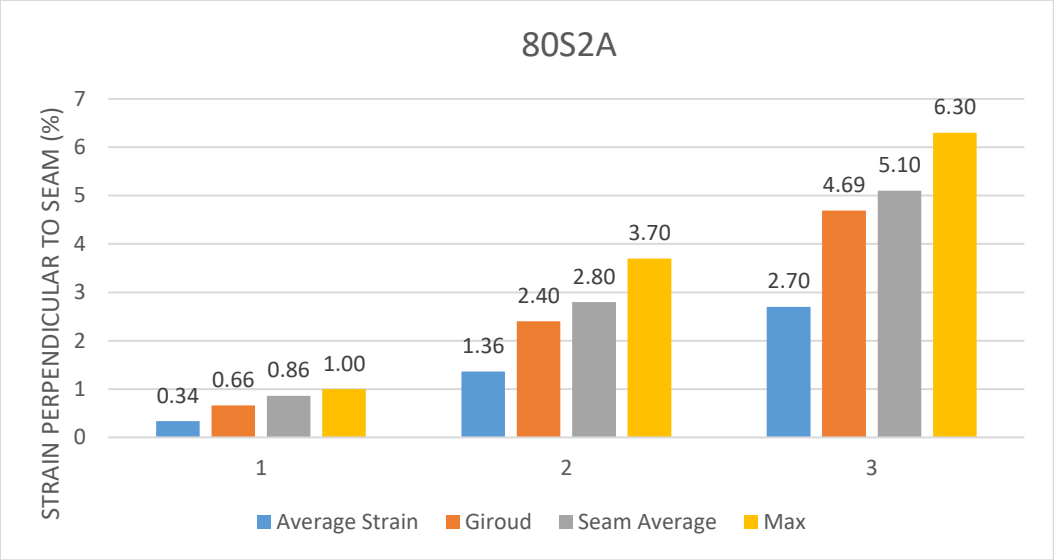

Figure 4-16: Histogram for 2 mm (80-mil) extrusion fillet seam strains (Sample 80S2A)

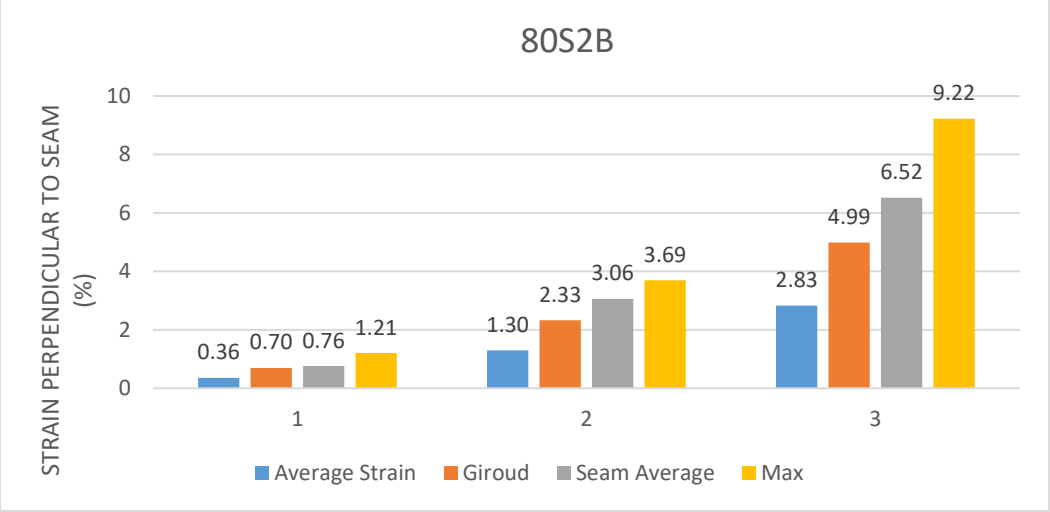

Figure 4-17: Histogram for 2 mm (80-mil) dual hot wedge seam strains (Sample 80S2B)

The results presented herein clearly demonstrate the importance of considering strain concentrations adjacent to the seams in a geomembrane that are perpendicular to an applied tensile load. While the Giroud et al. (1995) strain concentration factors do a reasonable job in predicting the average values of these strain concentrations, the maximum strain concentrations in the geomembrane seams is significantly higher than that predicted by Giroud (2005). Table 4-3 compares quantitatively the strains adjacent to the seam

calculated using the Giroud et al. (1995) equations with the average and maximum strains adjacent to the seam acquired through the DIC procedure for an average tensile strain over the sample on the order of 3%. The ratio of the average strain adjacent to the seam measured using DIC to the theoretical strain adjacent to the seam calculated based upon Giroud et al. (1995) (i.e., the strain due to seam strain concentration) for nominal average sample strains on the order of 3% ranged from 0.9 to 1.4, depending on thickness and seam type. The ratio of maximum strain adjacent to the seam measured using DIC to the theoretical strain adjacent to the seam calculated based upon the Giroud et al. (1995) equations for average sample strains on the order of 3% ranged from 1.4 to 2.0, depending on thickness and seam type. The ratio of the maximum strain adjacent to the seam measured using DIC to the nominal average sample strain for nominal average sample strains on the order of 3% ranged from 2.3 to 4.0, depending on thickness and seam type.

Table 4-3: Comparison of the seam strain

Sample	ε_{AVG}	ε_{Giroud}	$(\varepsilon_{DIC})_{AVG}$	$(\varepsilon_{DIC})_{MAX}$	$\frac{(\varepsilon_{DIC})_{AVG}}{\varepsilon_{Giroud}}$	$\frac{(\varepsilon_{DIC})_{MAX}}{\varepsilon_{Giroud}}$	$\frac{(\varepsilon_{DIC})_{MAX}}{\varepsilon_{AVG}}$
40S1C	78%	5.44%	7.44%	9.50%	1.4	1.8	3.4
40S2B	50%	6.03%	5.48%	11.40%	0.9	1.9	3.3
40S2C	61%	6.23%	8.88%	10.87%	1.4	1.7	3.0
80S1C	89%	5.72%	5.59%	11.60%	1.0	2.0	4.0
80S2A	70%	4.59%	5.10%	6.30%	1.1	1.4	2.3
80S2B	83%	4.99%	6.52%	9.22%	1.3	1.9	3.3

4.8. Conclusions

Strain concentrations at HDPE geomembrane seams loaded in uniaxial tension perpendicular to the seam were measured experimentally. A modified soil triaxial test apparatus was employed to apply a tensile load to wide-width HDPE geomembrane

samples with extrusion or fusion seams in them. The strain field over the entire sample, including strain concentration adjacent to the seam, from images captured as the sample was being strained was evaluated using DIC. The strain field computed using DIC provided the location and magnitude of strain concentration adjacent to the seam in the HDPE sample. The experimental results were compared to the theoretical values for seam strain concentration calculated using equations developed by Giroud et al. (1995).

The results of the analysis clearly show the existence of strain concentrations at the locations adjacent the seams as predicted by Giroud et al. (1995) and as illustrated in Figure 4-1. However, while the average strain concentrations measured experimentally using DIC were reasonably close to those established using the Giroud et al. (1995) strain concentration equations, the maximum strains adjacent to the seams measured using DIC were significantly greater than the strains adjacent to the seam predicted using the Giroud et al. (1995) equations. For average tensile strains over the geomembrane samples on the order of 3% (the nominal average strain), the maximum tensile strains adjacent to the seams varied from 1.4 to 2.0 times the strains predicted using the Giroud et al. (1995) equations and up to four times the nominal average strain over the sample.

The authors believe the additional incremental strain adjacent to the seam measured experimentally compared to that predicted theoretically using the equations developed by Giroud et al. (1995) is likely due to non-uniformities and imperceptible imperfections along the seam. Considering that the seams tested herein were fabricated specifically for this project by a manufacturer under controlled conditions, imperfections and non-uniformities in field seams are likely to be even greater than the seams tested herein, resulting in even

larger seam strain concentrations. Testing of field seams should be conducted to see if this hypothesis is valid.

These findings have significant implications with respect to allowable tensile strains in geomembranes and to construction quality assurance (CQA) practices for collecting geomembrane seam samples for destructive testing. Testing conducted herein suggests that allowable tensile strain in a HDPE geomembrane should likely be less than 4% to prevent yielding in the seam, particularly if the supposition that imperfections and strain concentrations in field seams are likely to be greater than in the factory-prepared seams tested herein is correct. These findings also suggest that it is prudent to avoid seams oriented perpendicular to an applied tensile load and that recovery of CQA samples for destructive testing from areas where the geomembrane may be loaded in tension, e.g. at the crest of a slope or near an anchor trench, should be avoided, as the patches applied in these areas after the CQA samples are recovered will always have a seam perpendicular to the applied tensile load. This conclusion is supported by the observation that the tears in the geomembrane at the Chiquita Canyon landfill detected after the Northridge earthquake appeared to emanate from patches applied to locations near the crest of the slope from which samples for destructive CQA testing were recovered (EMCON, 1994). Strain concentrations due to scratches in the geomembrane (also evaluated by Giroud et al. 1995) and due to other irregularities on the surface of the geomembrane should also be considered when establishing allowable strains and CQA practices.

Notations

Basic SI units given in parentheses

CQA construction quality assurance

DIC	digital image correlation
HDPE	high density polyethylene
t_{gm}	geomembrane thickness mm)
t_s	seam thickness (mm)
W	width of seam (mm^3)
ε_{AVG}	global average strain of the HDPE sample (%)
ε_{Giroud}	theoretical maximum strain from Giroud et al. (1995) equations (%)
$(\varepsilon_{DIC})_{MAX}$	maximum strain adjacent to seam (%)
$(\varepsilon_{DIC})_{AVG}$	average strain of geomembrane adjacent to seam (%)

References

ASTM (2011), "Standard Test Method for Determining Performance Strength of Geomembranes by the Wide Strip Tensile Method," Test Method D4885-01, ASTM International, West Conshohocken, PA.

Correlated Solutions (2016), "VIC-3D™ System," Correlated Solutions, Inc., www.correlatedsolutions.com/products/#vic3d.

EMCON Associates (1994), "Northridge Earthquake Seismic Evaluation, Chiquita Canyon Landfill," EMCON Associates, San Jose, California, April.

Giroud, J. P., Tisseau, B., Soderman, K.L., & Beech, J.F. (1995), "Analysis of Strain Concentration Next to Geomembrane Seams, *Geosynthetics International*, Vol. 2, No. 6, pp. 1049-1097.

Giroud, J. P. (2005), "Quantification of Geosynthetic Behavior," *Geosynthetics International,* Special Issue on the Giroud Lectures, Vol. 12, No. 1, 2-27.

Kavazanjian, E., Arab, M., & Matasovic, N. (2013), "SOAP-5: Performance of Two Geosynthetic-lined Landfills in the Northridge Earthquake," *Proceedings of the 7th International Conference on Case Histories in Geotechnical Engineering,* Missouri University of Science and Technology, Rolla, Missouri (on CD ROM).

Peggs, I.D., Schmucker, B., and Carey, P. (2005), "Assessment of Maximum Allowable Strains in Polyethylene and Polypropylene Geomembranes," *Proceedings of GeoFrontiers 2015: Waste Containment and Remediation,* Geotechnical Special

Publication 142, ASCE, DOI:
http://dx.doi.org.ezproxy1.lib.asu.edu/10.1061/40789(168)23

Take, W.A. (2015), “Thirty-Sixth Canadian Geotechnical Colloquium: Advances in visualization of geotechnical processes through digital image correlation,” *Canadian Geotechnical Journal*, 52 (9), 1199-1220, doi: 10.1139/cgj-2014-0080

CHAPTER 5. EXPERIMENTAL EVALUATION OF GEOMEMBRANE SEAM STRAIN CONCENTRATIONS IN FIELD SEAMS

5.1 Introduction

The results of the experimental work presented in Chapter 4 indicate that the maximum tensile strain adjacent to a seam in a laboratory prepared geomembrane may be on the order of four times the nominal tensile strain. The change in geometry between the seam and the adjacent geomembranes contributes to the increased strain adjacent to the seam. The seaming process during installation creates the seam geometry. Installation factors such as heating consistency, bead thickness, liner thickness, and equipment placement contribute to the potential for strain concentrations. The incremental bending strain associated with a geomembrane seam depends upon the geometry of the seam itself (Giroud, 1995). It is reasonable to assume that the maximum bending strain depends upon the geometry and therefore the installation of the seam. As field conditions result in greater variation than controlled laboratory conditions, the installation process must be considered when evaluating the potential strain concentrations. Any parameters or equations developed for design should be based upon data collected from samples of equivalent quality to the seams which are welded during installation. As the strain concentrations assessed in the previous chapter were based upon seams prepared in the laboratory under controlled conditions, it seemed necessary to test actual field seams to develop guidelines on the acceptable strain in practice.

The state of practice in landfills in the United States and Europe is based upon limiting allowable global tensile strain magnitudes (Peggs et al 2005). As such, knowing the maximum expected strain in a geomembrane as a function of the global tensile strain

is desirable. Furthermore, identification of the nominal tensile strain which is expected, with a reasonable degree of confidence, to not induce maximum strains which exceed yield is necessary. A testing program was developed to experimentally evaluate the seam strain concentrations at HDPE field seams loaded in tension perpendicular to the seam for typical seam types, thicknesses, and surface textures used in practice. Digital image correlation (DIC) was used to measure the average strain and the localized maximum strain induced in the geomembrane sample. The expected maximum strain in the geomembrane was generated as a function of the nominal tensile strain. The nominal tensile strain which is expected to induce maximum strains which do not exceed yield with 90 percent and 95 percent levels of confidence was calculated for the different types of seams tested in this study.

5.2 HDPE Geomembrane Field Samples

Remnants of HDPE geomembrane field samples cut from liner installations for quality assurance / quality control (QC/QA) purposes were supplied by United States geomembrane testing laboratories and installers. 1 mm (40 mil) and 1.5 mm (60 mil) thick samples were provided and included smooth and textured geomembrane seam samples as well as samples wherein a smooth geomembrane was welded to a textured geomembrane. Both dual track fusion welded and extrusion fillet welded samples were provided. The samples were supplied in roughly rectangular coupons which were later trimmed to fit the grip apparatus (150 mm wide) used for testing. The sample length was cut so that the area in between the grips was 75 mm to satisfy the requirements of ASTM D4885-01 (ASTM 2011). The initial sample preparation included cleansing and fitting of the geomembrane sample to the length of the friction load plates used to grip the sample.

The trimming process included the removal of overlapping, non-welded sections of geomembrane, providing a clear line of view for image capture in the zones of interest.

Table 5-1 presents detail of the testing program on HDPE field geomembrane samples. All samples were tested in uniaxial tension. Digital image correlation (DIC) was used to evaluate the tensile strain perpendicular to the seam across the surface of the samples.

Table 5-1: HDPE Field Geomembrane Samples

Sample Type	Thickness	Surfacing	Number of Samples	Average Seam Width (mm)	Average Seam Thickness
Dual Hot Wedge	1 mm	Smooth	14	47.5	2.35
		Textured	21	49.2	2.5
		Smooth-Textured	5	49.5	2.6
	1.5 mm	Smooth	41	52.7	3.0
		Textured	27	54	3.3
		Smooth-Textured	6	54.8	3.1
Extrusion Fillet	1 mm	Textured	12	33.7	3.4
		Smooth-Textured	3	33.3	3.81
	1.5 mm	Textured	11	47.2	4.7
		Smooth Textured	4	39.1	4.1

The dual hot wedge seam width ranged from 44.4 mm to 58.8 mm. The 1 mm dual hot wedge seam samples had seam thicknesses ranging from 2.0 to 3.0 mm. The 1.5 mm dual hot wedge seam samples had seam thicknesses ranging from 2.5 mm to 3.6 mm. The 1 mm extrusion fillet seam samples had seam thicknesses ranging from 2.7 to 4.8 mm. The 1.5 mm extrusion fillet seam samples had seam thicknesses ranging from 3.0 mm to 5.0 mm.

5.3 Testing Apparatus and Equipment Setup

5.3.1 Tensile Test Load Frame

All testing was performed using a GCTS load frame with modified grips to secure the lower and upper geomembrane respectively. The base grip was bolted firmly to the load frame base and the upper grip was allowed to rotate freely. The geomembrane samples were secured using textured stainless steel friction plates pressed together with ten bolts spread evenly across the plate length. The grips were tightened to securely fasten the geomembrane while refraining from crushing or otherwise damaging the material. Figure 5-1 shows the front view of the upper geomembrane grip which is 150 mm wide. Figure 5-2 shows a side view of the upper grip including the textured friction plates. Figure 5-3 shows the friction load plate, with dimensions 150 mm wide by 30 mm tall.

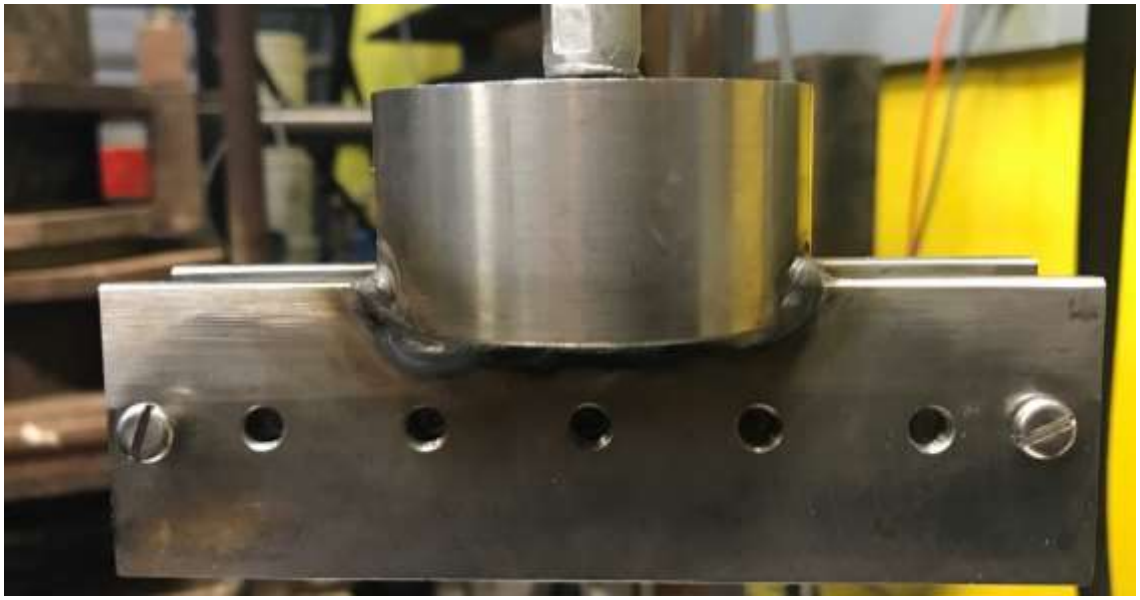

Figure 5-1: Upper grip apparatus (front view)

Figure 5-2: Upper grip apparatus with textured load plates (side view)

Figure 5-3: Friction plate with dimensions 150 mm wide by 30 mm tall

The GCTS system allows measurement of deformation and load from LVDT and load cell measurements respectively. The nominal average tensile strain in the sample may be calculated considering the original and deformed sample length. Slippage may occur at times between the geomembrane and grip apparatus Sample slippage was minimized by applying an even pressure across the grip plates, with as high a magnitude as possible without crushing or harming the sample. More importantly, any such sample slippage was noted during the test so the effect on the LVDT measurements of the deformation between the grips (used to calculate the nominal strain) past the point of slippage could be considered in the analysis. Measurement of nominal (average) strain across the sample surface was also measured using DIC. The DIC method of strain measurement is independent of slipping between the sample and friction plates.

5.3.2 **DIC Image Capture**

Image capture was facilitated using two Point Grey cameras with Xenoplan 1.9/35-0901 lens from Schneider – Kreuznach. Light was supplied by two LED lights from Visual Instrumentation Corp. (Model 900420W). The apparatus was supported on a standard tripod attached to a mounting rack with adjustable mounts for the cameras and lights. The apparatus was placed level with the sample and the cameras adjusted with overlapping fields of view. The focus was adjusted to be clear and consistent between the two cameras. The exposure was set by first adjusting the lighting so that exposure was equal between the two cameras and across the sample. Small adjustments were then made to the camera exposure. The consequences of improper configuration are an inadequate data calibration due to excessive projection error and poor or discontinuous deformation data (i.e. the algorithm is unable to find appropriate matches of color intensity). Figure 5-

4 shows the DIC image capture equipment setup. The image capture software used on this project was VIC Snap (Correlated Solutions, 2016).

Figure 5-4: DIC image capture equipment setup

5.3.3 DIC Calibration

Calibration of the DIC setup consisted of inserting a 105 mm wide x 75 mm-high calibration plate with black dots 1.5 mm in diameter spaced 7.5 mm center to center in a square grid pattern. Figure 5-4 presents an image of the calibration plate. The calibration plate is rotated along its three axes by hand. While the calibration plate is being rotated, a series of photos are taken with the cameras. These photos are then imported into VIC3D and used to calibrate the test setup. The calibration process compares the differences

between each image that is imported into VIC3D. A score is given that reflects the differences in the calculated calibration plate geometry for each camera at the end of the calibration. This score indicates the cumulative error, the basis for determining if the test setup is adequate. If the cumulative error is below 1%, the calibration is satisfactory and testing may be conducted. If not calibration images are retaken and another calibration analysis is conducted as sometimes the calibration is not satisfactory due to human effort. If the calibration still yields unsatisfactory results the equipment must be re-aligned. The result of improper setup and calibration is increased projection error. Because the cameras have overlapping fields of view, a theoretical line may be drawn along an image taken by camera one and the same line projected onto an image taken by camera two. The difference between the two theoretical lines is the projection error. The theoretical value should be zero, but a small projection error is normal due to small differences in camera view. A successful calibration takes these differences into account.

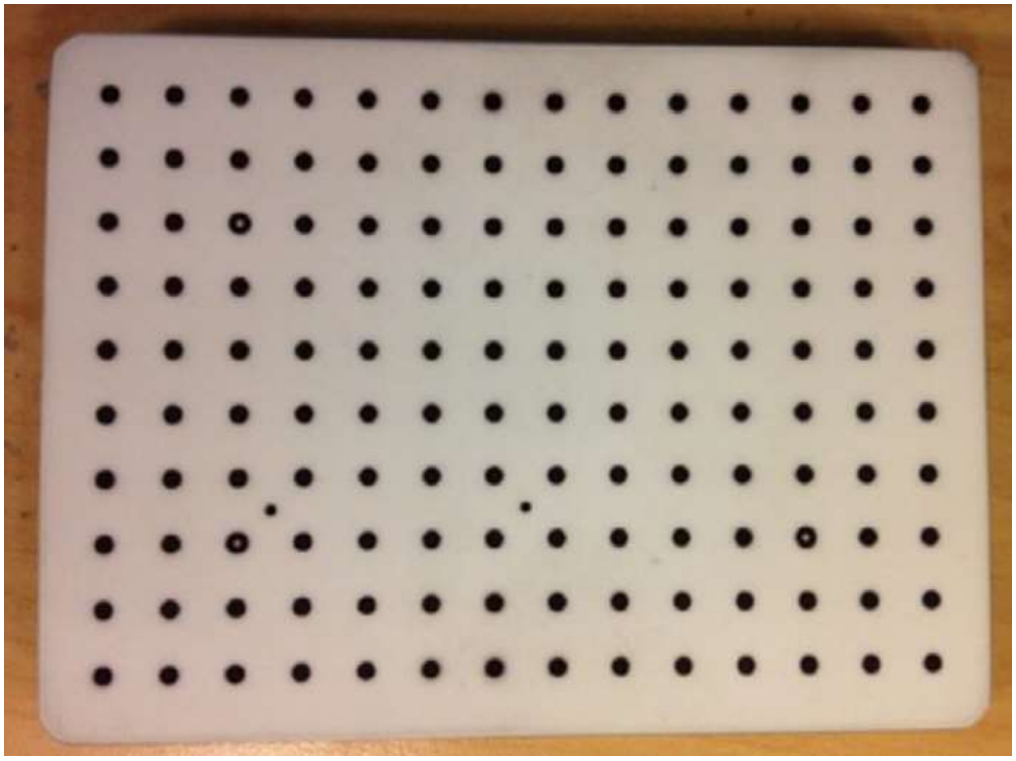

Figure 5-4: Calibration plate for DIC testing

5.3.4 Tensile Test Apparatus Setup

Once calibration of the DIC setup was complete, the geomembrane sample was slid into place between the friction load plates of the modified uniaxial tensile testing apparatus. Once the sample was in place, the grip apparatus was firmly tightened with pressure applied equally across the textured plates. A seating load was applied to remove slack from the sample and to place the sample in a slight degree of tension, evaluated visually, to seat the sample. Following seating, the sample was deformed in tension at a strain rate of 10% per minute in accordance with the ASTM 4885 standard for wide-width tensile testing of geomembranes. The tests were typically conducted up to strains of 12% to 15%. Tests were terminated in the event of slipping between the sample and friction load plates.

5.3.5 **HDPE Geomembrane Sample Preparation**

Because the strain concentrations associated with a geomembrane seam are extremely localized, they cannot be measured using strain gages or other conventional strain measurement techniques. Therefore, DIC was employed to measure the strain field around the seam (and over the entire geomembrane sample). The most important factor affecting accurate measurements using DIC is sample preparation (Take, 2014). The surface of the sample must be prepared in a manner such that distortions of the sample can be optically detected. A sample of uniform color or texture, e.g. an entirely black sample, would not be amenable to DIC measurements. High gloss surfaces can also make DIC measurement ineffective due to reflections from the high intensity lighting used to illuminate the sample. Therefore, preparation of the samples for DIC measurements consisted of first applying a uniform coat of white non-gloss paint on the surface of the sample. Once the white non-gloss paint was dry, a random pattern of black speckles was applied over the white background and allowed to dry.

The details of the speckle pattern are of great importance in acquiring proper results from the DIC measurements. If a speckle is too large, a data gap is created in the analysis. However, if a speckle is too small the image analysis program may not recognize it. Changes in speckle density can also create gaps in the data. Figure 5-6 shows an un-seamed HDPE sample prepared for image capture to be used in digital image correlation.

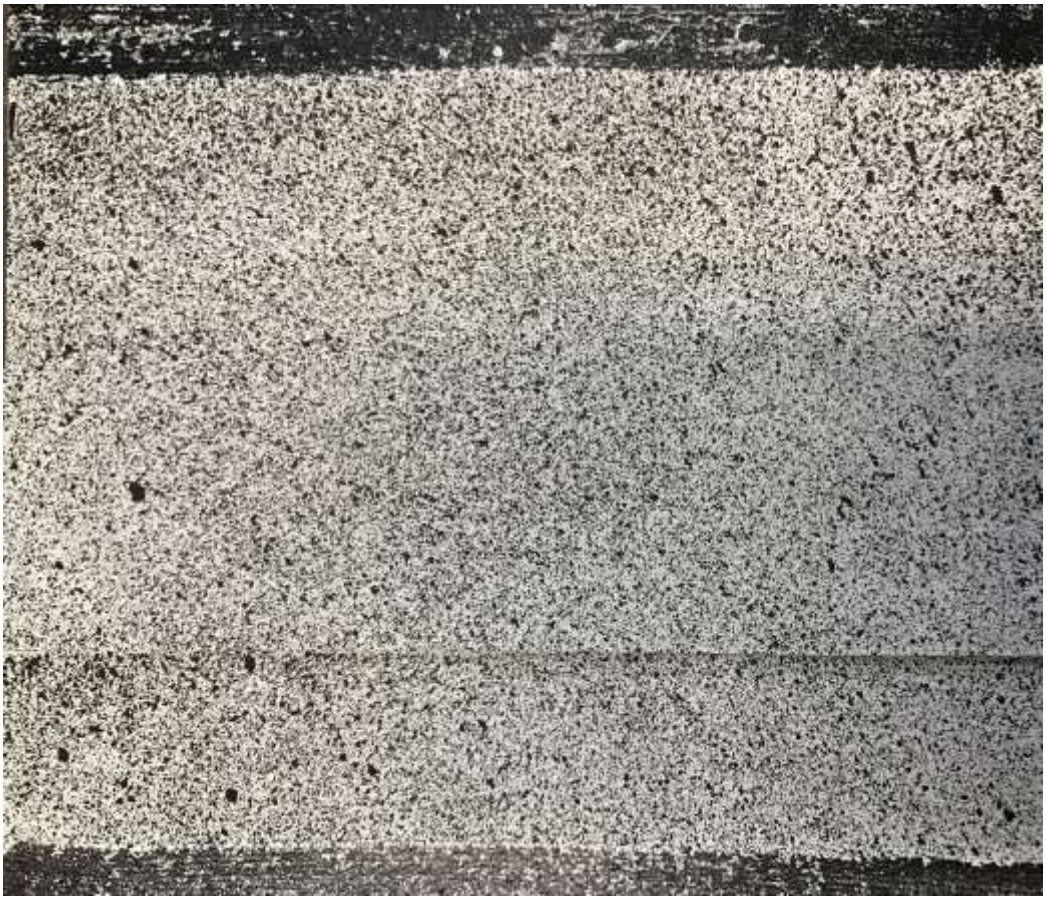

Figure 5-6: HDPE sample prepared with speckle pattern for DIC analysis

5.4 Accuracy and Precision of DIC Measurements

Tests were conducted on unseamed samples to evaluate the accuracy and precision of the DIC measurements. Accuracy was evaluated by comparing the average global strain evaluated by the DIC measurements using VIC 3D to the nominal global strain evaluated based upon the length of the sample between the grips and measurements of the displacement of the grips securing the sample made using a linear varying displacement transducer (LVDT). Precision was evaluated by loading the sample to a strain below yield five times and comparing the DIC strain measurements from each trial at nominal strains

(strains based upon LVDT measurements) of 0.17, 0.35, 1, and 3 percent. The accuracy and precision measurements were made on 2 different samples.

VIC 3D calculates the strain field based upon differentiation of the displacement field of the sample determined by comparison of two images taken at different times. Therefore, a reference image for the unstrained state of the sample is required upon which the DIC analysis is based. In this testing program, the reference image was taken after the seating load was applied to the geomembrane samples. Using the reference image as the baseline, VIC 3D computes a deformation and strain field over the area of interest based upon the relative movement of the speckles.

Results of the accuracy and precision tests are presented in Table 5-2. The mean strain from 5 trials based upon the DIC measurements was typically within 10 percent of the strain based LVDT measurements. Except at the smaller nominal strains (0.17 and 0.35 %), the strain from the DIC measurements was greater than the nominal strain from the LVDT measurements. The standard deviation from 5 measurements on the same sample was increased as the strain increased, but the variance (the standard deviation divided by the mean) decreased as the strain increased. While the variance at the smaller nominal strains (0.17 and 0.35 %) for Sample 1 was relatively high (up to 45%), at the largest nominal strain (3 %) was only 6% for Sample 1 and 3% for Sample 2.

Table 5-2: Comparison of nominal percent strain based upon LVDT measurements to mean and standard deviation percent strain from DIC measurements on an unseamed sample loaded below yield five times

LVDT	Sample 1			Sample 2		
	Mean	Std. Dev.	Variance	Mean	Std. Dev.	Variance
0.17	0.153	0.067	44%	0.171	0.016	9%
0.33	0.326	0.101	31%	0.359	0.012	11%
1.00	1.073	0.129	12%	1.110	0.029	3%
3.00	3.330	0.200	6%	3.389	0.086	3%

5.5 HDPE Geomembrane Field Sample Testing

The field seam samples were assigned an identifier based primarily upon their source and test date. The samples were typically tested in groups based upon the time of sample preparation. samples tested on the same day all share the same calibration. Therefore, 1.1, 1.2, and 1.3, indicates three samples which were all tested on day 1 of testing and therefore share the same calibration file.

The tensile tests were conducted up to strains of 12 to 15% and were terminated based upon sample slipping and excessive load placed upon the grip apparatus. The nominal tensile strain based upon grip separation was calculated from the initial distance between the grips. The average tensile strain over the entire sample was calculated using DIC, as was the maximum strain at several points throughout the test. The number of data points was determined by the number of images taken during the test. The image capture rate was one image every two seconds.

5.6 Data Analysis

5.6.1 VIC 3D Analysis

The images were analyzed with the DIC algorithm to calculate the relative deformation and resulting strain profile. The analysis was performed for every image, which represents a discrete point during the test. The average and maximum tensile strain in the sample were calculated from the strain profile.

Figures 5-7 through 5-9 show the strain field for an unseamed HDPE sample. At low average strains of 2%, the range of strain in the sample is low and the maximum strain is 2.9% (Figure 5-7). At medium average strain (7.9%), the distribution of strain becomes more varied, with a maximum tensile strain of 10.5% for Figure 5-7. At a high average strain of 12%, at which point the sample begins to yield, a larger strain range with a maximum strain of 18.8% was calculated. A greater variation in strain is expected following material yield, and variation at high strain may be in part due to necking effects. The strain pattern observed in Figures 5-7 through 5-9 is consistent with the strain pattern observed in Chapter 4 and is clearly different than the strain pattern observed in a seamed geomembrane sample.

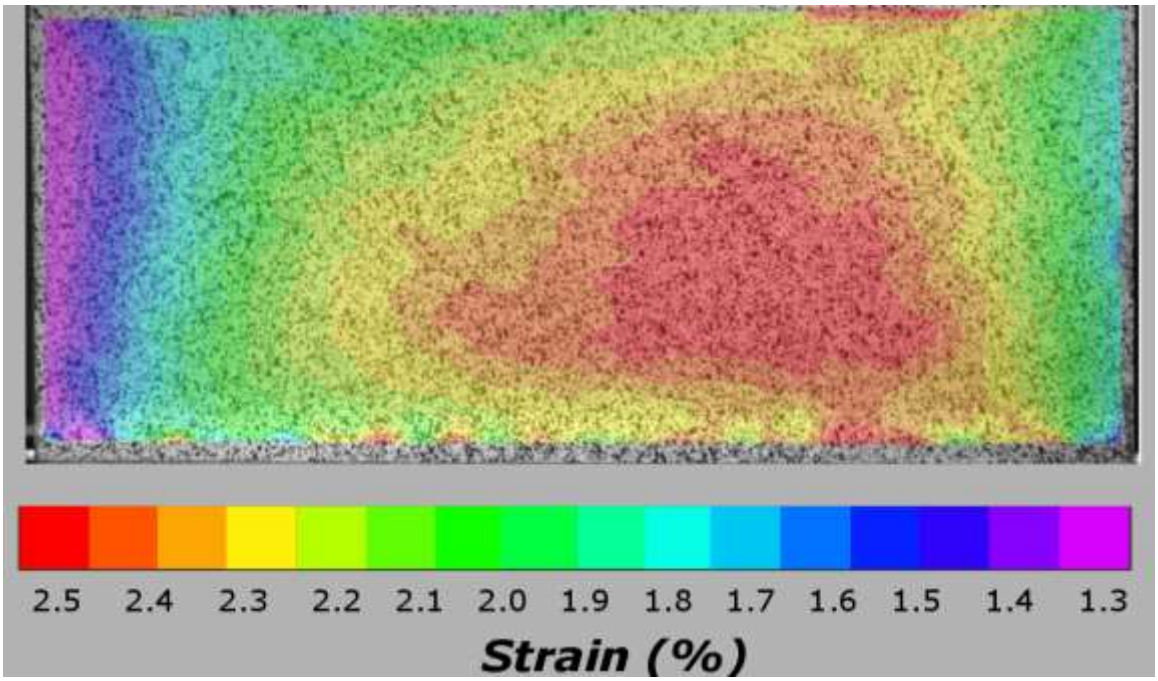

Figure 5-7: Strain field from DIC for 1 mm unseamed sample at 2.2% average strain

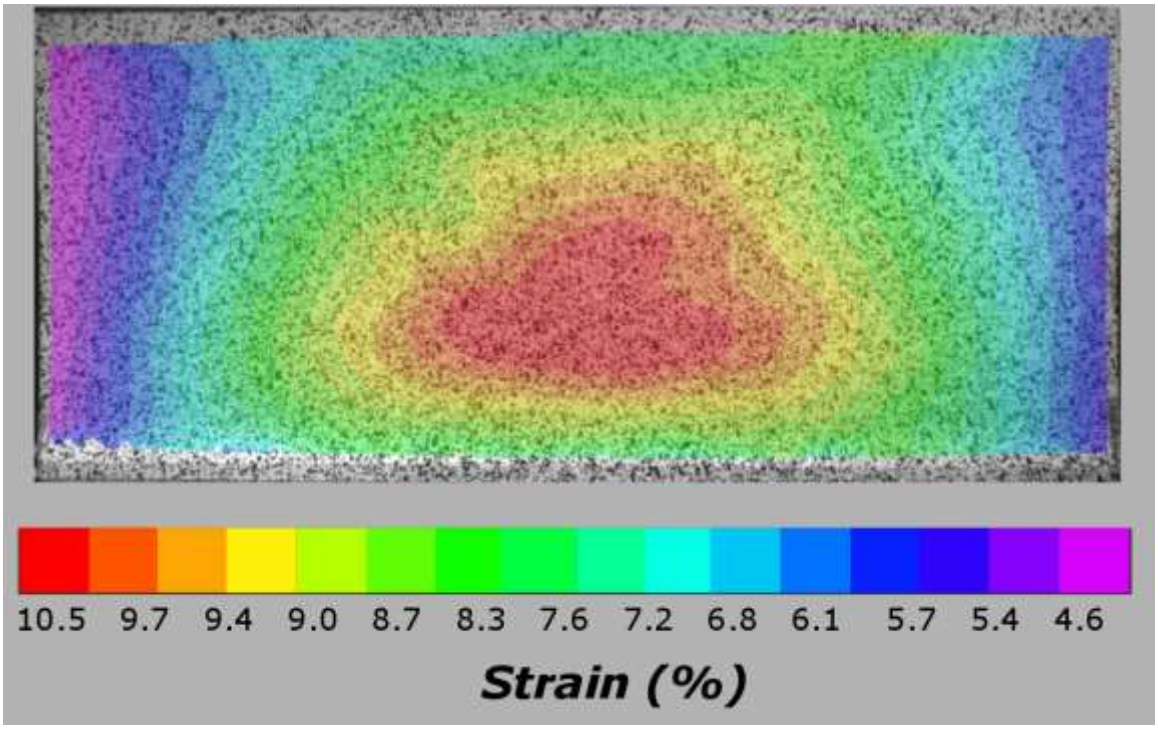

Figure 5-8: Strain field from DIC for 1 mm unseamed sample at 7.9% average strain

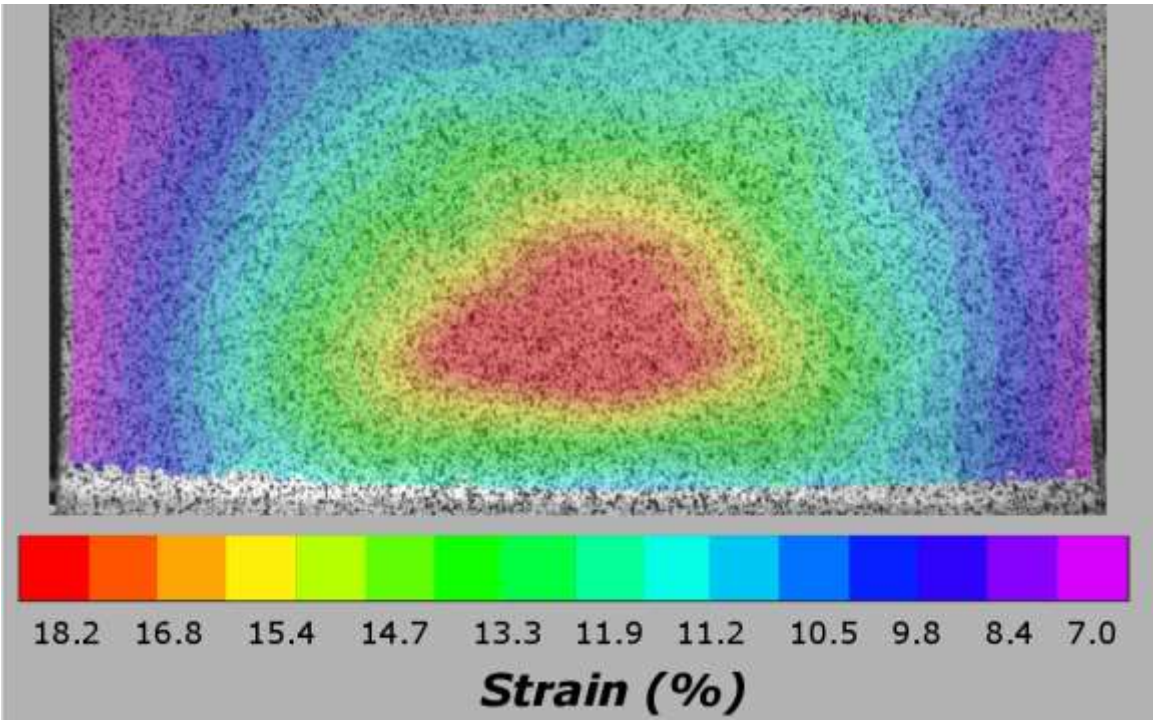

Figure 5-9: Strain field from DIC for 1 mm unseamed sample at 12.0% average strain

Figure 5-10 shows the VIC3D results for a 1 mm geomembrane sample with an extrusion fillet seam and textured surfacing. The average (global strain) in the sample is 4.2% and the maximum strain is 10.3%. The strain band adjacent to the seam along the breadth of the sample has a calculated average strain of 7.9%, very close to the strain of 7.6% calculated from the Giroud et al. (1995) strain concentration factors.

Figure 5-8 shows the computed strain field for a 1 mm (40-mil) dual hot wedge seam sample at an average strain over the sample surface of 6.2%. The strain concentration is clearly visible in the lower geomembrane as a red and yellow band along the breadth of the sample. The average strain in this zone is 8.1% and the maximum strain is 22.3%.

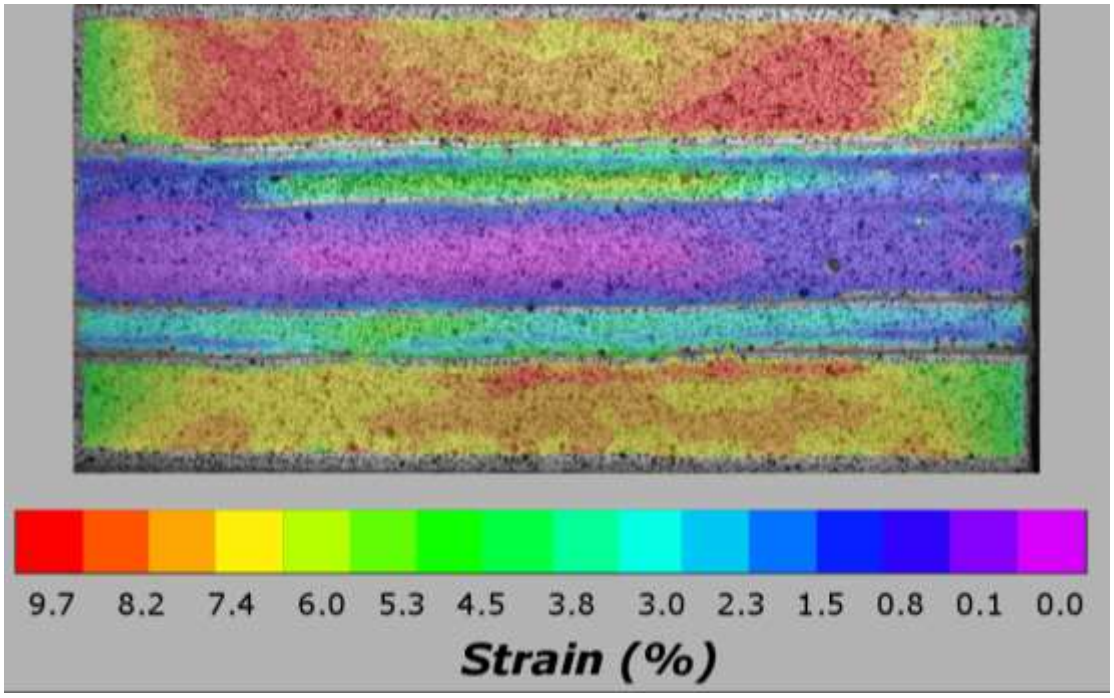

Figure 5-10: Strain field from DIC for 1 mm extrusion fillet sample at 4.2% average strain (Sample 21.1)

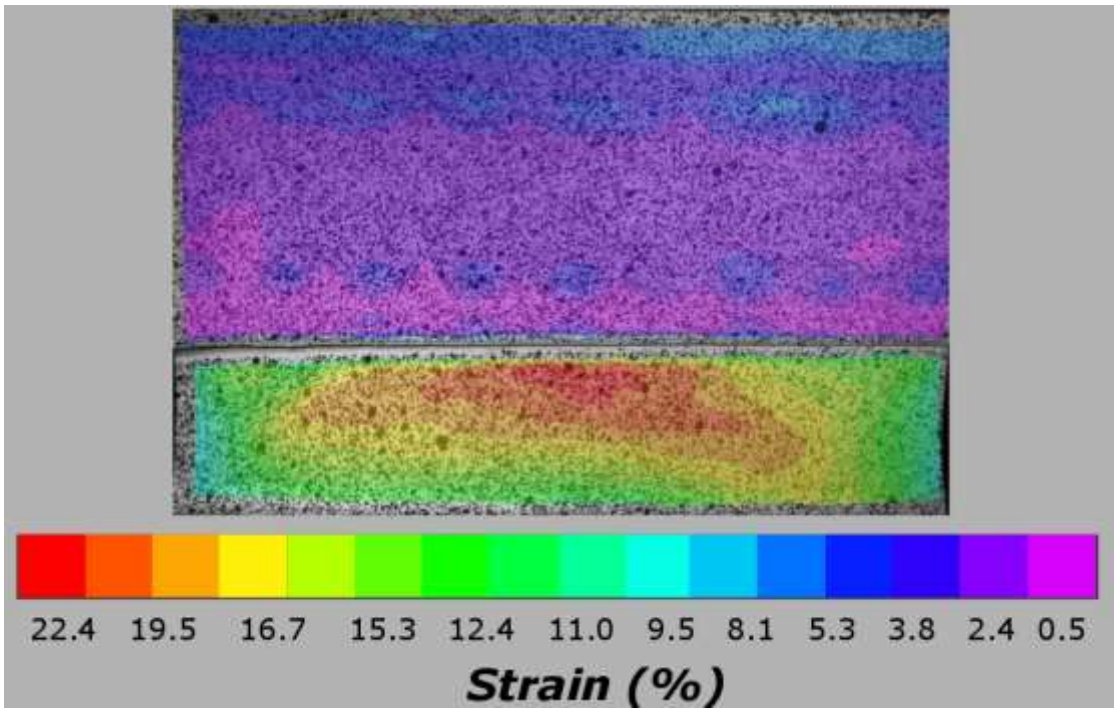

Figure 5-11: Strain field from DIC for 1 mm dual hot wedge sample at 6.2% average strain (Sample 21.1)

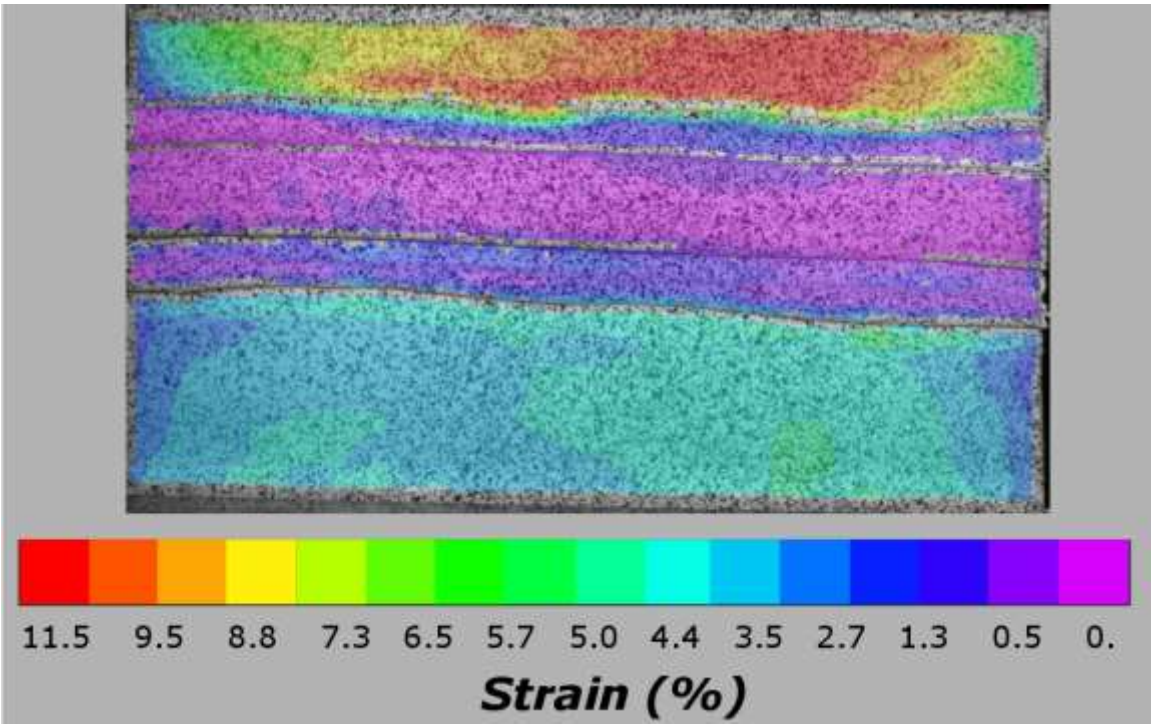

Figure 5-12: Strain field from DIC for 1 mm extrusion fillet sample at 3.0% average strain (Sample 20.1)

Figure 5-12 shows an example strain field of a 1 mm extrusion fillet seam sample at 3.0% average strain. The sample surfacing consists of a smooth geomembrane welded to a textured geomembrane. The strain concentration is identifiable in the geomembrane adjacent to the seam, averaging 8.7% strain. The difference between the strain in the welded section of the geomembrane and the strain in the geomembrane adjacent to the seam is pronounced in this sample. The average strain in the weld is 0.5%. The difference in thickness between the geomembrane and the weld contributes to relative strain magnitudes. The principal is illustrated well in Figure 5-12, as the weld thickness is 4.8 mm and the geomembrane thickness is 1 mm. The increased thickness of the seamed area results in a low strain. The maximum strain in the sample was measured at 11.9%.

5.6.2 **Significance Tests**

To determine if there were significant differences between the maximum strain induced in different types of samples, a series of two-sample t tests were performed on segregated data based upon seam thickness and surface texture. The significance tests were performed at each image capture. The significance tests were performed at every discrete point throughout the tensile test where data was collected (i.e. an image was captures), An example is shown below, describing the significance testing.

To determine the difference in the data taken from the 1.5 mm dual hot wedge samples with smooth surfacing and the 1 mm dual hot wedge samples with smooth surfacing, the following methodology was adopted. First, the null hypothesis is stated:

$$H_0: \mu_1 - \mu_2 = 0 \qquad \text{(equation 5-1)}$$

The null hypothesis states that the mean of the maximum strain calculated in 1.5 mm dual hot wedge samples with smooth surfacing is equal to the mean of the maximum strain calculated in the 1 mm dual hot wedge samples with smooth surfacing.

The standard deviation of the maximum tensile strain measured in the 1.5 mm dual hot wedge samples with smooth surfaces were similar to the standard deviation of the maximum tensile strain measured in the 1 mm dual hot wedge samples with smooth surfaces, i.e. no more than twice the magnitude. Therefore a pooled standard deviation was calculated. Furthermore, since the pooled sample population exceeds 30, the data can be assumed to conform to a normal distribution. A demonstration of adherence to the normal distribution is presented in Figure 5-13. Therefore, the pooled standard deviation, s_p, may be evaluated as:

$$s_p = \sqrt{\frac{(n_1-1)s_1^2+(n_2-1)s_2^2}{n_1+n_2-2}} \qquad \text{(equation 5-2)}$$

The test statistic, t*, was then calculated for each data point (every nominal strain level) where the average maximum strain at that time step was taken as the variable of interest and the mean value was approximated by the sample means, $\bar{x}_1$ and $\bar{x}_2$.

$$t^* = \frac{\bar{x}_1-\bar{x}_2}{s_p\sqrt{\frac{1}{n_1}+\frac{1}{n_2}}} \qquad \text{(equation 5-3)}$$

A typical significance level (alpha) was chosen, 10%. The significance level determines the level of confidence in the test. In the context of the significance test, an alpha of 10% means that there is a 10% chance that the mean maximum strain of the two samples will be statistically different, but misclassified as the same.

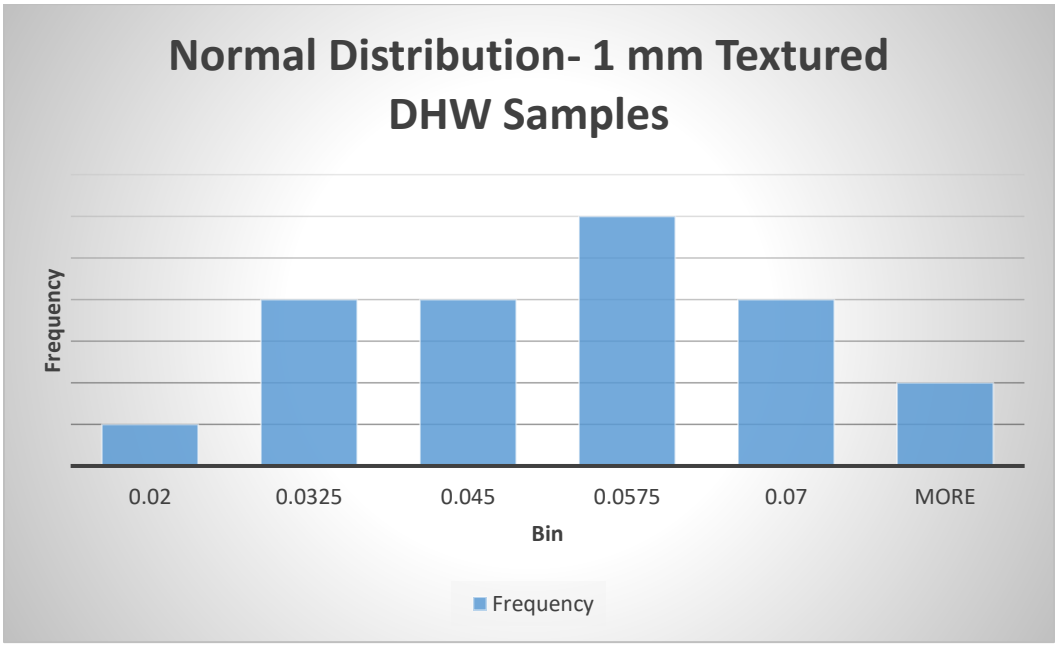

Figure 5-13: Distribution of maximum tensile strain for 1 mm textured dual hot wedge samples at a nominal tensile strain of 2%

The significance tests were performed at each data point from 0% to 10% strain and the results are presented in Table 5-3.

Table 5-3: Significance Test Results

Sample 1	Sample 2	Pooled Sample Size	Statistically Significant Difference at alpha of 0.1?
1 mm Dual Hot Wedge Smooth surfacing	1.5 mm Dual Hot Wedge Smooth Surfacing	55	Yes
1 mm Dual Hot Wedge Textured Surfacing	1.5 mm Dual Hot Wedge Textured Surfacing	48	No
1 mm Dual Hot Wedge Textured Surfacing	1 mm Dual hot Wedge Smooth surfacing	35	No
1.5 mm Dual Hot Wedge Textured Surfacing	1.5 mm Dual Hot Wedge Smooth Surfacing	68	No
1 mm Extrusion Fillet Textured/Smooth	1 mm Extrusion Fillet Textured surfacing	15	No
1.5 mm Extrusion Fillet Textured/Smooth	1.5 mm Extrusion Fillet Textured Surfacing	13	Yes
1 mm Extrusion Fillet Textured/Smooth	1.5 mm Extrusion Fillet Textured /Smooth	7	Yes
1 mm Extrusion Fillet Textured Surfacing	1.5 mm Extrusion Fillet Textured Surfacing	21	Yes

Based upon the significance test results summarized in Table 5.3, the mean maximum strain for the 1 mm samples with textured surfacing was found to be the same as the mean maximum strain for the 1 mm samples with smooth surfacing. As such, the two sample pools were combined in subsequent analysis. The same was found to be true for the 1.5 mm samples with respect to the surfacing. No statistical difference was found between the mean maximum strain of seams samples welding textured to smooth surfaces and textured surfaces only, for 1 mm extrusion fillet seamed samples. There was a statistical difference for the other mean maximum strain sample populations. It should be

noted that the number of extrusion fillet seamed samples was limited and far less than the sample size of the dual hot wedge seamed sample population (for example, 21 extrusion fillet textured samples and 48 dual hot wedge textured samples).

5.7 Summary of Test Results

5.7.1 Maximum Strain as a Function of Nominal Tensile Strain

Figure 5-14 summarizes the test data for 1 mm (40mil) dual hot wedge seamed samples, presenting the maximum tensile strain as a function of the nominal (global) tensile strain. The blue data points are the mean maximum strain for the 40mil dual hot wedge samples and the orange data points are the mean maximum strain plus two standard deviations. The sample pool includes both textured and smooth surfaced samples because, as explained above, the difference between the mean of the sample data was found to be statistically insignificant at all measured strain levels. The maximum strain adjacent to the seam was calculated by DIC for each induced nominal strain. The mean of the sample is presented on the chart below. Furthermore, the mean plus two standard deviations is also presented. At low strains, i.e., strains between about 0.1% and 2%, the mean maximum strain is relatively flat, at a typical value of around 5%. Furthermore, the standard deviation at this level is small. At nominal strains between 2% and 8%, the maximum strain is typically on the order of 3 times the nominal strain, and the sample standard deviation is observed to increase with increasing nominal strain above nominal strains of 4%. At nominal strains above 8%, the variation increases, and the mean maximum strain is typically between 3 to 4 times the nominal tensile strain.

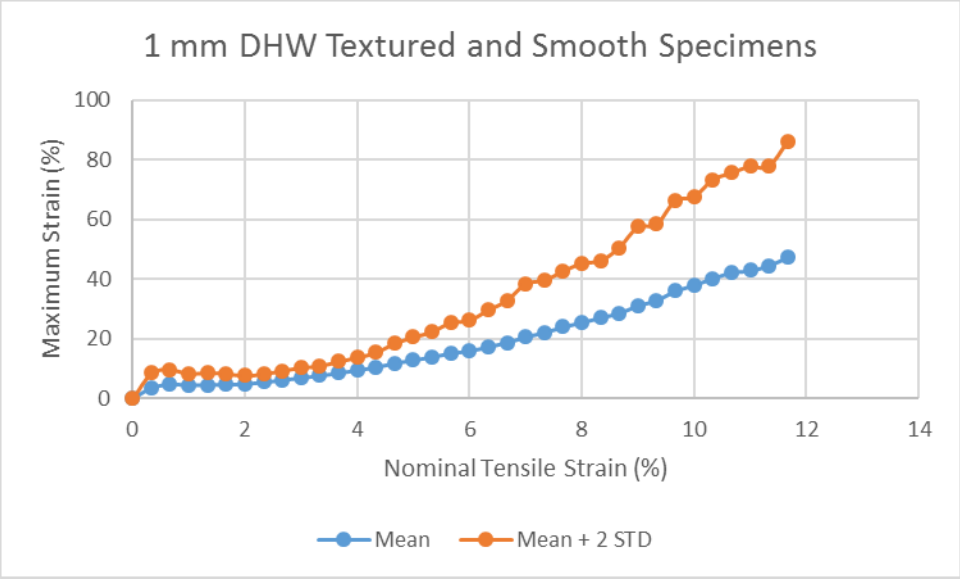

Figure 5-14: 1 mm dual hot wedge samples: Maximum induced strain as a function of the nominal tensile strain

Figure 5-15 shows the data for 1.5 mm dual hot wedge samples. The mean maximum strain pattern is similar to that of the 1 mm dual hot wedge samples, as a function of nominal tensile strain. However, the strain concentrations are greater in general, particularly at nominal tensile strains above 6%, though, the general trend with regard to the maximum expected strain is consistent. At nominal strains below 6%, a magnification factor of 3 is common, with respect to the nominal tensile strain. Nominal strains above 6% are expected to induce higher magnification factors. The mean maximum strain induced in the 1.5 mm dual hot wedge samples as a result of a 10% nominal strain is 47% (suggesting that localized yield occurred at a significantly lower nominal strain).

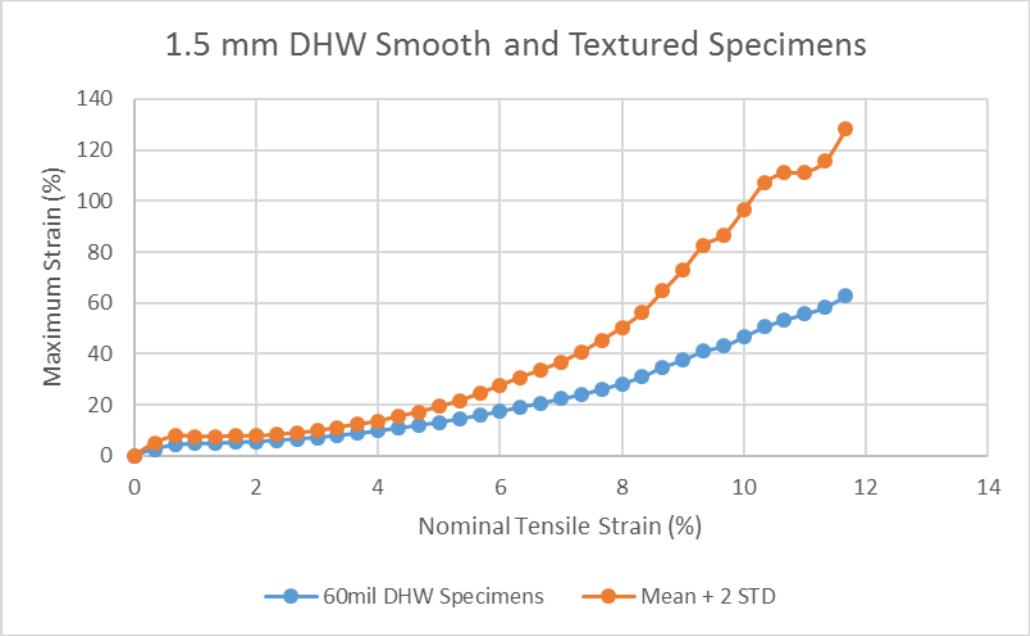

Figure 5-15: 1.5 mm dual hot wedge samples: Maximum induced tensile strain as a function of nominal tensile strain

The extrusion fillet seam samples displayed more variation in mean maximum tensile strain than the dual hot wedge seam samples. Figures 5-16 and 5-17 show plots of the mean maximum strain (blue) and the mean plus two standard deviations (orange) for the 1 mm and 1.5 mm samples. The mean maximum strain curve shows a similar behavior to that of the dual hot wedge mean maximum strain curve for 40-mil samples. Below nominal strains of 2%, the maximum strain is not a strong function of nominal strain. Above 2%, the mean maximum strain is approximately four times the nominal tensile strain and the standard deviation remains relatively low. Above 4%, both the potential magnitude and the variation of the mean maximum strain increases. For example, at a nominal tensile strain of 8%, the mean maximum strain is 40%, a magnification factor of 5.

The mean maximum strain of the 1.5 mm extrusion fillet samples is shown in Figure 5-17. The 1.5 mm samples exhibit similar strain concentrations at lower nominal strains when compared to the mean maximum strain in the 40 mil samples. At higher nominal strains, the magnification factor is less in the 60mil samples. For example, at a nominal strain of 8%, the mean maximum strain is 32%, compared to the 40% observed in the 40mil extrusion fillet seamed samples. Furthermore, the variation is lower, based upon the curves plotted in Figures 5-16 and 5-17 wherein the mean plus two standard deviations is presented against the nominal tensile strain. The standard deviation remains relatively low in the 60mil mean strain curve up until a nominal strain of 8% and greater.

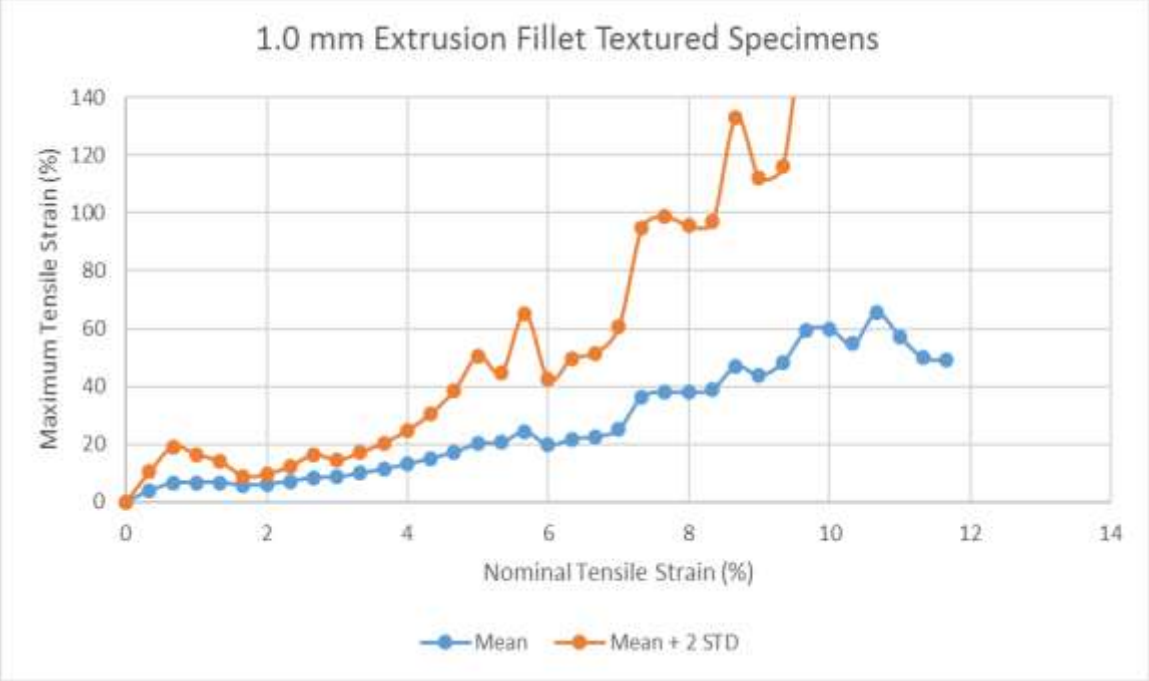

Figure 5-16: 1 mm extrusion fillet textured samples: Maximum induced tensile strain as a function of nominal tensile strain

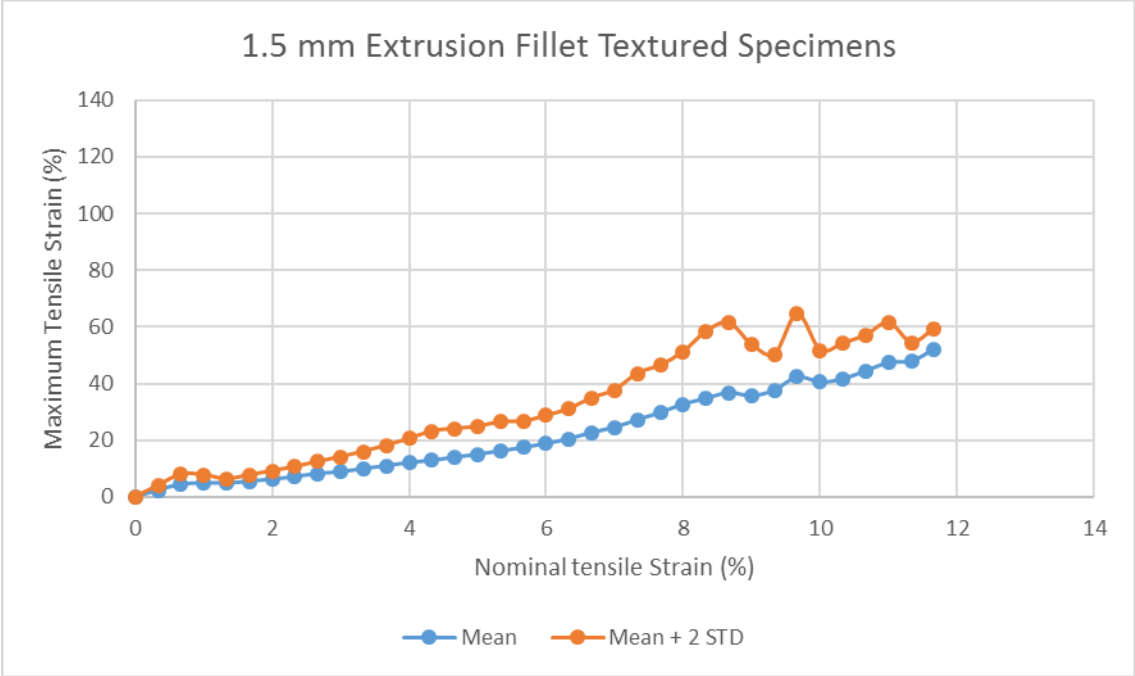

Figure 5-17: 1.5 mm extrusion fillet textured samples: Maximum induced tensile strain as a function of nominal tensile strain

5.7.2 Allowable Nominal Tensile Strain

Based upon general data conformance to a normal distribution, the nominal tensile strain expected to induce maximum strains no greater than 11% (assumed to correspond to the yield strain) was calculated for each statistically distinct group. The results of this calculation are shown in Table 5-4.

Table 5-4: Allowable nominal tensile strain

Sample Type	Allowable Nominal Tensile Strain 95% confidence	Allowable Nominal Tensile Strain 90% Confidence	Assumed Yield Strain
1 mm Dual Hot Wedge	3.3%	3.6%	11%
1.5 mm Dual Hot Wedge	3.7%	3.8	11%
1 mm Extrusion Fillet	2.2	2.4	11%

Sample Type	Allowable Nominal Tensile Strain 95% confidence	Allowable Nominal Tensile Strain 90% Confidence	Assumed Yield Strain
1.5 mm Extrusion Fillet	2.5	2.7	11%

5.8 Conclusions

The maximum tensile strain in HDPE geomembranes adjacent to seams loaded in uniaxial tension perpendicular to the seam were measured experimentally on 144 samples of field seams. The tested samples were remnants of samples collected from field installed geomembrane seams during CQA. The samples were trimmed and fitted to a modified triaxial test apparatus used to apply a tensile strain per ASTM D4885 for wide width tensile testing. The strain was measured across the sample using DIC. DIC allows the measurement of extremely localized strain concentrations. The experimental results were used to quantify the magnitude of the maximum strain expected in the field as a function of nominal tensile strain.

The testing program included dual hot wedge and extrusion fillet seamed samples and geomembrane thicknesses of 1 mm and 1.5 mm. Textured and smooth surfaced samples were included in the study. The maximum measured strain was calculated for all samples at 2 second intervals as the sample was strained. The associated nominal tensile strain was measured at 0.5 second intervals. The mean maximum tensile strain and the standard deviation of the maximum tensile strain was calculated for each time step (associated with a captured image). Significance testing was performed to evaluate the statistical differences among the different types of seams (based upon the characteristics of the seamed geomembranes) in the test data. Two sample t-tests with pooled standard

deviations were used to evaluate the difference in mean maximum strain in the 1.5 mm and 40mil dual hot wedge seamed samples as well as the difference in mean maximum strain in the textured and smooth surfaced samples. A similar process was followed in determining the statistical difference in mean maximum strain for the extrusion fillet seamed samples. The results of the significance tests are presented in Table 5-3. The mean maximum strain in the dual hot wedge samples was found to be independent of geomembrane surfacing for both 1 mm and 1.5 mm geomembranes. The mean maximum strain in the extrusion fillet samples was found to be dependent upon both seam thickness and geomembrane surfacing.

The mean maximum strain induced in the geomembrane samples was developed as a function of the nominal tensile strain. Figures 5-14 through 5-17 provide graphical representations of this relationship. The extrusion fillet seam samples were found to demonstrate greater variation in maximum strain when compared to the dual hot wedge samples. Furthermore, the 1 mm extrusion fillet seam samples displayed more variation at all strain levels, whereas the 1.5 mm extrusion fillet seam samples had much smaller standard deviations at low strain levels (below 4%). The dual hot wedge seamed samples typically had calculated maximum strains of between 3 to 4 times the nominal strain. The extrusion fillet seamed samples typically had calculated maximum strains of 4 times the nominal strain at low strain values (nominal strains below 4%) and had showed higher strain magnification at higher strain values.

The allowable tensile strain expected to induce maximum strains no greater than the yield of HDPE (assumed to be 11%) were developed. The results are included in Table 5-4. A dual hot wedge seamed geomembrane may sustain nominal tensile strains

on the order of 3.3 to 3.7% while remaining below yield. However, extrusion fillet seams may sustain nominal tensile strains of 2.2 to 2.7 while remaining below yield, with a 95% level of confidence.

The variation in the maximum induced tensile strain, particularly in geomembranes adjacent to extrusion fillet seams have implication with respect to allowable strain in geomembranes. Construction quality assurance practices dictate the collection of seam samples for destructive testing, consequentially creating two locations where an extrusion fillet seam is perpendicular to an applied axial load on the geomembrane. Based upon the results of this study, placing an extrusion fillet seam at a location where the nominal tensile strain exceeds 2.2% may result in maximum strains exceeding yield, while still complying with general industry practices (i.e. allowable global strains of 3% and 4%). Furthermore, dual hot wedge seams induce greater strain concentration in the adjacent geomembrane than previously anticipated, suggesting that the allowable global strain of 4% is too high and should be reduced to 3%.

CHAPTER 6. EXPERIMENTAL EVALUATION OF STRAIN CONCENTRATIONS IN GEOMEMBRANES DUE TO SCRATCHES AND DEFECTS

6.1 Introduction

Scratches, defects, and an associated reduction of thickness in geomembrane liners may occur in any stage of liner construction, i.e., during manufacture, handling, and installation. Giroud, et. al (1994) established that reduction in thickness of a geomembrane results in a stress concentration and a resulting localized increase in strain. Defects near seams will contribute to the strain concentration adjacent to the seam, magnifying the additional strain due to bending (Giroud, 2005). The work presented in Chapter 5 captures the effects of installation in the field on strain concentrations adjacent to seams as the analyses are based upon data taken from seams in the field. Small scratches and defects near the seam associated with the welding process such as grinding may be captured in these analyses. However, defects and reductions in thickness also occur away from the seam such as scratches during installation and compression of a stiff geonet into the softer geomembrane by overburden. Giroud et al. (1994) quantifies the reduction in HDPE geomembrane yield strain due to scratches, using a rational approach based upon the material properties and stress strain relationship. The methodology has never been evaluated experimentally. Therefore, a testing program was developed to compare the yield strain of scratched geomembranes to that of unscratched geomembrane samples.

6.2 Background Theory and Previous Work

Giroud et al. (1984) hypothesizes the following failure mechanism for geomembranes which fail due to a strain concentration caused by thickness reductions,

(e.g., a scratch) for geomembranes characterized by a yield peak in the stress strain relationship. Consider a geomembrane scratched and loaded in tension perpendicular to the scratch. The reduced thickness causes an increase in stress at the location of the scratch, as shown in Figure 6-1 from Giroud et al. (1994).

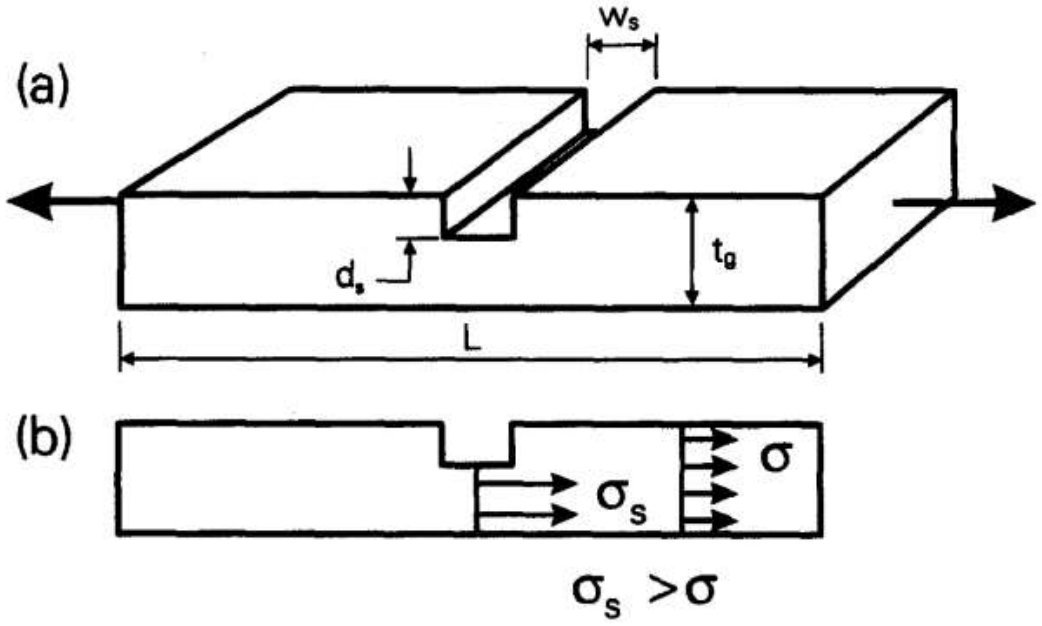

Figure 6-1: Development of stress concentrations in geomembranes subject to thickness reductions

The yield stress is reached at the scratch, but the stress in the unmarred geomembrane remains below yield. A large strain may be exhibited at the scratch while a relatively small strain (governed by the geomembrane stress-strain relationship) is exhibited in most of the geomembrane. The result is an induced failure despite an acceptably low average strain across the geomembrane.

Giroud et al. (1994) developed an approach to calculate the yield strain of a scratched geomembrane. The dependent variable is the ratio of the defective geomembrane yield strain to the intact geomembrane yield strain. The independent variable is the ratio of the thickness reduction to the intact geomembrane thickness. The

expectation is that a unit increase in stress will cause a disproportionate concentration in strain due to inelastic behavior, as illustrated in Figure 6-2 from Giroud (2005). Figure 6-3 presents the graphical relationship (and the corresponding equation) of the reduction in yield strain as a function of scratch depth derived by Giroud (2005).

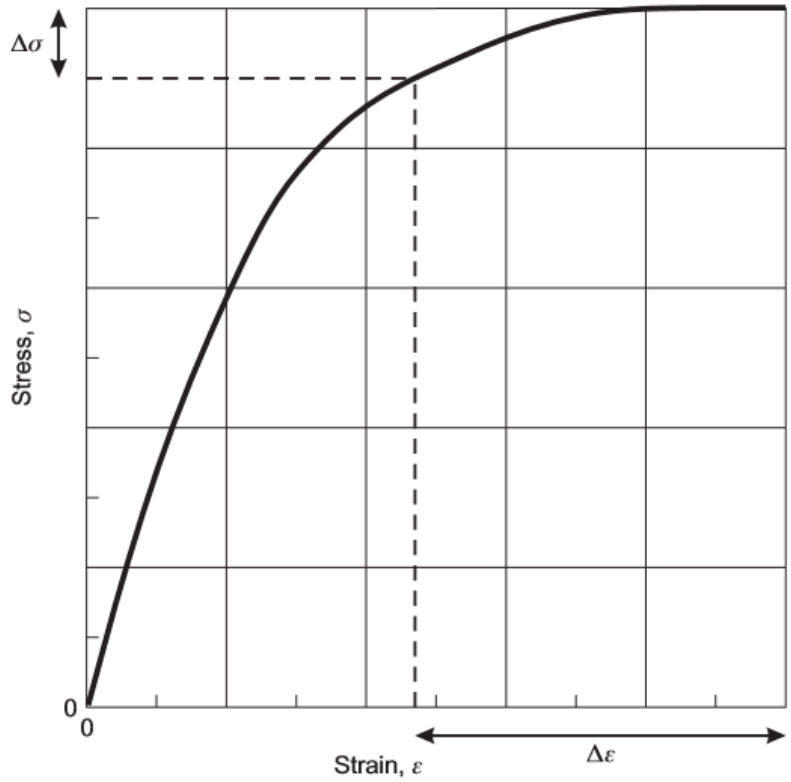

Figure 6-2: Disproportional strain increase in response to a unit stress increase in geomembranes

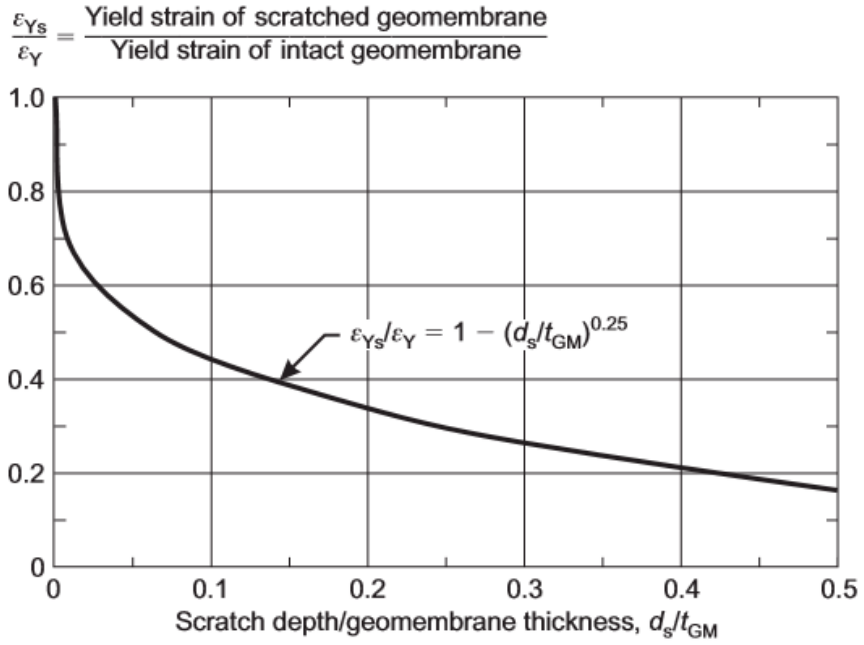

Figure 6-3: Yield strain of marred geomembranes as a ratio of the intact geomembrane yield strain

6.3 HDPE Geomembrane Samples

Six (6) 1 mm HDPE geomembrane samples were supplied by a leading United States geomembrane manufacturer for use in this testing program. The samples measured 130 mm wide by 100 mm tall. Each sample was clamped between 3 0mm tall friction plates, so that the strained section of the geomembrane section satisfies the requirements of ASTM D4885 for wide-width tensile testing (ASTM 2011). Three (3) samples were left unmarred and three (3) samples were subjected to a controlled thickness reduction (i.e., a longitudinal scratch of constant depth. The strain field in each sample throughout the tensile test was calculated using digital image correlation (DIC).

6.4 Testing Apparatus and Equipment Setup

6.4.1 Tensile Test Load Frame

All testing was performed using a GCTS load frame with modified grips to secure the lower and upper ends of the geomembrane. The base grip was bolted firmly to the load frame base and the upper grip was allowed to rotate freely to minimize bending strains in the geomembrane sample. The geomembrane samples were secured using textured stainless steel load plates pressed together with 5 bolts spread evenly across the plate length, for both friction load plates. Two guide bolts holes were machined into both the grip apparatus and friction plates, shown in Figure6-4. The grips were tightened to securely fasten the geomembrane while refraining from crushing or otherwise damaging the material. Figure 6-4 shows the front view of the upper geomembrane grip which is 150mm wide. Figure 6-5 shows a side view of the upper grip including the textured plates.

Figure 6-4: Upper grip apparatus (front view)

Figure 6-5: Upper grip apparatus with textured load plates (side view)

The GCTS system allows measurement of deformation and load from LVDT and load cell measurements respectively. The nominal average tensile strain in the sample was calculated considering the original sample length and the deformed sample length measured by the LVDT. Slippage may occur at times between the geomembrane and grip apparatus Slippage was minimized by applying an even pressure across the grip plates, with as high a magnitude as possible without crushing or harming the sample. Visible sample slippage was noted during the test so that its effect on strain and the LVDT measurements of the deformation between the grips (used to calculate the nominal strain) past the point of slippage could be considered in the analysis. Measurement of nominal (average) strain across the specimen surface was also measured using DIC. The DIC method of strain measurement is independent of slipping between the specimen and the friction plates.

6.4.2 **DIC Image Capture**

Image capture was facilitated with two Point Grey cameras with Xenoplan 1.9/35-0901 lens from Schneider – Kreuznach. Light was supplied by two LED lights from Visual Instrumentation Corp. (Model 900420W). The apparatus was supported on a standard tripod attached to a mounting rack with adjustable mounts for the cameras and lights. The apparatus was placed level with the sample and the cameras adjusted so that the viewing window was equivalent (to the degree possible). The camera focus was likewise adjusted to be near equivalent. The exposure was set by first adjusting the lighting so that exposure was equal between the two cameras and across the sample. Small adjustments were then made to the camera exposure. The configuration of the image capture components was found to affect the quality of the data collection with consequences including an inadequate data calibration due to excessive projection error and poor or discontinuous deformation data (i.e. the algorithm was unable to find appropriate matches of color intensity). Figure 6-6 shows the DIC image capture equipment setup. The image capturing software used on this project was VIC Snap (Correlated Solutions, 2016).

Figure 6-6: DIC image capture equipment setup

6.4.3 **DIC Calibration**

Calibration of the DIC setup consisted of inserting a 105 mm wide x 75 mm-high calibration plate with black dots 1.5 mm in diameter spaced 7.5 mm center to center in a square grid pattern. Figure 6-7 presents an image of the calibration plate. The calibration plate is rotated along its three axes by hand. While the calibration plate is being rotated, a series of photos are taken with the cameras. These photos are then imported into VIC3D and used to calibrate the test setup. The calibration process compares the differences between each image that is imported into VIC3D. A score is given that reflects the differences in the calculated calibration plate geometry for each camera is given at the

end of the calibration. This score indicates the cumulative error, the basis for determining if the test setup is adequate. If the cumulative error is below 1%, the calibration is satisfactory and testing may be conducted. If not calibration images are retaken and another calibration analysis is conducted as sometimes the calibration is not satisfactory due to human effort. If the calibration still yields unsatisfactory results the equipment must be re-aligned. The result of an improper setup and calibration is increased projection error. Because the cameras have overlapping fields of view, a theoretical line may be drawn along an image taken by camera one and the same line projected onto an image taken by camera two. The difference between the two theoretical lines is the projection error. The theoretical value should be zero, but a small projection error is normal due to small differences in camera view. A successful calibration takes these differences into account.

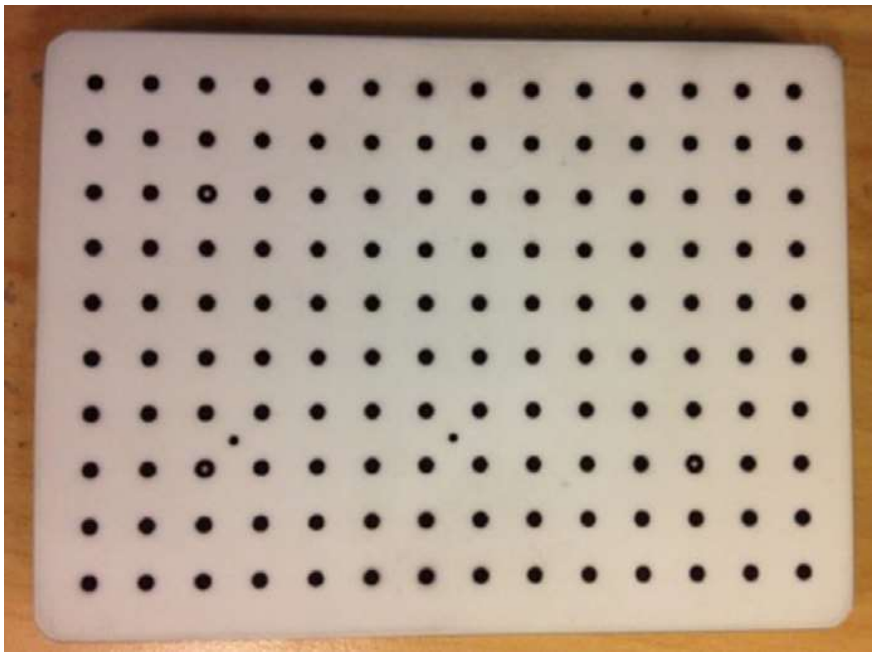

Figure 6-7: Calibration plate for DIC testing

6.4.4 **Tensile Test Apparatus Setup**

Once calibration of the DIC setup was complete, the geomembrane sample was slid into place between the jaws of the uniaxial tensile testing apparatus. Once the sample was in place, the grip apparatus was firmly tightened with pressure applied equally across the textured plates. A seating load was applied to remove slack from the sample and to place the sample in a slight degree of tension, evaluated visually, to seat the sample. Following seating, the sample was deformed in tension at a strain rate of 10% per minute in accordance with the ASTM 4885 standard for wide-width tensile testing of geomembranes. The tests were typically conducted up to strains of 12% to 15%. Tests were terminated in the event of slipping between the sample and the friction load plates

6.5 HDPE Geomembrane Sample Preparation

Three HDPE geomembrane samples were left unmarred to obtain baseline strain profiles and stress-curves for the material. Three additional HDPE geomembrane samples were prepared by applying controlled longitudinal scratches at the center of the sample with a width of 38 mm and depths of 10 percent, 20 percent, and 40 percent of the geomembrane thickness.

DIC was employed to measure the tensile strain in the sample. For a DIC test to be effective, the surface of the sample must be prepared in a manner such that distortions of the sample can be optically detected. A sample of uniform color or texture, e.g. an entirely black sample, would not be amenable to DIC measurements. High gloss surfaces can also make DIC measurement ineffective due to reflections from the high intensity lighting used to illuminate the sample. Therefore, preparation of the samples for DIC measurements consisted of first applying a uniform coat of white non-gloss paint on the surface of the

sample. Once the white non-gloss paint was dry, a random pattern of black speckles was applied over the white background and allowed to dry.

The details of the speckle pattern are of great importance in acquiring proper results from the DIC measurements. If a speckle is too large, a data gap is created in the analysis. However, if a speckle is too small the image analysis program may not recognize it. Changes in speckle density can also create gaps in the data. Figure 5-8 shows an un-seamed HDPE sample properly prepared for DIC strain field measurements.

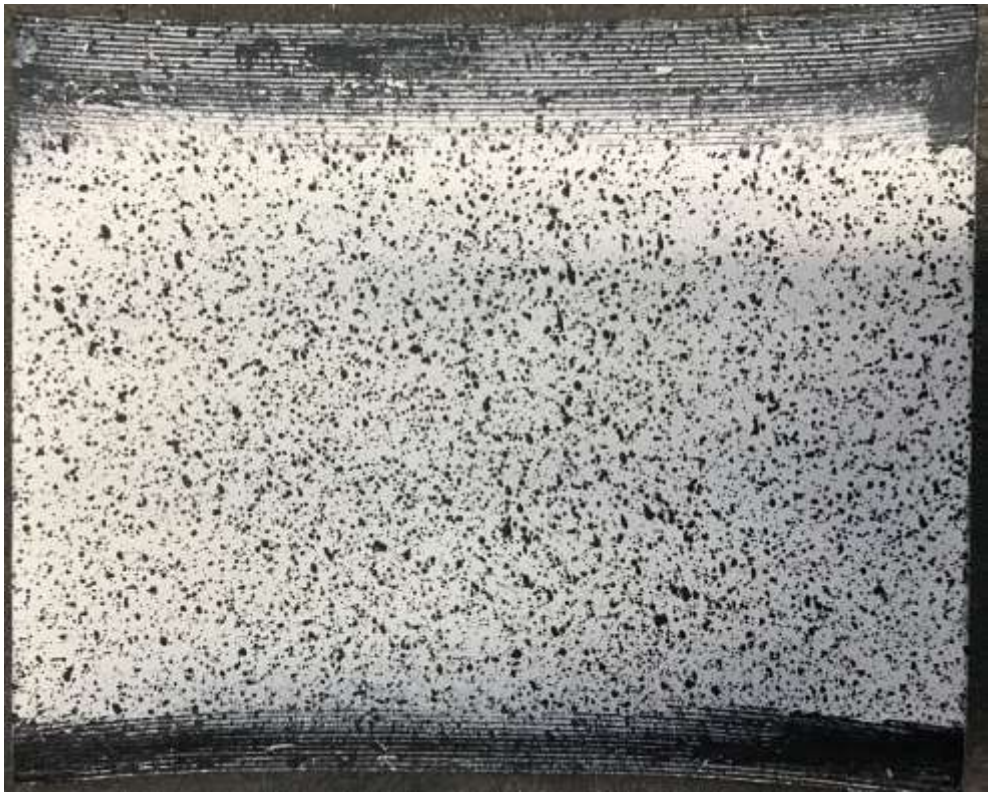

Figure 6-8: HDPE sample prepared with speckle pattern for DIC analysis

6.6 Accuracy and Precision of DIC Measurements

Tests were conducted on unseamed samples to evaluate the accuracy and precision of the DIC measurements. Accuracy was evaluated by comparing the average global strain evaluated by the DIC measurements using VIC 3D to the nominal global strain evaluated

based upon the length of the sample between the grips and measurements of the displacement of the grips securing the sample made using a linear varying displacement transducer (LVDT). Precision was evaluated by loading the sample to a strain below yield five times and comparing the DIC strain measurements from each trial at nominal strains (strains based upon LVDT measurements) of 0.17, 0.35, 1, and 3 percent. The accuracy and precision measurements were made on 2 different samples.

VIC 3D calculates the strain field based upon differentiation of the displacement field of the sample determined by comparison of two images taken at different times. Therefore, a reference image for the unstrained state of the sample is required upon which the DIC analysis is based. In this testing program, the reference image was taken after the seating load was applied to the geomembrane samples. Using the reference image as the baseline, VIC 3D computes a deformation and strain field over the area of interest based upon the relative movement of the speckles.

Results of the accuracy and precision tests are presented in Table 6-1. The mean strain from 5 trials based upon the DIC measurements was typically within 10 percent of the strain based LVDT measurements. Except at the smaller nominal strains (0.17 and 0.35 %), the strain from the DIC measurements was greater than the nominal strain from the LVDT measurements. The standard deviation from 5 measurements on the same sample was increased as the strain increased, but the variance (the standard deviation divided by the mean) decreased as the strain increased. While the variance at the smaller nominal strains (0.17 and 0.35 %) for Sample 1 was relatively high (up to 45%), at the largest nominal strain (3 %) was only 6% for Sample 1 and 3% for Sample 2.

Table 6-1: Comparison of nominal percent strain based upon LVDT measurements to mean and standard deviation percent strain from DIC measurements on an unseamed sample loaded below yield five times

LVDT	Sample 1			Sample 2		
	Mean	Std. Dev.	Variance	Mean	Std. Dev.	Variance
0.17	0.153	0.067	44%	0.171	0.016	9%
0.33	0.326	0.101	31%	0.359	0.012	11%
1.00	1.073	0.129	12%	1.110	0.029	3%
3.00	3.330	0.200	6%	3.389	0.086	3%

6.7 HDPE Geomembrane Testing

6.7.1 Testing Schedule

A total of six tests were performed, three baseline tests (A,B, and C) and three tests designed to evaluate the strain concentrations in a scratched geomembrane (D, E, and F). Table 6-2 below summarizes the sample characteristics. Strains of up to 15% were applied to the samples at a strain controlled rate of 10% strain per minute.

Table 6-2: HDPE geomembrane test samples

Sample	Thickness	Scratched	Depth of Scratch	Depth Percentage
A	1mm	No	N/A	N/A
B	1mm	No	N/A	N/A
C	1mm	No	N/A	N/A
D	1mm	Yes	0.1mm	10%
E	1mm	Yes	0.2mm	20%
F	1mm	Yes	0.4mm	40%

6.7.2 **VIC DIC Analysis**

The strain field in each geomembrane sample was developed graphically at discrete time increments throughout the test with the goal of visualization of the material behavior away from the scratch. The nominal strain referenced below is the strain measured using DIC, over the visible surface of the sample.

Figure 6-9 and Figure 6-10 show the computed strain field for a 1 mm geomembrane sample with a scratch depth of 10% of the intact geomembrane (Sample D) for nominal strains of 4.9% and 19.3% respectively. The strain concentration adjacent to the scratch (shown as a black line for visualization) is directly over the scratch and as expected.

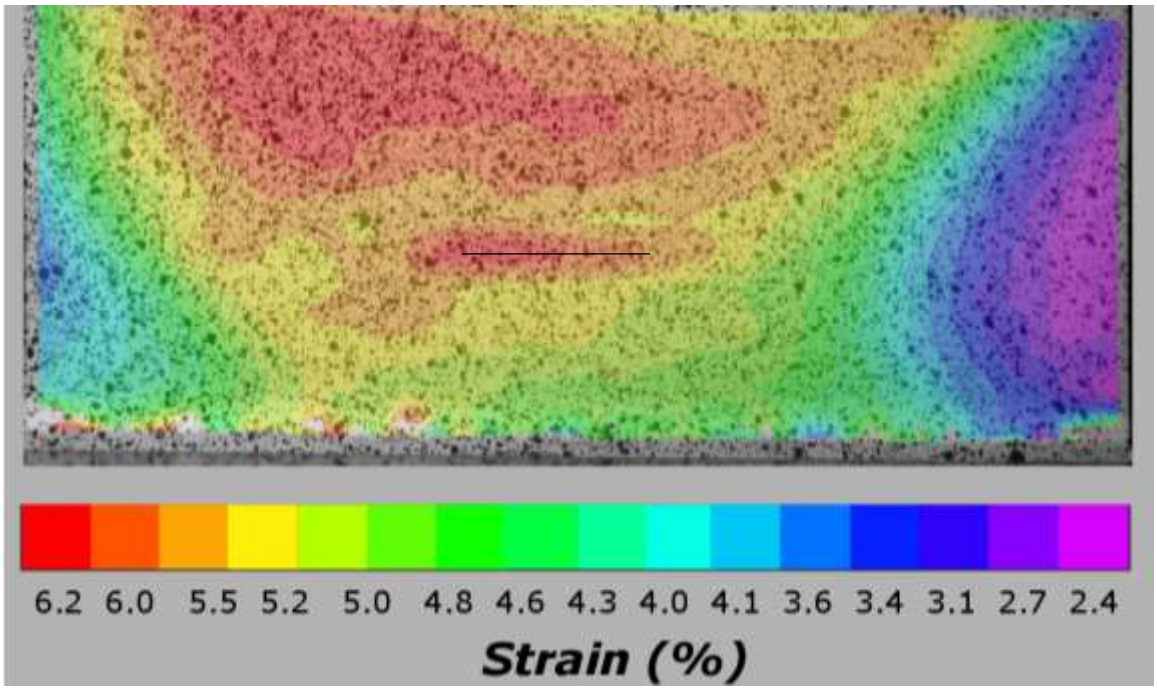

Figure 6-9: 1 mm geomembrane sample with 0.1 mm scratch. Average strain: 4.9. Maximum strain: 8.0% (Sample A)

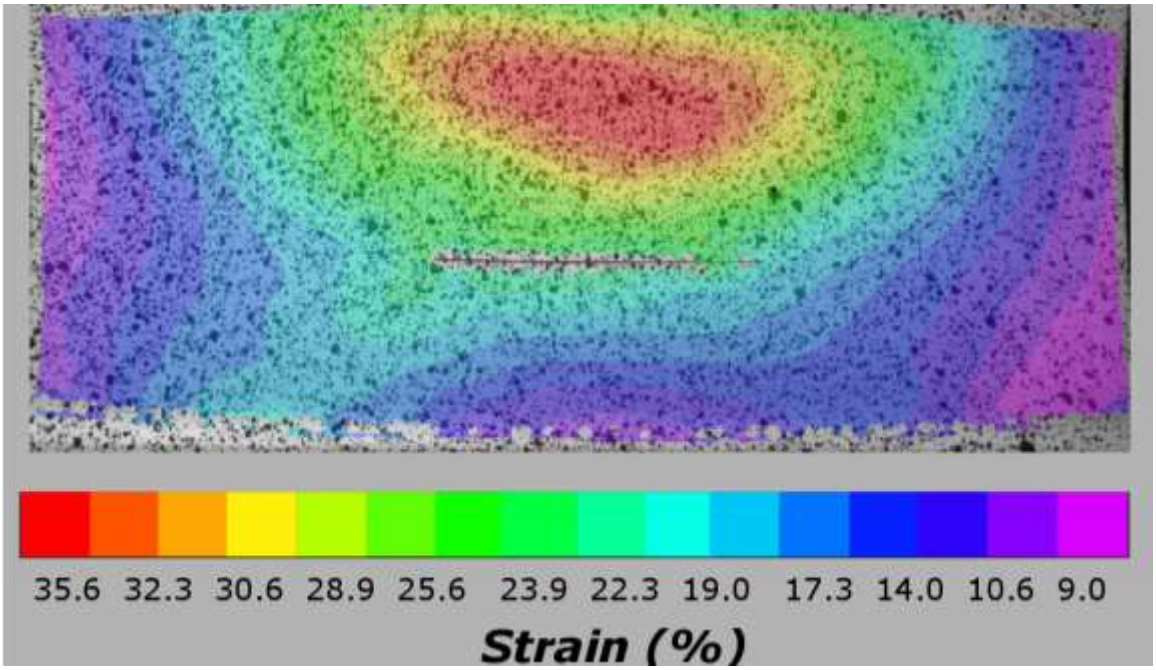

Figure 6-10: 1 mm geomembrane sample with a 0.1 mm scratch. Average strain 19.3 %. Maximum strain 26.4 % (Sample D)

Figure 6-11 and Figure 6-12 show the computed strain field for a 1 mm geomembrane sample with a scratch depth of 20% of the intact geomembrane (Sample E) for average strains of 4.4% and 14.0% respectively. The strain concentration adjacent to the scratch (shown as a black line for visualization) is concentrated around the scratch. Furthermore, the sample is shown to rupture at an average strain of 14 percent (Figure 12) whereas the anticipated rupture strain of HDPE is estimated at over 100%. Because the sample ruptured and disrupted the speckling pattern, the true maximum strain cannot be determined However, the maximum calculated tensile strain prior to rupture of 38.7 percent occurred at the corners of the rupture.

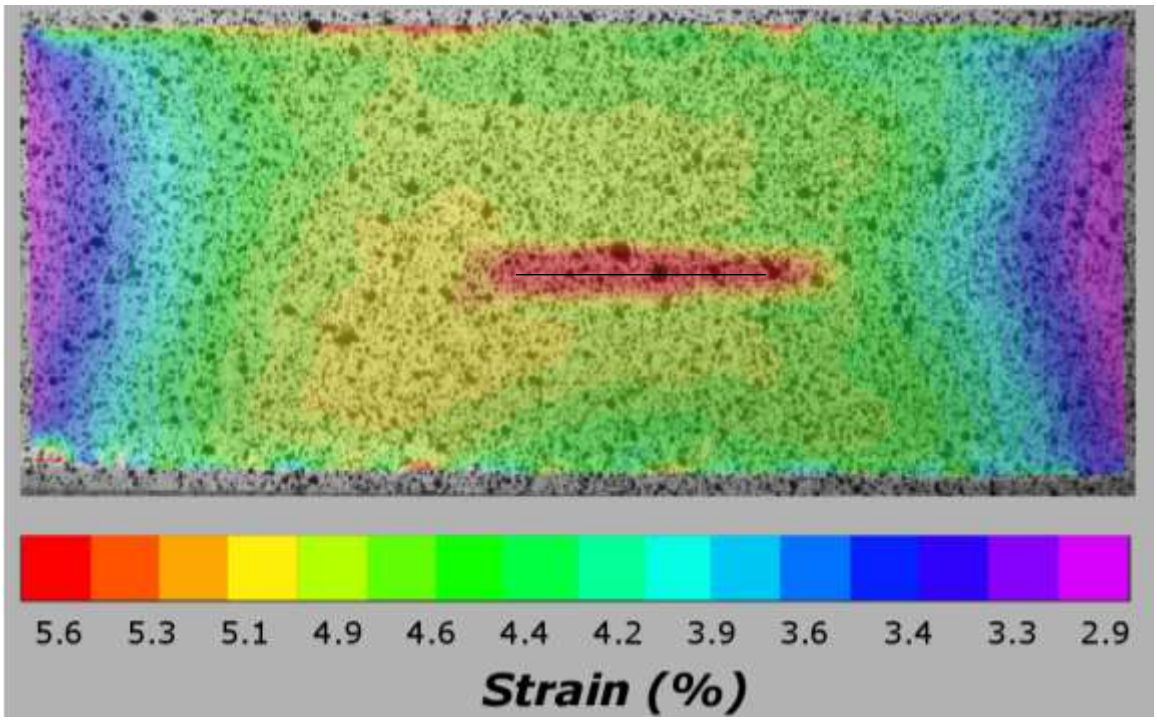

Figure 6-11: 1 mm geomembrane with a 0.2 mm scratch. Average strain: 4.4 %. Maximum strain 6.3 % (Sample E)

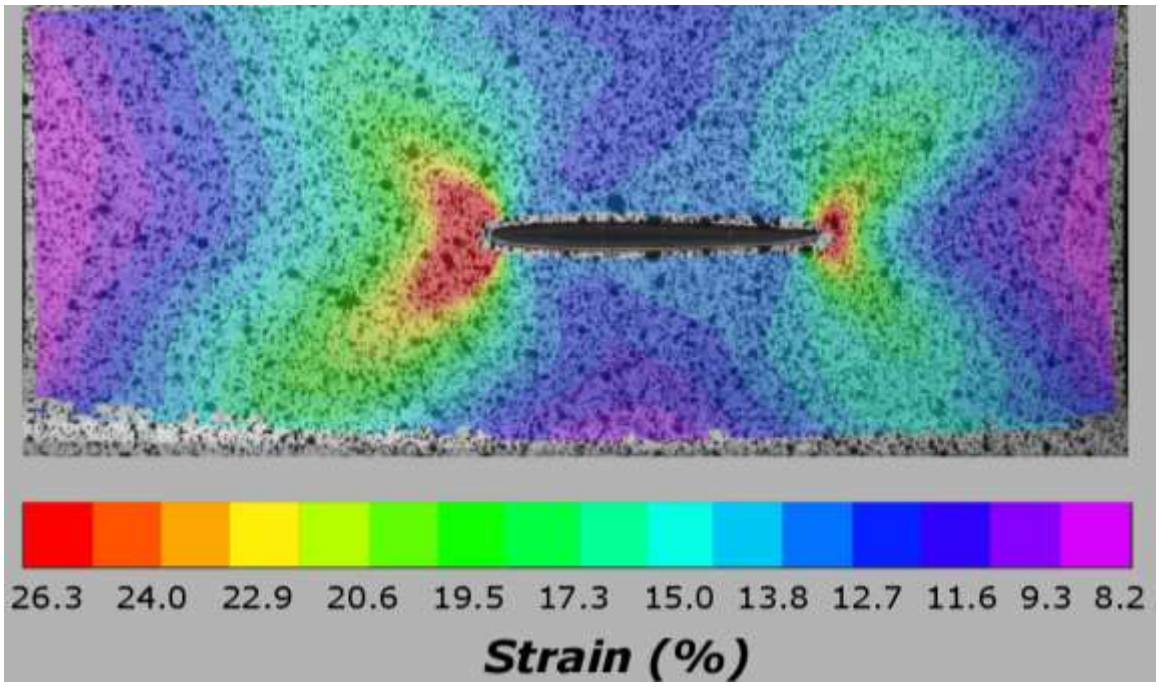

Figure 6-12: 1 mm geomembrane with a 0.2 mm scratch. Average strain 14.0%. Maximum strain: 38.7 % (Sample E)

Figure 6-13 through Figure 6-15 show the computed strain field for a 1 mm geomembrane with a scratch depth of 40% of the intact thickness (Specimen F) at three different strain levels. The strain fields are shown for the sample at an average strain of 2.1, 4.0, and 5.5 percent. At low average strains, the strain near the scratch is quite high, as expected. The strain concentration remains very localized, as seen in Figure x. The average strain is 4.0%, and the maximum calculated tensile strain is only 6.0%, but the sample has started to rupture. The phenomena is evident in Figure 6-15, wherein a low average strain of 5.5% in the sample has resulted in a clear rupture.

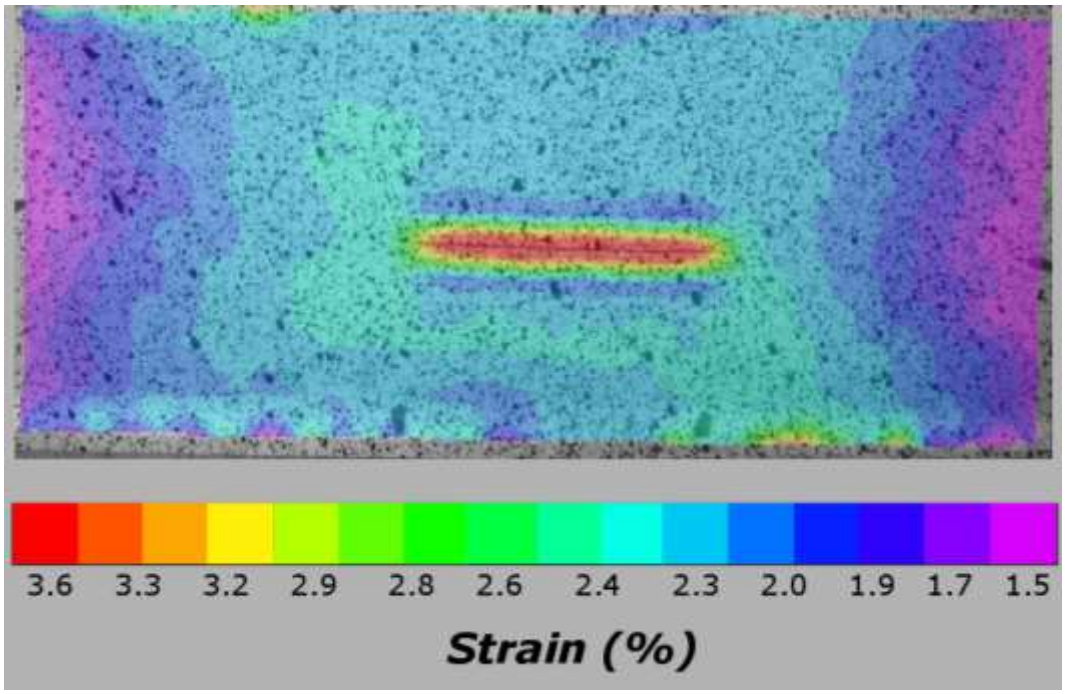

Figure 6-13: 1 mm geomembrane with a 0.4 mm scratch. Average strain 2.1 %. Maximum strain: 4.0% (Sample F)

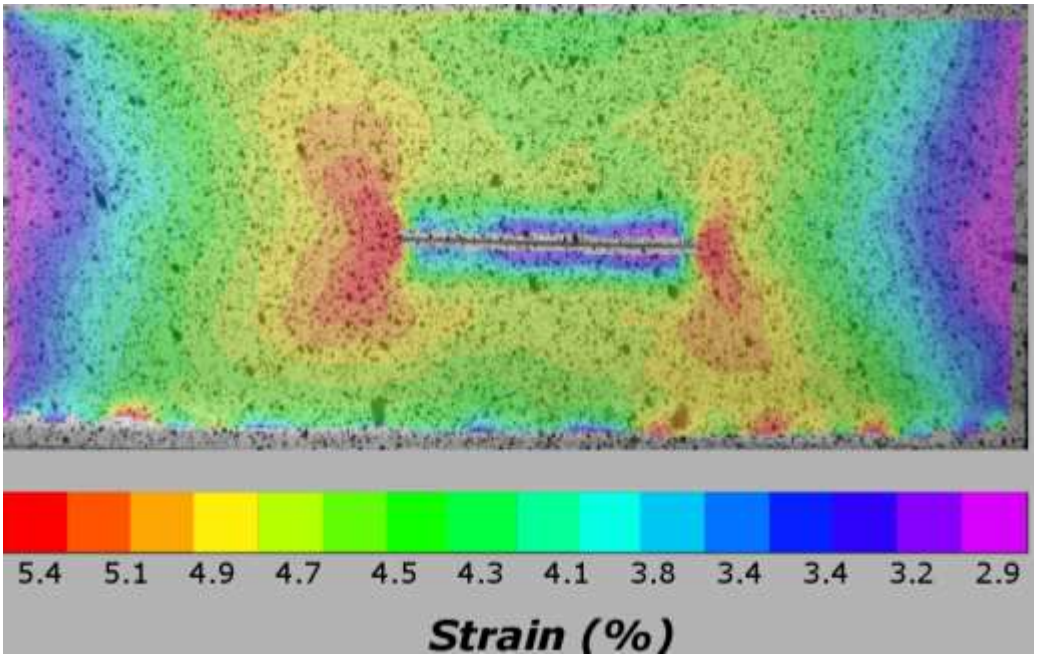

Figure 6-14: 1 mm geomembrane with a 0.4 mm scratch. Average strain: 4.3 %. Maximum strain 6.0%. (Sample F)

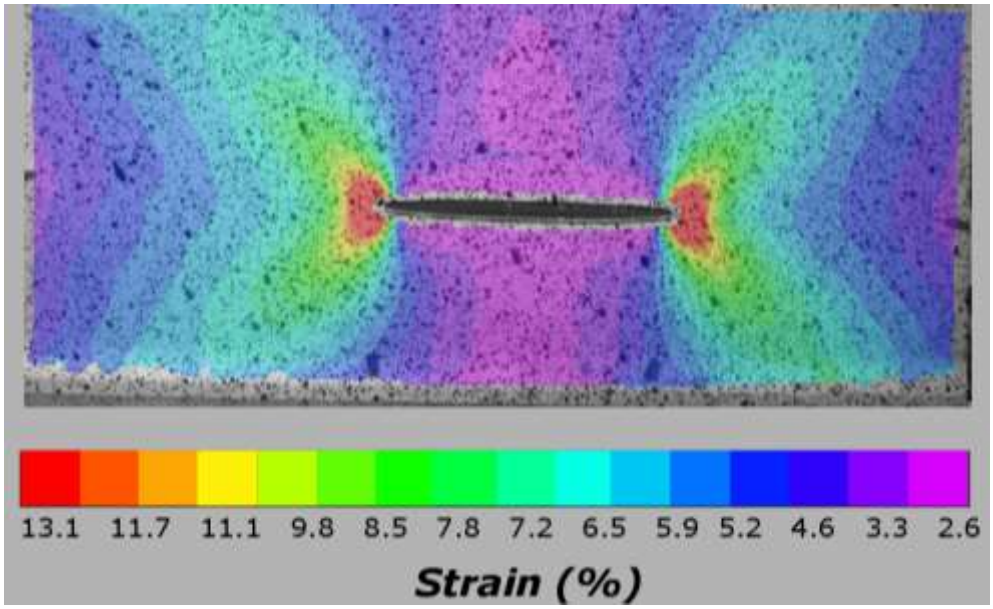

Figure 6-15: 1 mm geomembrane with a 0.4 mm scratch. Average strain 5.5 %. Maximum strain 18.0% (Sample F)

6.8 Experimental Results

The stress strain curves for the intact geomembranes (samples A, B, and C) are presented in Figure 5-17 for the average strain across the sample surface as measured using DIC. Furthermore, Figure 6-16 compares the stress strain relationship for sample A using the nominal tensile strain (as measured using grip separation) and the average strain across the sample surface (measured using DIC). This comparison shows that the two methods for measuring the global stress-strain response of the geomembrane samples are essentially equivalent. Figure 6-16 compares the stress-strain curves generated using the grip separation method to calculate the strain and the average strain calculated across the surface of the sample using DIC. The only significant difference is in the strain softening region. The strain increases gradually as the induced stress relaxes in the grip separation generated strain curve (at a rate of 10% per minute as dictated by the test parameters). The average strain (measured using DIC) appears to stay relatively constant as the stress relaxes, creating a more abrupt drop in strength.

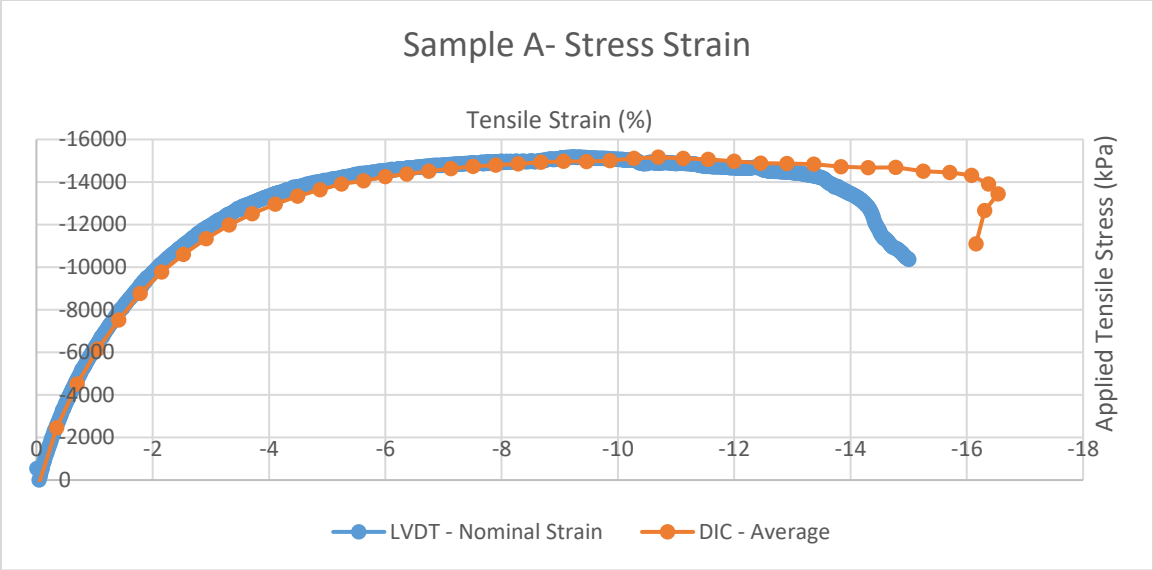

Figure 6-16: Stress strain curve for Sample A, comparing the strain calculated using grip separation and digital image correlation

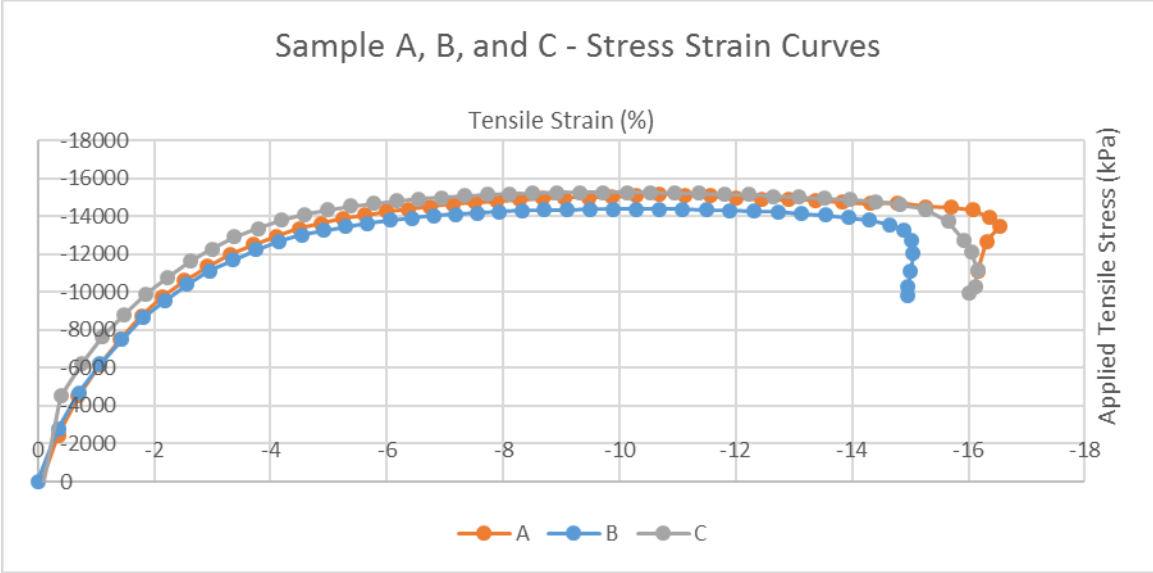

Figure 6-17: Stress strain curves for unmarred Samples

The peak strain occurs at approximately 11 percent to 12 percent strain in the intact samples (A, B, and C). A significant post-peak decrease in strength occurs at between 15 percent and 16 percent.

Figure 6-18 and Figure 6-19 show the stress strain curves generated for samples D and E respectively. The curves reach similar peak strengths and exhibit noticeable strength loss between 10% and 13% in the case of Sample E, with a 20% scratch depth with respect to the intact geomembrane thickness. The strength loss is not obvious in the stress strain curves based upon an average strain approach. The increased strain calculated using DIC is likely due to the high strain concentrations near the scratch, not captured by the grip separation method.

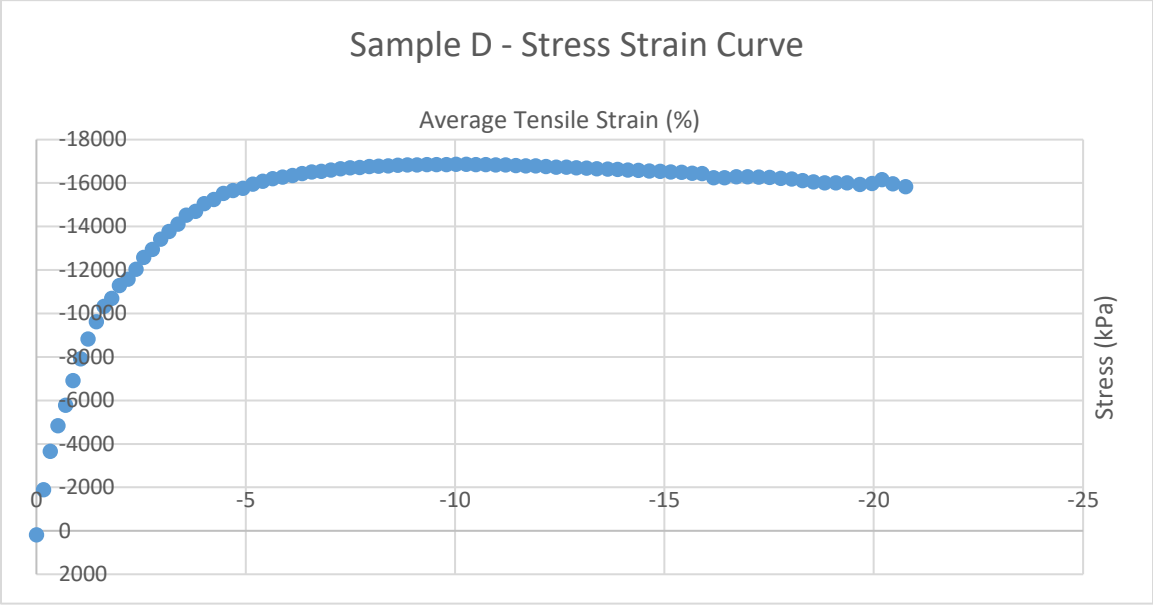

Figure 6-18: Stress strain curve for a 1 mm HDPE geomembrane with a 10% thickness scratch, strain measured using DIC (Sample D)

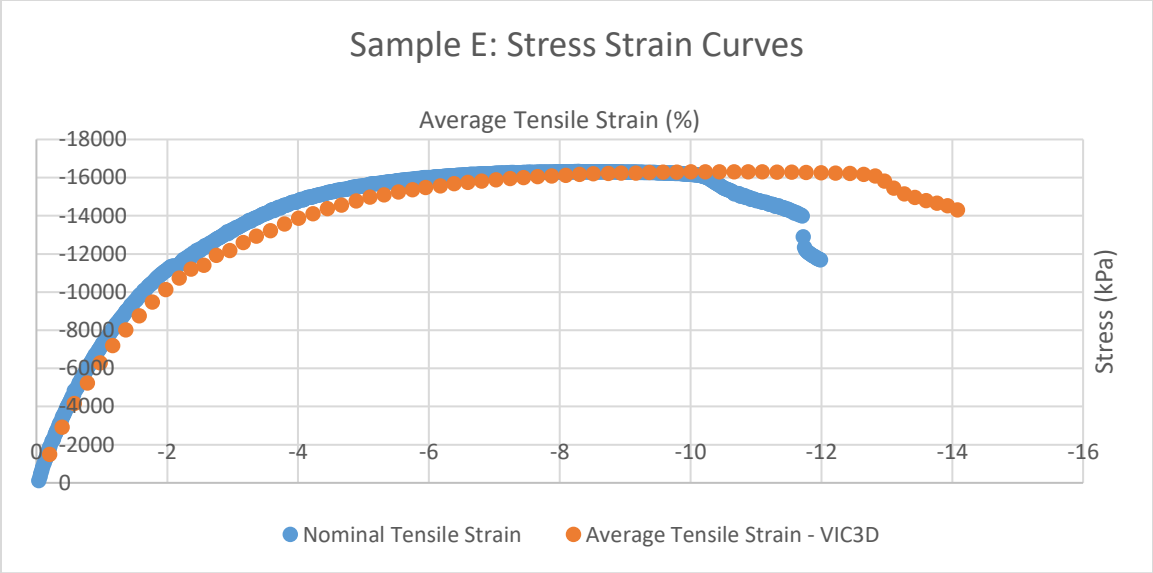

Figure 6-19: Stress strain curve for a 1 mm HDPE geomembrane with a 20% thickness scratch (Sample E)

Figure 6-20 shows the stress strain curves for Sample F, with a 40% scratch depth with respect to the intact geomembrane thickness. The shape of the curves are similar, both showing a noticeable strength decrease at approximately 4% to 5% tensile strain. The scratched area opened at a low tensile average strain for Sample F (a strain of approximately 4.3%.) The image capture is unable to calculate the excessive strains in this area because of the discontinuity at rupture, leading the average strain to be approximately equal to the nominal tensile strain as measured using grip separation.

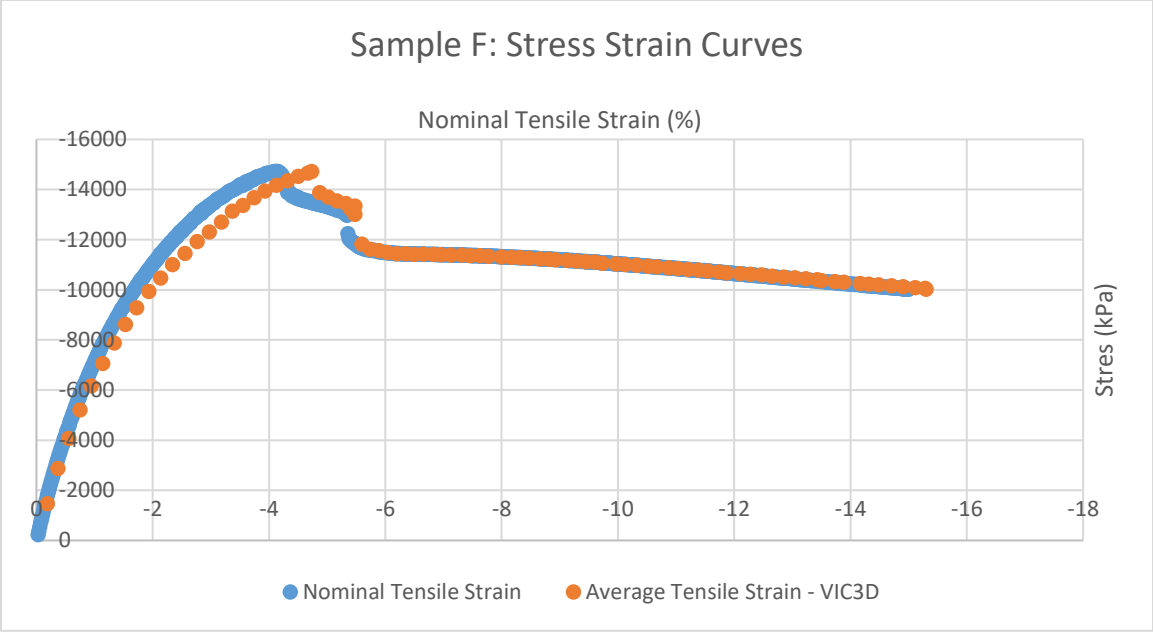

Figure 6-20: Stress strain curve for a 1 mm HDPE geomembrane with a 40% thickness scratch (Sample F)

Table 6-3 presents the primary results of the study, including the data for samples D, E, and F. The scratch depth is listed as a percentage of the unscratched geomembrane thickness (1 mm). The unmarred yield strain refers to the yield strain of an intact, unscratched HDPE geomembrane, taken as 12% based upon Figure 6-17. The yield strain ratio, $\frac{\varepsilon_{YS}}{\varepsilon_{Y}}$, was calculated based upon the equations derived in Giroud (1993). The yield strain ratio and the unmarred yield strain are multiplied to calculate the predicted yield strain. The yield strain based upon the first observed drop in stress from the stress strain curves (Figures 6-18, 6-19, and 6-20) is reported under Yield Strain Using Stress Strain Plot. The nominal tensile strain which induced a maximum tensile strain equal to the yield strain is reported under Nominal Strain Limiting Maximum Strain to Yield.

Table 6-3: Yield strain results for Samples D, E, and F.

Sample	Scratch Depth	Unmarred Yield Strain	$\frac{\varepsilon_{Ys}}{\varepsilon_{Y}}$	Predicted Yield Strain	Yield Strain Using Stress Strain Plot	Nominal Strain Limiting Maximum Strain to Yield
D	10%	12%	0.44	5.2%	12.5	8.3
E	20%	12%	0.33	4.0%	10.0	8.3
F	40%	12%	0.20	2.4%	4.0	4.67

6.9 Conclusions

The reduction in yield strain due to scratches in HDPE geomembranes loaded in uniaxial tension perpendicular to the scratch were evaluated experimentally on three samples with a 1 mm thickness. A modified soil triaxial test apparatus was employed to apply tension to the samples at a constant nominal strain rate. The geomembrane samples fit into the grip apparatus, fulfilling the requirements stated in ASTM D4885 for wide width tensile testing. The strain was measured using digital image correlation, allowing the capture of localized pockets of strain. The experimentally measured yield strains were compared to theoretical values obtained using equations presented by Giroud et al. (2005).

The testing program included three scratched HDPE 1 mm geomembrane samples and three unscratched HDPE 1 mm geomembrane samples. The geomembrane samples had smooth surfacing. The maximum measured strain was calculated for all specimens at 2 second intervals as the sample was strained, as was the associated nominal tensile strain (measured using both DIC and the LVDT on the load frame). The unscratched HDPE

geomembranes were tested to understand the stress-strain relationship, illustrated in Figure 6-17. The geomembranes were found to have an approximate yield strain of 12%, and showed reproducible results from the test apparatus. Figure 6-16 confirms that the nominal tensile strain as measured using DIC and the deformation from the LVDT measurements are similar, as expected. The nominal tensile strain which induced a maximum tensile strain exceeding yield was observed from the test data and compared to the yield strain calculated using the stress strain plots and the yield strain prediction calculated using the equations from Giroud (2005).

The analysis results show a clear weakening in the geomembrane resulting from even small scratches (i.e. 10% of the intact thickness). The theoretical reduced yield strain for a scratch with a 0.1 mm scratch in a 1 mm thick geomembrane is 5.2%, based upon an N-order polynomial derived by Giroud et al. (1984) fit to the typical yield behavior of HDPE. The data did not show a drastic reduction in yield strain. The nominal tensile strain which induced a maximum strain greater than yield was 8.3%. The Giroud equation is based upon a scratch across the length of the geomembrane, making it conservative and appropriate for design.

The yield strain obtained from a typical stress strain curve does not properly capture the effects of scratches in seams. The average tensile strain in the sample may remain within allowable limits, but still induce rupture. A scratched geomembrane was found to rupture at very low average strains as in the case of Sample F (Figure 5-15). The scratched geomembrane showed rupture at average strains of 5.5%, and a measured maximum strain of 18%. It must be further noted that linear features are not captured well by DIC. In the case of a geomembrane rupture, the sample texturing is disrupted and the

DIC algorithm is no longer able to accurately measure the deformation and calculate the strain.

Further work may be warranted with a larger sample size and a developed method for determining the exact moment of yield or rupture using DIC. This may include a much faster rate of image capture (on the order of 1 image every 0.5 seconds).

CHAPTER 7. SUMMARY AND CONCLUSIONS

Strain concentrations in HDPE geomembranes due to the presence of seams and scratches were evaluated through tensile testing of laboratory prepared and field installed samples. A modified triaxial load frame was used with appropriate modifications to apply axial uniaxial tension with a strain controlled test program. The strain over the sample surfaces was captured using digital image correlation. The results of the strain evaluation on 6 laboratory prepared samples indicate that the maximum strain in the geomembrane adjacent to the seam is on the order of 4 times the global average strain. The zone of increased strain adjacent to the seam was measured to have average strain magnitudes similar to those predicted using the Giroud (1994) equations for incremental bending strain in geomembranes adjacent to seams. Therefore, the equations are thought to be an accurate measure of bending strain. However, as the maximum induced strain far exceeds the prediction, small changes in geometry and inconsistencies within the geomembrane are thought to induce strain magnitudes not captured in the analytical solution.

Geomembrane seams welded during liner installations are thought to exhibit a greater degree of variability in geometry than laboratory prepared geomembrane samples. The variability was captured by evaluating strains in field samples taken for QA/QC purposes. The samples were prepared and subjected to tensile loading, perpendicular to the seam. The strain across the sample surface was captured with DIC and the maximum strain was evaluated as a function of the nominal tensile strain. The geomembrane sample groups were separated based upon surfacing and thickness according to the results of statistical significance test. The resulting relationships are presented in Figures 5-14 and 5-17. Furthermore, the nominal tensile strain expected to induce maximum tensile strains

less than or equal to the yield of HDPE was found to be 3.2 to 3.7% for geomembranes with dual hot wedge seams and 2.2 to 2.7% for geomembranes with extrusion fillet seams.

Geomembranes subject to scratches and defects have a lowered yield strain compared to an intact geomembrane with the same material properties. The nature of this relationship was evaluated using a continuous deformation measurement approach. Tensile strain fields were calculated across the surface of the test samples, which were subjected to scratching. The test results showed that the measured and observed yield strain based upon the analysis was higher than the yield strain prediction developed with equations from Giroud 2005. However, while the overall sample did not yield at low nominal strain, the geomembrane was found to have yielded, and in some cases ruptured, at low nominal tensile strain magnitudes of under 5%.

The allowable tensile strain in geomembrane liners may need to be reevaluated based upon the results presented herein. The current practice of construction quality assurance (CQA) requires the collection of geomembrane seam samples for destructive testing. The patch must be covered with an extrusion fillet seam, resulting in a dual seam with two edges perpendicular to the potential tensile loading. Furthermore, the extrusion fillet seam used to seal the patch is likely to induce higher magnitude strains in the adjacent geomembrane than the dual hot wedge seam which it covers. Therefore, the geomembrane seam may need to be left intact in specific location of the liner subject to higher design strains. Specifically, the global tensile strain in the area of extrusion fillet seams should be limited to magnitudes of 2.5% and global tensile strain in the area of dual hot wedge seams should be limited to 3.0%.

Future effort to quantify the strain concentrations in geomembranes subjected to tensile loading adjacent to scratches may include a larger sample size and a wider range of scratch depths. Test programs using DIC should consider the effect of the image capture rate. Decreasing the time-step between images may help to identify the exact moment at which the geomembranes experience maximum strains at or above yield and when rupture occurs. The magnitude of strain in geomembrane samples loaded to tension with scratches across the width of the sample should be compared to the results of this study to determine the effect of an increased strain at the corner of the scratch. Also, the effect of uncontrolled scratches with varying thickness and length may be necessary.

CHAPTER 8. CULMINATING EXPERIENCE SUMMARY

The research and analysis involved in publication of the journal paper "Experimental Evaluation of HDPE Geomembrane Seam Strain Concentrations" served as a starting point for a great deal of the work contained herein. The clear presence of large strain concentrations and the value in quantifying the expected strains in the field motivated further research. The lab procedures and data collection techniques developed for this study were modified and applied to later testing schedules designed to capture the strain concentrations in field geomembrane samples. Similarly, the software used was applied in a similar manner on later research projects to analyze the collected data, making the experience invaluable, leading to increased efficiency on later projects. With regard to future work, the natural progression of the research contained in the journal paper has been followed as a part of this culminating experience document. As such, the future of the work is described in Chapter 7, and is based upon the results of additional studies, included in Chapter 5 and 6.

REFERENCES

ASTM (2011), "Standard Practice for Pressurized Air Channel Evaluation of Dual Seamed Geomembranes," Test Method D5820-95, ASTM International, West Conshohocken, PA.

ASTM (2011), "Standard Test Method for Determining Performance Strength of Geomembranes by the Wide Strip Tensile Method," Test Method D4885-01, ASTM International, West Conshohocken, PA.

ASTM (2012), "Standard test Method for Determining the Integrity of Nonreinforced Geomembrane Seams Produced Using Thermo-Fusion Methods," Test Method D6392-12, ASTM International, West Conshocken, PA.

Arab, G. A. (2011) "The Integrity of Geosynthetic Elements of Waste Containment Barrier Systems Subject to Seismic Loading," PhD. thesis, Arizona State University, Tempe, Arizona, USA.

Augello, A. J., Matasovic, N., Bray, J.D., Kavazanjian, E., Jr., and Seed, R.B. (1995) ''Evaluation of Solid Waste Landfill Performance during the Northridge Earthquake," Earthquake Design and Performance of Solid Waste Landfills, ASCE Geotechnical Special Publication No. 54, 17-50.

Correlated Solutions (2016), "VIC-3D^{TM} System," Correlated Solutions, Inc., www.correlatedsolutions.com/products/#vic3d.

EMCON Associates (1994) "Northridge Earthquake Seismic Evaluation, Chiquita Canyon Landfill," April.

Giroud, J.P. (1984). Analysis of stresses and elongations in geomembranes. In Proceedings of the International Conference on Geomembranes (vol. 2). IFAI, MN, USA, pp. 482-6.

Giroud, J. P., Beech, J.F., Soderman, K.L. (1994). Yield of scratched geomembranes. Geotextiles and Geomembranes, **13**, pp. 231-246.

Giroud, J. P., Tisseau, G. Soderman, K. L. & Beech J. F. (1995). Analysis of strain concentrations next to geomembrane seams. *Geotext. Geomb.*

Giroud, J. P. (2005). "Quantifcation of geosynthetic behavior". Geosynthetics International, Special Issue on the Giroud Lectures, **12**, NO 1, 2-27.

Kavazanjian, E., Jr., Arab, M., and Matasovic, N. (2013) "Performance of two Geosynthetics-Lined Landfill in the Northridge Earthquake," Proceedings of the 7th International Conference on Case Histories in Geotechnical Engineering and Symposium in Honor of Clyde Baker, Chicago, April.

Matasovic, N., Kavazanjian, E., Jr., Augello, A.J., Bray, J.D. and Seed, R.B. (1995) "Solid Waste Landfill Damage Caused by 17 January 1994 Northridge Earthquake," In: Woods, Mary C. and Seiple, Ray W., Eds., The Northridge, California, Earthquake of 17 January 1994: California Department of Conservation, Division of Mines and Geology Special Publication 116, Sacramento, Calif., 221-229

Müller, Werner W."*HDPE Geomembranes in Geotechnics"*. Berlin: Springer, 2007. 379-404. Print.

Perez, J.A., Coppieters, S., Debruyne, D. (2015) "Influence of the Paint Coating Thickness in Digital Image Correlation Experiments," World Academy of Science, Engineering and Technology International Journal of Computer, Electrical, Automation, Control and Information Engineering, **7,** pp 1660-1664

Take, W.A. (2015), "Thirty-Sixth Canadian Geotechnical Colloquium: Advances in visualization of geotechnical processes through digital image correlation," Canadian Geotechnical Journal, 52 (9), 1199-1220, doi: 10.1139/cgj-2014-0080.

APPENDIX A

STATEMENT OF PERMISSION

All authors of the journal paper “Experimental Evaluation of HDPE Geomembrane Seam Strain Concentrations” have granted their permission for the work to be included in this thesis as part of a culminating experience document.